2009-02-12

# Role of Supervillin, a Membrane Raft Protein, in Cytoskeletal Organization and Invadopodia Function

Jessica Lynn Crowley
*University of Massachusetts Medical School*

# THE ROLE OF SUPERVILLIN, A MEMBRANE RAFT PROTEIN, IN CYTOSKELETAL ORGANIZATION AND INVADOPODIA FUNCTION

A dissertation presented by

Jessica Lynn Crowley

Submitted to the Faculty of the

University of Massachusetts Graduate School of Biomedical Sciences, Worcester

in partial fulfillment of the requirements for the degree of

DOCTOR OF PHILOSOPHY

February 12, 2009

Interdisciplinary Graduate Program

**THE ROLE OF SUPERVILLIN, A MEMBRANE RAFT PROTEIN, IN CYTOSKELETAL ORGANIZATION AND INVADOPODIA FUNCTION**

A Dissertation Presented By

Jessica Lynn Crowley

The signatures of the Dissertation Defense Committee signifies completion and approval as to style and content of the Dissertation

Elizabeth Luna, Ph.D., Thesis Advisor

Dannel McCollum, Ph.D., Member of Committee

Trudy Morrison, Ph.D., Member of Committee

Susette Mueller, Ph.D., Member of Committee

Leslie Shaw, Ph.D., Member of Committee

The signature of the Chair of the Committee signifies that the written Dissertation meets the requirements of the Dissertation Committee

Peter Pryciak, Ph.D., Chair of Committee

The signature of the Dean of the Graduate School of Biomedical Sciences signifies that the student has met all graduation requirements of the School

Anthony Carruthers, Ph.D.
Dean of the Graduate School of Biomedical Sciences

Interdisciplinary Graduate Program
February 12, 2009

Dedicated to the memory of my parents,

who were lovingly supportive of me during all of my endeavors.

# Acknowledgments

First, I would like to thank my mentor, Dr. Elizabeth Luna for her support and guidance throughout my graduate career. Beth has challenged me to really think about how things work and where the important questions lie. She always has an open door for helpful discussions and her enthusiasm for science is unmatched. I also appreciate the support I've received from members of the Luna lab (past and present): Thomas Nebl, Sang Oh, Steve Palmieri, Yu Chen, Norio Takizawa, Nacima Hadjout, Joline Jacques and Zhiyou Fang. I especially thank Tara Smith, for helpful comments on this dissertation, as well as acting as a sounding board for experimental design many, many times.

I would also like to thank all members of my committee (past and present): Drs. Peter Pryciak, Trudy Morrison, Dannel McCollum, Leslie Shaw, Yu-Li Wang and Stephen Lambert. I am very grateful for all of your helpful advice and guidance over the years. You were instrumental in keeping me focused and forcing me to think about the big picture. Also, thank you to Dr. Susette Mueller for serving as my outside committee member, as well as providing thoughtful comments and suggestions on my paper.

In addition, my time in graduate school would not have been as enjoyable were it not for my friends, as well all of the members of the Biotech IV community. This scientific utopia (like the Amish, with pipets*) is ever supportive and never dull. You have all become like a second family to me. Josh Nordberg of the Sluder lab was extremely helpful with all things imaging. I especially thank Shelly and Satoe for keeping me (or trying to) sane during this process.

Finally, I need to thank my family. My husband, Josh, has been remarkably patient during this long and difficult journey. For his love and support, I am truly

grateful. Our son, Owen, has provided more joy than I could have imagined (but much less sleep!) during his first year with us. My sisters, Jen and Beck, and their families have provided much in the way of emotional support, comic relief and nourishment. And thank you to the rest of my (large) extended family for all of the little things that supported me along the way.

*M. Winters ca. 2007

## Abstract

Crucial to a cell's ability to migrate is the organization of its plasma membrane and associated proteins in a polarized manner to interact with and respond to its surrounding environment. Cells interact with the extracellular matrix (ECM) through specialized contact sites, including podosomes and invadopodia. Tumor cells use F-actin-rich invadopodia to degrade ECM and invade tissues; related structures, termed podosomes, are sites of dynamic ECM interaction and degradation. We show here that supervillin (SV), a peripheral membrane protein that binds F-actin and myosin II, reorganizes the actin cytoskeleton and potentiates invadopodial function. Overexpressed SV increases the number of F-actin punctae, which are highly dynamic and co-localize with markers of podosomes and invadopodia. Endogenous SV localizes to the cores of Src-generated podosomes in COS-7 cells and with invadopodia in MDA-MB-231 cells. EGFP-SV overexpression increases the average amount of matrix degradation; RNAi-mediated downregulation of SV decreases degradation. Cortactin, an essential component of both podosomes and invadopodia, binds SV sequences in vitro and contributes to the formation of EGFP-SV induced punctae. Additionally, SV affects cortactin localization, which could provide a mechanism for SV action at invadopodia.

The formation of cholesterol-rich membrane rafts is one method of plasma membrane organization. A property of membrane rafts is resistance to extraction with cold Triton X-100 and subsequent flotation to low buoyant densities. The actin cytoskeleton has been implicated in many signaling events localized to membrane rafts, but interactions between actin and raft components are not well characterized. Our laboratory isolated a heavy detergent resistant membrane fraction from neutrophils,

called DRM-H, that contains at least 23 plasma membrane proteins. DRM-H is rich in cytoskeletal proteins, including fodrin, actin, myosin II, as well as supervillin. DRM-H also contains proteins implicated in both raft organization and membrane-mediated signaling. DRM-H complexes exhibit a higher buoyant density than do most DRMs (referred to as DRM-L), which are deficient in cytoskeletal proteins. By using similar purification methods, I find that COS-7 cells also contain cytoskeleton-associated DRMs. In addition, when transfected into COS-7 cells, estrogen receptor (ER)α associates with DRM-H, while ERβ is seen in both DRM-L and DRM-H populations, suggesting a role for DRM-H in nongenomic estrogen signaling. Thus, the cytoskeleton-associated DRM-H not limited to hematopoietic cells and could constitute a scaffold for membrane raft-cytoskeleton signaling events in many cells.

Taken together, our results show that SV is a component of cytoskeleton-associated membrane rafts as well as podosomes and invadopodia, and that SV plays a role in invadopodial function. SV, with its connections to both membrane rafts and the cytoskeleton, is well situated to mediate cortactin localization, activation state, and/or dynamics of matrix metalloproteases at the ventral cell surface for proper matrix degradation through invadopodia. The molecular dissection of invadopodia formation and function may contribute to a greater understanding of in vivo invasion, and thus, tumor cell metastasis.

# Table of Contents

## List of Figures

### Chapter 1 Figures



### Chapter 2 Figures

## List of Abbreviations

SV: supervillin

AV: archvillin, the muscle specific form of supervillin

DRM: detergent resistant membrane

DRM-L: DRM-light buoyant density

DRM-H: DRM-heavy buoyant density

ECM: extracellular matrix

GPI: glycosylphosphotidylinositol

## Preface

Portions of this dissertation are represented in the following publications:

Nebl T., Pestonjamasp K.N., Leszyk J.D., **Crowley J.L.**, Oh S.W. and Luna E.J. (2002). Proteomic analysis of a detergent-resistant membrane skeleton from neutrophil plasma membranes. *J Biol Chem*, 277, 43399-409.

Oh S.W., Pope R.K., Smith K.P., **Crowley J.L.**, Nebl T., Lawrence J.B. and Luna E.J. (2003). Archvillin, a muscle-specific isoform of supervillin, is an early expressed component of the costameric membrane skeleton. *J Cell Sci*, 116, 2261-75.

Chen Y., Takizawa N., **Crowley J.L.**, Oh S.W., Gatto C.L., Kambara T., Sato O., Li X.D., Ikebe M. and Luna E.J. (2003). F-actin and myosin II binding domains in supervillin. *J Biol Chem*. 278, 46094-106.

Takizawa N., Smith T.C., Nebl T., **Crowley J.L**., Palmieri S.J., Lifshitz L.M., Ehrhardt A.G., Hoffman L.M., Beckerle M.C. and Luna E.J. (2006). Supervillin modulation of focal adhesions involving TRIP6/ZRP-1. *J Cell Biol.* 174, 447-58.

**Crowley J.L.**, Smith T.C., Takizawa N. and Luna E.J. (2008). Supervillin reorganizes the actin cytoskeleton and increases invadopodial efficiency. *Mol Biol Cell*. 2008 Dec 24. [Epub ahead of print].

Figures 1-1 and 1-2 were reprinted with copyright permission, as indicated in the text.

Figures 2-2, 2-3 and 2-16 were contributed by E.J. Luna. T. Smith provided the data for Figures 2-5B and 2-6. Z. Fang provided the data for Figure 2-7A. N. Takizawa provided the data for Figure 2-5C. Figure 3-1 was contributed by T. Nebl.

# Chapter I

## General Introduction

Adhesion, motility and invasion are three basic cell biological properties that are necessary steps in a wide variety of fundamental biological processes. Motility underlies virtually every stage of progression of a single cell to a multicellular organism, during development, from the mass migration of cells during gastrulation, to the formation of blood vessels. These processes also play key roles in maintenance of health, including tissue repair and immunological defense against pathogens. In order to recognize foreign substances, immune cells undergo invasive cell movement to reach sites of infection and adhere to antigen presenting cells. Adhesion, motility and invasion also contribute to disease states such as cancer cell metastasis. In order to metastasize, primary tumor cells must lose adhesion to detach from neighboring cells, increase motility and invasion to intravasate to blood vessels, travel in the circulatory system or the lymph, then extravasate into and colonize a secondary tissue.

Cell motility involves several distinct steps (Lauffenburger and Horwitz, 1996; Ridley *et al*., 2003). Cells initiate migration by polarization of plasma membrane and cytoskeletal components to form membrane protrusions, including lamellipodia and filopodia. Cells then form attachments at their leading edge to stabilize protrusions, primarily through integrin transmembrane receptors which couple the extracellular matrix (ECM) to the actin cytoskeleton on the inside of the cell (Geiger *et al.*, 2001; Wehrle-Haller and Imhof, 2002). Myosin-based contractility is required to translocate the cell

body forward, followed by detachment of adhesions at the rear of the cell (Broussard *et al.*, 2008).

Crucial to a cell's ability to migrate is the organization of plasma membrane and associated proteins in a polarized manner to interact with and respond to their surrounding environment. For many years, the fluid mosaic model, where proteins float in a sea of lipids, was the textbook view of the plasma membrane (Singer and Nicolson, 1972). This view has been challenged by the appreciation of a more ordered phase of the plasma membrane, referred to as lipid rafts, or, more precisely, membrane rafts. Membrane rafts are defined as "small (10-200 nm), heterogeneous, highly dynamic, sterol- and/or sphingolipid-enriched domains that compartmentalize cellular processes. Small rafts can sometimes be stabilized to form larger platforms through protein-protein and protein-lipid interactions" (Pike, 2006). Membrane rafts are distributed asymmetrically during migration in many cell types and may be a mechanism for proper distribution of membrane receptors, including chemosensory receptors and ECM interacting proteins (Gomez-Mouton *et al.*, 2001; Seveau *et al.*, 2001; Manes *et al.*, 2003). These membrane domains serve to organize lipids and proteins for a variety of signal cascades and trafficking events (Simons and Toomre, 2000; Echarri *et al.*, 2007). Additionally, there is a role for the underlying cytoskeleton in organization of membrane domains (Holowka *et al.*, 2000; Viola and Gupta, 2007). Kusumi and colleagues have proposed a picket fence model of membrane organization. Diffusion of membrane proteins and lipids is limited by the membrane skeleton meshwork (fence) as well as

transmembrane proteins anchored to the meshwork (pickets), and proteins and lipids "hop" from one zone to the next (Kusumi *et al.*, 2005).

Formation of ECM contacts also contributes to cell polarity and motility. The most studied cell-ECM contact site, typically found in fibroblasts, is the focal adhesion: large, relatively stable, integrin based adhesion structures located at the ends of stress fiber bundles (Wehrle-Haller and Imhof, 2003; Zaidel-Bar *et al.*, 2004). In addition to focal adhesions, cells interact with the ECM via other actin-rich structures, termed podosomes and invadopodia. Podosomes and invadopodia contain many focal adhesion molecules, but are quite distinct in appearance and function (Block *et al.*, 2008). Although podosomes are similar to invadopodia and the terms are sometimes used interchangeably, the current convention is to refer to structures found in normal cells and in Src-transformed fibroblasts as podosomes, and the structures in tumor cells as invadopodia (Gimona *et al.*, 2008).

Podosomes are highly dynamic structures that come in close contact with the substrate and consist of a core of F-actin surrounded by a ring of adhesion proteins, including integrins, vinculin and talin (**Figure 1-1**) (Linder and Aepfelbacher, 2003). Podosomes have a diameter of ~0.3 μm and a height of ~0.5 μm and are highly dynamic, with a half-life of 2-12 minutes (Destaing *et al.*, 2003; Evans *et al.*, 2003). While some podosomes are formed de novo, many arise from precursor structures (Evans *et al.*, 2003). The actin assembly molecules Arp2/3 and WASp/N-WASp are essential for podosome formation (Linder *et al.*, 1999; Linder *et al.*, 2000). Src kinase activity is a

potent inducer of podosomes (Destaing *et al.*, 2008), and it was in Rous sarcoma virus-transformed fibroblasts that the "peculiar dot-like" podosomes were described early in the field (Marchisio *et al.*, 1987). Very recently, initial events in podosome formation have been examined in Src-transformed fibroblasts (Oikawa *et al.*, 2008), showing that Src activation leads to a rapid increase in the accumulation of phosphoinositide-3,4-bisphosphate ($PI(3,4)P_2$), followed by recruitment of the Src substrate and protease-binding protein Tks5 and the adaptor protein Grb2. Tks5 contains 5 SH3 domains that bind to N-WASp and may thereby contribute to actin polymerization at podosomes.

Podosomes engage in matrix remodeling and tissue invasion and thus are prominent in cell types that cross tissue boundaries, including cells of monocytic lineage (osteoclasts, macrophages and dendritic cells) (Marchisio *et al.*, 1984; Linder *et al.*, 1999; Burns *et al.*, 2001). Podosomes have also been detected after induction with phorbol esters or cytokines in smooth muscle cells and epithelial cells, respectively (Hai *et al.*, 2002; Osiak *et al.*, 2005; Varon *et al.*, 2006). Podosomes function in bone resorption in osteoclasts by adhesion to the bone and subsequent formation of a sealing zone around the resorption pit (Inui *et al.*, 1999; Stenbeck and Horton, 2000; Chabadel *et al.*, 2007). Podosome assembly is blocked in cells from mice deficient in gelsolin, an actin severing and capping protein, and these mice show increased bone mass due to decreased osteoclast function (Chellaiah *et al.*, 2000). The precise function of podosomes in macrophages is less well defined, but podosome deficient macrophages have impaired adhesion and motility (Linder *et al.*, 1999).

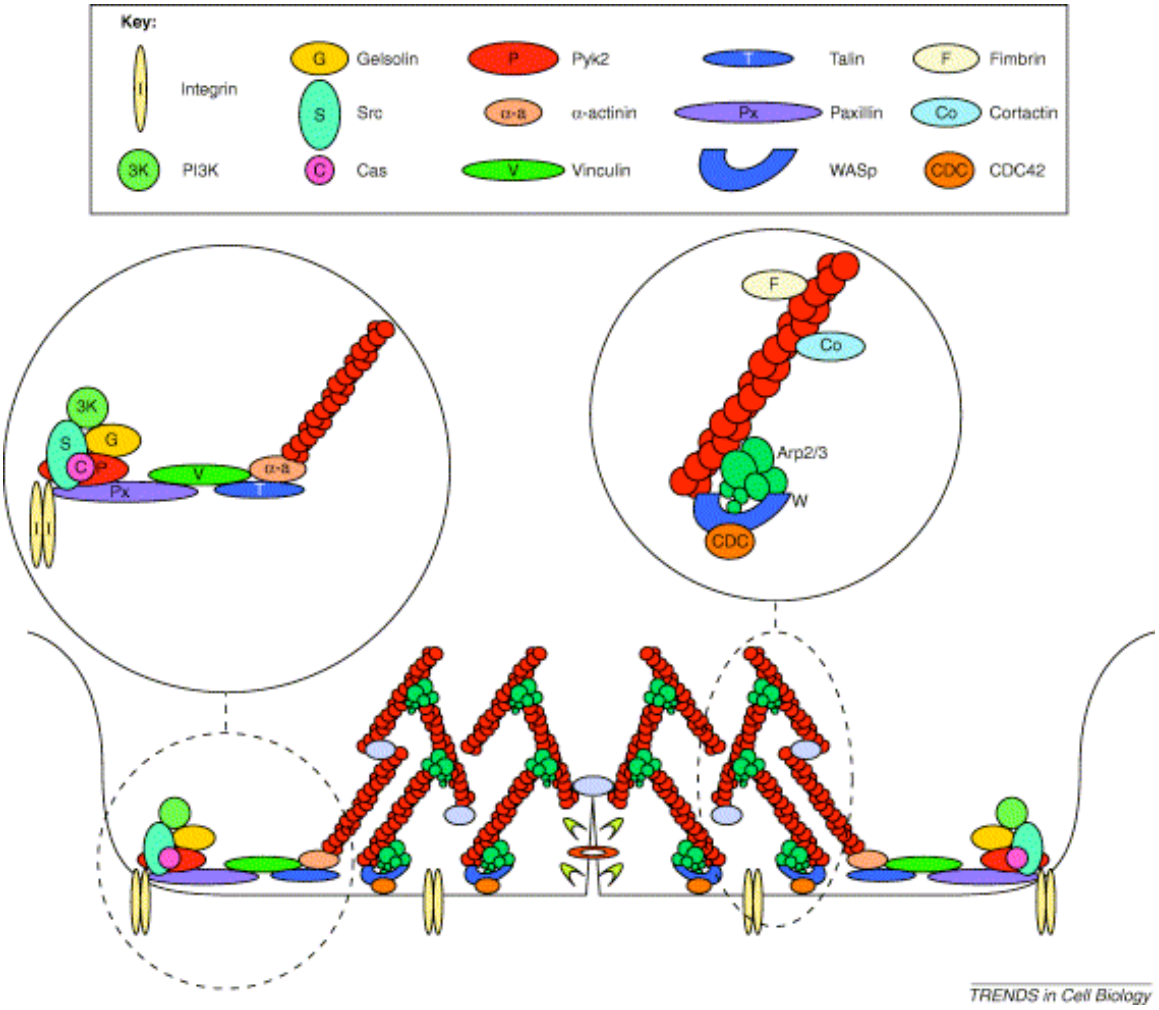


**Figure 1-1.** Model of podosome organization.

Ring structure detail is shown in the upper left panel. Integrins link signaling molecules to the actin core via paxillin, vinculin, talin and alpha-actinin.

The upper right panel shows a detailed view of the podosome core proteins. The podosome core consists of a branched network of actin filaments nucleated by cdc42-activated WASp and Arp2/3. The central core of F-actin filaments surrounds an invagination of the plasma membrane.

Reprinted with permission (Linder and Aepfelbacher, 2003).

Invadopodia are protrusive structures responsible for focalized matrix degradation in invasive cancer cell lines (Chen, 1989; Gimona *et al.*, 2008). Though related to podosomes by the presence of an F-actin core, they do not have such a well-defined, regular ring structure. Instead, invadopodia appear as irregularly shaped F-actin punctae at ventral cell surfaces with associated invaginations and protrusions of the plasma membrane (Baldassarre *et al.*, 2003). Invadopodial structures can be long-lived, some lasting up to 2 hours (Baldassarre *et al.*, 2006; Yamaguchi and Condeelis, 2007). Integrin engagement provides the initial trigger for invadopodia formation, and plays a role in the docking and activation of proteases at these structures (Mueller and Chen, 1991; Nakahara *et al.*, 1998; Mueller *et al.*, 1999; Deryugina *et al.*, 2001). Like podosomes, invadopodia depend on Src kinase activity and branched actin assembly, with essential contributions from N-WASp, cortactin Arp2/3, AMAP1, dynamin 2, and Arf6 (Stylli *et al.*, 2008).

The observation that invadopodia are important mediators of matrix degradation in cultured cells may be extended to a role for such structures in vivo. The presence of invadopodia in various cell lines has been correlated with other measures of metastasis (Coopman *et al.*, 1998). In addition, isolated tumor cells also form invadopodia, showing that they are not artifacts of culture conditions (Clark *et al.*, 2007; Stylli *et al.*, 2008). Advances in intravital imaging have revealed intravasating carcinoma cells with invadopodia-like protrusions that penetrate blood vessel walls (Condeelis and Segall, 2003; Yamaguchi *et al.*, 2005b). A paracrine signaling loop has been proposed for cooperative tumor invasion in which carcinoma cells secrete colony stimulating factor-1

(CSF-1) to promote podosome formation in tumor associated macrophages, and macrophages secrete epidermal growth factor (EGF) to stimulate invadopodia formation (Yamaguchi *et al.*, 2006). Taken together, these data suggest that both podosomes and invadopodial action may be required for cancer cells to break through the basement membrane (**Figure 1-2**) (Yamaguchi *et al.*, 2005b).

Cortactin is necessary for both podosome and invadopodia formation and function (Artym *et al.*, 2006; Webb *et al.*, 2006a; Clark *et al.*, 2007; Webb *et al.*, 2007). Cortactin is a multidomain Src substrate that stimulates Arp2/3 induced actin polymerization and activation of N-WASp (Wu and Parsons, 1993; Uruno *et al.*, 2001; Weaver *et al.*, 2001). ERK phosphorylation of cortactin positively regulates its ability to activate N-WASp in vitro, whereas Src phosphorylation is a negative regulator (Martinez-Quiles *et al.*, 2004). Cortactin promotes cell motility, invadopodia formation and invasion through matrix barriers (Weaver, 2008). Gene amplification at chromosome 11q13, a poor prognostic indicator, frequently results in cortactin overexpression in breast as well as head and neck cancers (Schuuring *et al.*, 1992; Weaver, 2008). Although cortactin is not suspected in tumor initiation, a dominant negative non-phosphorylatable cortactin (Y421, 466, 482F) mutant inhibited bone metastasis in an in vivo mouse model (Li *et al.*, 2001). Thus, cortactin is an important actin regulatory protein involved in invasion, and possibly tumor progression.

In an effort to understand the composition of membrane skeletons in highly motile cells, the Luna laboratory identified supervillin (SV) as an F-actin binding protein in

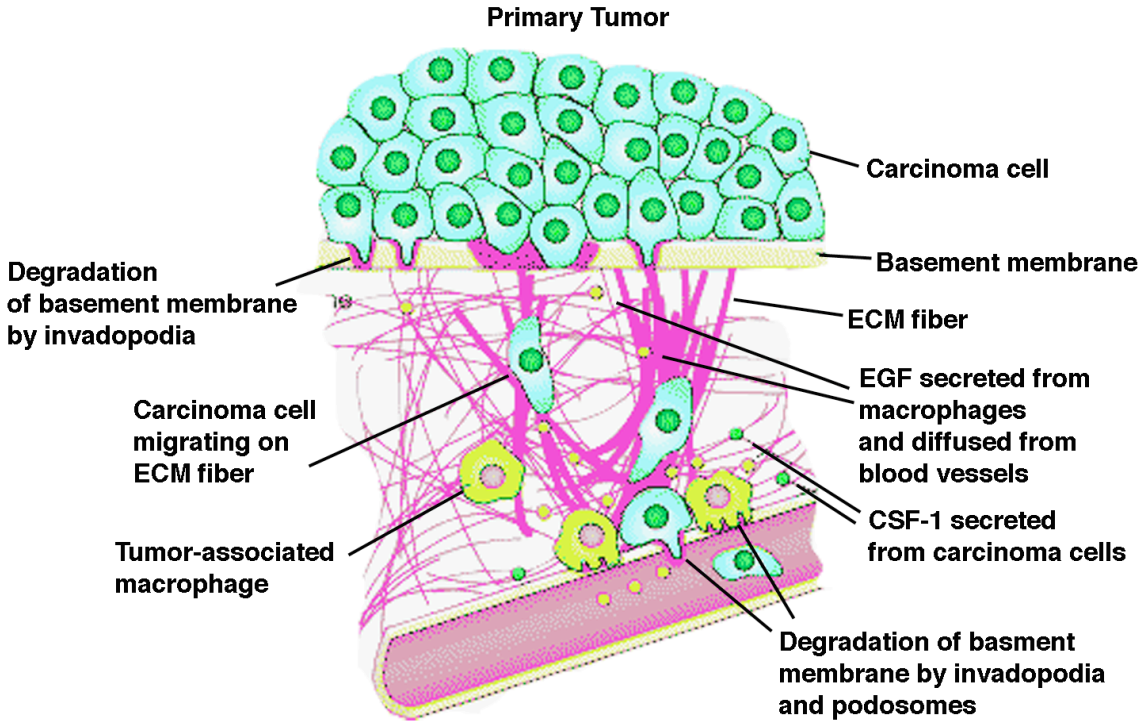


**Figure 1-2.** Model for intravasation of cancer cells.

Migratory carcinoma cells detach from neighboring cells and degrade the basement membrane through invadopodial action. These cells travel along ECM fibers with stimulation from EGF secreted by tumor associated macrophages. The tumor cells secrete CSF-1, thereby stimulating macrophages to form podosomes. This results in cooperative invasion into the bloodstream.

Reprinted with permission (Yamaguchi *et al.*, 2005b).

neutrophils (Pestonjamasp *et al.*, 1995). SV is a tightly bound peripheral membrane protein with a highly conserved C-terminus with homology to the actin-reorganizing proteins villin and gelsolin (Pestonjamasp *et al.*, 1997). Thus, SV derives its name from being one of the largest members of the villin/gelsolin superfamily (Pestonjamasp *et al.*, 1997; Silacci *et al.*, 2004; Khurana and George, 2008). Abundant levels of SV message have been reported in HeLa cervical adenocarcinoma, SW480 colorectal adenocarcinoma, and A549 lung carcinoma cells (Pope *et al.*, 1998). Also, more SV protein is present on immunoblots of whole cell lysates from HeLa cells than in lysates from NIH-3T3 fibroblasts, COS7 cells, or kidney epithelial cell lines (Pestonjamasp *et al.*, 1997). In Madin-Darby bovine kidney (MDBK) epithelial cells, SV localizes in a punctate manner at the membrane and in the cytoplasm in low-density cultures, and to areas of cell-cell contact at higher cell density. In addition, co-localization with the cell-cell adhesion protein E-cadherin increased upon transition to a more confluent culture (Pestonjamasp *et al.*, 1997).

Biochemical purifications and domain analysis of SV has identified many binding partners. An initial surprise resulted in the demonstration that the F-actin binding motif resides in the novel SV N-terminus, not as expected in the villin/gelsolin homologous sequences. (Wulfkuhle *et al.*, 1999) This study also revealed functional nuclear targeting domains in the center of the protein (SV-830-1009) (Wulfkuhle *et al.*, 1999). Finer mapping of the SV N-terminus identified at least three F-actin binding sites, as well as binding sites for nonmuscle myosin II, the long form of myosin light chain kinase (L-MLCK) and thyroid receptor-interacting protein 6 (TRIP6), a LIM-domain containing

focal adhesion protein (Chen *et al.*, 2003; Takizawa *et al.*, 2006; Takizawa *et al.*, 2007). SV also co-purifies with a detergent resistant membrane fraction, called DRM-H, that contains ~23 neutrophil plasma membrane proteins (Nebl *et al.*, 2002). DRM-H is rich in cytoskeletal proteins, including fodrin, actin and myosins IG and II, in addition to membrane raft organizing proteins and signaling molecules. Taken together, these interactions point to a role for SV in integrating membrane-cytoskeleton signaling events.

In fact, SV has dramatic effects on the organization of the actin cytoskeleton and on focal adhesions (Wulfkuhle *et al.*, 1999; Takizawa *et al.*, 2006; Takizawa *et al.*, 2007). Overexpression of EGFP-SV in COS7-2 cells induces a change in the distribution of intracellular F-actin (Wulfkuhle *et al.*, 1999), along with decreases in the numbers of stress fibers and large focal adhesions (Takizawa *et al.*, 2006). There is an inverse correlation of SV levels and strength of adhesion to fibronectin-coated surfaces; SV overexpression decreases adhesion, whereas RNAi-mediated knockdown of SV increases adhesion (Takizawa *et al.*, 2006). A similar relationship exists regarding cell spreading. SV downregulation increases the rate of cell spreading and overexpression of SV slows spreading rates by upregulating myosin II activation at the plasma membrane (Takizawa *et al.*, 2007). An alternatively spliced form of SV, archvillin, found in skeletal muscle is involved in the organization of muscle costameres, and myogenic differentiation (Oh *et al.*, 2003). Smooth muscle archvillin (SmAV) is required for extracellular-signal-regulated kinase (ERK1/2) activation and stimulus-mediated contractility (Gangopadhyay *et al.*, 2004). Thus, SV is an interesting, multifunctional molecule that serves as a scaffold for membrane-cytoskeleton signaling.

**Objective of dissertation studies**

The goal of my thesis research was to unravel the cellular functions of SV, an actin-binding membrane protein. In Chapter II, I will show that SV reorganizes the actin cytoskeleton into dynamic, punctate structures that have characteristics of podosomes and invadopodia. Endogenous SV localizes to both Src-induced podosomes and invadopodia. Moreover, SV is important for the function of invadopodia in MDA-MB-231 cells, in which overexpression increases, and RNAi-mediated knockdown decreases, matrix degradation. SV, in conjunction with the related protein, gelsolin, contributes to Matrigel$^{TM}$ invasion. Chapter III investigates a SV-cytoskeleton-membrane raft complex, DRM-H, in COS-7 cells. Based on the finding that both ERα and ERβ fractionate with SV in DRM-H, a role for DRM-H is proposed in nongenomic estrogen signaling.

# Chapter II

## Supervillin Reorganizes the Actin Cytoskeleton and Increases Invadopodial Efficiency

## Abstract

Tumor cells use actin-rich protrusions called invadopodia to degrade extracellular matrix (ECM) and invade tissues; related structures, termed podosomes, are sites of dynamic ECM interaction. We show here that supervillin (SV), a peripheral membrane protein that binds F-actin and myosin II, reorganizes the actin cytoskeleton and potentiates invadopodial function. Overexpressed SV induces redistribution of lamellipodial cortactin and lamellipodin/RAPH1/PREL1 away from the cell periphery to internal sites and concomitantly increases the numbers of F-actin punctae. Most punctae are highly dynamic and co-localize with the podosome/invadopodial proteins, cortactin, Tks5, and cdc42. Cortactin binds SV sequences in vitro and contributes to the formation of EGFP-SV induced punctae. SV localizes to the cores of Src-generated podosomes in COS-7 cells and with invadopodia in MDA-MB-231 cells. EGFP-SV overexpression increases average numbers of ECM holes per cell; RNAi-mediated knockdown of SV decreases these numbers. While SV knockdown alone has no effect, simultaneous down-regulation of SV and the closely related protein, gelsolin, reduces invasion through ECM. Taken together, our results show that SV is a component of podosomes and invadopodia and that SV plays a role in invadopodial function, perhaps as a mediator of cortactin localization, activation state, and/or dynamics of MMPs at the ventral cell surface.

## Introduction

During metastasis, tumor cells invade the surrounding extracellular matrix (ECM), migrate into the bloodstream, and traverse endothelial barriers at secondary sites in distant organs (Condeelis *et al.*, 2005). ECM degradation, in vitro, involves specialized membrane-associated F-actin structures known as podosomes and invadopodia (Weaver, 2006; Linder, 2007; Gimona *et al.*, 2008; Machesky *et al.*, 2008). Podosomes are endogenously found in cell types that cross tissue boundaries or are involved in tissue remodeling, e.g. leukocytes and osteoclasts, respectively (Gimona *et al.*, 2008). Although podosomes contain many focal adhesion proteins and may mediate dynamic cell-ECM attachments, they are distinguishable from focal adhesions, which are ECM- and integrin-associated complexes that promote cell migration in fibroblasts (Zaidel-Bar *et al.*, 2004; Evans and Matsudaira, 2006; Lo, 2006; Romer *et al.*, 2006; Spinardi and Marchisio, 2006; Block *et al.*, 2008; Broussard *et al.*, 2008). Podosomes also turn over much faster than do focal adhesions and contain cores of actin filaments that are surrounded by rings of vinculin and other focal adhesion proteins (Gavazzi *et al.*, 1989; Ochoa *et al.*, 2000; Destaing *et al.*, 2003; Evans and Matsudaira, 2006). Electron micrographs of podosomes in Rous sarcoma virus-transformed fibroblasts show that the dense microfilamentous material in the core surrounds a central invaginating membrane tubule (Nitsch *et al.*, 1989; Ochoa *et al.*, 2000). Invadopodia mediate ECM degradation, are larger and longer-lived than podosomes, and are characterized by surface protrusions and large membrane invaginations (Chen and Wang, 1999; Baldassarre *et al.*, 2003; Yamaguchi and Condeelis, 2007; Stylli *et al.*, 2008).

Recent studies indicate many functional and compositional similarities between podosomes and invadopodia. Both these structures have been associated with secretion of matrix metalloproteinases (MMPs) and endocytosis of degraded matrix components (Ochoa *et al.*, 2000; Baldassarre *et al.*, 2003; Clark and Weaver, 2008). Also, both structures contain several proteins in common—including cortactin, Tks5/FISH, and Cdc42—in addition to many proteins also found at focal adhesions (Seals *et al.*, 2005; Linder, 2007; Yamaguchi and Condeelis, 2007; Block *et al.*, 2008). Current nomenclature is to use the term "invadopodia" for invasive structures in tumor cells and to use "podosome" for the invasive/adhesive structures in transformed fibroblasts and in cells—such as leukocytes, osteoclasts, endothelial and smooth muscle cells—with endogenous or inducible podosomes (Gimona *et al.*, 2008). However, vascular smooth muscle cells invade ECM, and tumor cells contain podosome-like, dynamic "pre-invadopodial complexes" with short lifetimes that mature into longer-lived invadopodia (Yamaguchi *et al.*, 2005a; Furmaniak-Kazmierczak *et al.*, 2007). In addition, invadopodium formation involves sequential stages of cortactin recruitment to membranes, MT1-MMP accumulation, matrix degradation, and cortactin dissociation (Artym *et al.*, 2006). Thus, the distinction between "podosomes" and "invadopodia" may be as much temporal as compositional, i.e. invasion structures may arise from more dynamic podosome-like precursors in both normal tissues and tumors (Linder and Aepfelbacher, 2003; Gimona *et al.*, 2008). Here, we use the current nomenclature for podosomes and invadopodia and refer to undefined structures as "actin punctae".

Supervillin (SV) is one of the largest members of the villin/gelsolin family of actin-organizing proteins, which have both overlapping and distinct functions (Silacci *et al.*, 2004; Archer *et al.*, 2005; Khurana and George, 2008). Villin is associated with pre-cancerous morphological changes in epithelia, and gelsolin is required for the formation and degradative activity of osteoclast podosomes; gelsolin also promotes cancer cell invasion and motility (MacLennan *et al.*, 1999; Chellaiah *et al.*, 2000; De Corte *et al.*, 2002; Rieder *et al.*, 2005; Van den Abbeele *et al.*, 2007). Nonmuscle SV co-purifies from neutrophil plasma membranes as a component of a lipid raft-like complex that also includes heterotrimeric G proteins, Src family kinases and membrane type 6 MMP (MT6-MMP) (Nebl *et al.*, 2002), all of which are involved in tumorigenesis and matrix degradation (Mareel and Leroy, 2003; Ingley, 2008; Sohail *et al.*, 2008). A smooth muscle isoform of SV, called SmAV, localizes to phorbol ester-induced podosomes in A7r5 cells with F-actin, nonmuscle myosin IIB, and extracellular-signal-regulated kinases (ERK1/2) (Gangopadhyay *et al.*, 2004). SmAV is required for normal ERK1/2 activation downstream of phenylephrine signaling in ferret aorta (Gangopadhyay *et al.*, 2004), but the functionality of SV isoforms in the formation of podosome-like structures has not been explored.

Based on its biochemical characteristics, SV is well positioned for a role in mediating alterations in the actin cytoskeleton at membranes. SV co-fractionates with membranes and binds very tightly to the membrane bilayer, resisting extraction with buffered solutions at pH <12 (Pestonjamasp *et al.*, 1997; Nebl *et al.*, 2002; Oh *et al.*,

2003). One site of membrane attachment is associated with SV amino acids 342-571 (SV342-571), which interact with the LIM domains of the focal adhesion proteins, thyroid receptor-interacting protein 6/zyxin-related protein 1 (TRIP6/ZRP1) and lipoma-preferred partner (LPP) (Takizawa *et al.*, 2006). SV also binds avidly to F-actin at three sites through which it can either bundle or crosslink actin filaments; to nonmuscle myosins IIA and IIB; to the long isoform of myosin light chain kinase (L-MLCK); and to calponin (Chen *et al.*, 2003; Takizawa *et al.*, 2007), a negative regulator of podosome formation in smooth muscle cells (Gimona *et al.*, 2003).

SV potentiates a process that negatively regulates focal adhesion function. Overexpressed SV decreases cell adhesion to fibronectin, whereas RNAi-mediated SV down-regulation increases cell attachment (Takizawa *et al.*, 2006). Sequences within the SV N-terminus (SV1-171) disrupt stress fibers by inducing apparent hypercontractility of myosin II (Takizawa *et al.*, 2006; Takizawa *et al.*, 2007). Another SV sequence (SV342-571) counteracts stress fiber and large focal adhesion formation or stability through the interaction with TRIP6 (Takizawa *et al.*, 2006). However, phalloidin staining of cytoplasmic F-actin is observed even after disruption of stress fibers in cells expressing elevated levels of SV or SV342-571 (Wulfkuhle *et al.*, 1999; Takizawa *et al.*, 2006). The nature of these phalloidin-stained structures has never been explored.

The mechanism by which SV and TRIP6 regulate adhesion also is imperfectly understood. Most investigations have focused on the roles of these proteins in "inside-

out" signaling through other proteins on the cytoplasmic sides of focal adhesions (Yi *et al.*, 2002; Lai *et al.*, 2005; Bai *et al.*, 2007; Lai *et al.*, 2007; Takizawa *et al.*, 2007). An alternative, non-mutually exclusive hypothesis, tested in this study, is that SV induces the loss of focal adhesion function by promoting the formation of podosomes, invadopodia, and ECM degradation.

## Materials and Methods

### Antibodies, reagents, and constructs

Mouse monoclonal anti-vinculin (hVIN1) and anti-gelsolin (Clone GS-2C4) antibodies were from Sigma (St. Louis MO), as was affinity-isolated rabbit anti-HA tag. Mouse monoclonal anti-cortactin (4F11) and anti-actin (clone C4) antibodies were from Millipore Corporation (Bedford, MA). Mouse monoclonal anti-phosphotyrosine (pTyr-100) and anti-myc (71D10) antibodies were from Cell Signaling Technology (Danvers, MA). Mouse monoclonal anti-phosphoFAK (pY397) antibody was from BD Transduction Laboratories (Franklin Lakes, NJ). AlexaFluor 488- and 568-conjugated secondary antibodies against rabbit and mouse IgGs, and fluorescein- and Texas red-conjugated phalloidin were from Invitrogen (Carlsbad, CA) and used at 1:2000 dilution. Affinity-purified rabbit polyclonal antibodies against SV (H340) and lamellipodin (3917) have been described (Nebl *et al.*, 2002; Oh *et al.*, 2003).

EGFP-C1 and EGFP-SV vectors were described previously (Wulfkuhle *et al.*, 1999). An untagged version of bovine SV was made by cloning the full-length SV cDNA into the KpnI and XbaI sites of pTracer-CMV (Invitrogen) (Wulfkuhle *et al.*, 1999). His-tagged cortactin(ΔSH3, aa 1-506) was generated from pdsRed-cortactin (gifted by Dr. Alan S. Mak, Queen's University, Kingston, Canada) (Webb *et al.*, 2006a) after digestion with BglII and cloning into pET30a vector (Invitrogen). Y527F-Src was from the Harold Varmus laboratory (NIH, Bethesda, Maryland). Myc-tagged Tks5 (myc-Tks5) (Lock *et al.*, 1998) and HA-tagged Cdc42 (Shinjo *et al.*, 1990) (HA-Cdc42), both

in the pEF-BOS expression vector (Mizushima and Nagata, 1990), were kind gifts from Drs. Sara Courtneidge (Scripps Research Institute, La Jolla, CA) and Dr. Kozo Kaibuchi (Nagoya University, Nagoya, Japan), respectively. EGFP-MT1-MMP was from Dr. Maria C. Montoya (Spanish Nacional Cancer Research Center (CNIO), Madrid, Spain) (Galvez *et al.*, 2002; Bravo-Cordero *et al.*, 2007).

**Immunoblotting**

Whole cell lysates were prepared in 1% SDS, PBS, 1 mM PMSF, and a protease inhibitor cocktail containing: 1 mg/ml aprotinin, 1 mM antipain, 2 mM ALLM (calpain inhibitor II), 1 mM benzamidine, 10 mME64, 1 mM leupeptin, and 1 mM pepstatin A. For each sample, 40 or 50 mg of protein, as determined by BCA Protein Assay (Pierce, Rockford, Il), were run on SDS-polyacrylamide gels (Laemmli, 1970), transferred to nitrocellulose membranes (Towbin *et al.*, 1979), and probed with primary antibodies against supervillin (0.2 – 0.4 μg/ml) and gelsolin (1:5000); β-actin (1:5000 antibody dilution) was used as a loading control. HRP-conjugated goat anti-mouse or goat anti-rabbit secondary antibodies (Jackson Laboratories, West Grove, PA), diluted 1:20,000, were detected by Pierce SuperSignal WestPico chemiluminescence. Band densities were determined using ImageJ (Rasband, W.S., U. S. National Institutes of Health, Bethesda, Maryland, http://rsb.info.nih.gov/ij/). EGFP-SV expression levels were determined by comparing band intensities with endogenous SV and correcting for transfection efficiency.

**Cell culture and transfection**

COS7-2 cells, a highly transfectable clone of COS-7 (Kowalczyk *et al.*, 1997), were a generous gift from Dr. Kathleen J. Green (Northwestern University, IL). COS-7 cells were grown in Dulbecco's modified Eagle high glucose media (DMEM, Invitrogen, GIBCO #11995) supplemented with 10% fetal calf serum (FCS) for 20 passages. MDA-MB-231 breast carcinoma cells were obtained from ATCC (American Type Culture Collection, Rockville, MD) and from the Tissue Culture Shared Resource of the Lombardi Cancer Center, courtesy of Dr. Susette Mueller (Georgetown University, DC). G418-resistant MDA-MB-231 cells that stably overexpress wild-type c-Src (MDA-MB-231/WT Src cells) were a kind gift from Dr. Toshiyuki Yoneda (U. Texas Health Science Center, San Antonio) and Dr. Mueller (Myoui *et al.*, 2003; Bowden *et al.*, 2006). MDA-MB-231 cells without (ATCC) and with WT c-Src overexpression were grown in DMEM supplemented with 10% FCS and 2 mM L-glutamine (Invitrogen, GIBCO 25030). Cultured cells for immunoblots were generously supplied by Drs. Greenfield Sluder (primary human foreskin fibroblasts and hTERT-RPE1, Clontech), Lucia Languino (LNCaP), K.C. Balaji (LNCaP, C4-2, DU-145), and Arthur Mercurio (MCF10A series).

Transfection methods have been described (Takizawa *et al.*, 2006). Briefly, for plasmids, COS-7 cells were transfected using Effectene Transfection Reagent (Qiagen Inc.) for 24 hours with the Y527F-Src, HA-Cdc42, and myc-Tks5 plasmids or for 24 or 48 hours with the EGFP-SV plasmid. For siRNAs, COS-7 cells were transfected with Lipofectamine 2000 (Invitrogen). MDA-MB-231/WT Src cells were transfected using the Nucleofector system (Amaxa, Inc. Gaithersburg, MD), according to manufacturer's

instructions. Briefly, for each Nucleofection, 1 x $10^6$ adherent cells were trypsinized, rinsed with Dulbecco's PBS, modified (D-PBS, Invitrogen, GIBCO #14190), resuspended with 100 µl solution V and with either 40 nM Stealth siRNA or 2 µg plasmid, and treated using program X13. Cells treated with siRNA were incubated for 4 days prior to experiments, whereas cells treated with plasmid were incubated for 2 days.

The dsRNAs targeting COS-7 cell SV have been described (Takizawa *et al.*, 2007). Two dsRNAs targeting human SV were made as Stealth duplexes (Invitrogen): human (h)SV1, 5'-CAGCCAUAAGGAAUCUAAAUAUGCU-3' (coding nucleotides 1680-1704) and hSV2, 5'-GCGAUGUUUGCUGCUGGAGAGAUCA-3' (coding nucleotides 2026-2050). The Stealth duplex sequence, 5'-GAACUAUGAAGGACCACCAGAGAUA-3', was used as a control dsRNA. A dsRNA targeting human gelsolin was also made as a Stealth Duplex with the sequence 5'-CAGTTCTATGGAGGCGACAGCTACA-3' (coding nucleotides 1460-1484). Two dsRNAs targeting primate cortactins were made as Stealth duplexes: CT1 5' UCUUGUUCCACACCAAAUUUCCCUC 3' and CT2 5' GAGGGAAAUUUGGUGUGGAACAAGA 3'.

**Recombinant protein purification and in vitro pulldown assay**

GST-SV fusion fragment proteins were expressed after IPTG induction in BL21(DE3)pLysS cells and purified with glutathione-Sepharose™ as previously described (Chen *et al.*, 2003). His-cortactin(ΔSH3) was expressed after induction by IPTG and purified by using Ni-NTA Agarose (Qiagen Inc., Valencia, CA). Eluted

proteins were dialyzed in dialysis buffer (50mM Tris pH 8.0, 150 mM NaCl, 1mM DTT, 10% glycerol). Dialyzed proteins were frozen quickly in liquid nitrogen and stored at -80ºC.

Purified GST-SV fragments were mixed with His-cortactin(ΔSH3) in binding buffer (50 mM Tris pH 8.0, 300 mM NaCl, 1% Triton X-100, 1 mM DTT, 10% glycerol, 1 mM PMSF and protease inhibitor cocktail) and incubated with glutathione-Sepharose™ beads for 1 hour at 4ºC with shaking. The mixtures were then washed five times with binding buffer followed by centrifugation at 3000 rpm for 2 min. Beads were resuspended in 2X SDS sample buffer and heated to 95ºC for 5 minutes. Proteins were separated by SDS-PAGE, and transferred to a nitrocellulose membrane. His-cortactin(ΔSH3) was identified by immunoblotting with monoclonal anti-His antibody (clone 27E8, Cell Signaling Technology).

**Live cell imaging**

COS-7 cells transfected with EGFP-SV were cultured on 22 mm square coverslips and sealed into chambers with DMEM, 10% FCS, 10 mM HEPES, without phenol red. After temperature equilibration in a Plexiglass environmental chamber heated to 37°C, images focused on the ventral cell surface were acquired for EGFP, using an HCX PL Apo, 63X, 1.32 NA, oil immersion objective lens on a DMIRE 2 inverted microscope (Leica Microsystems, Allendale, NJ), a Retiga Exi cooled CCD camera (QImaging Corp., Burnsby BC, Canada), and OpenLab 3.5.2 software (Improvision, Waltham, MA). Images were processed with OpenLab to enhance contrast and to

generate movie files. Labels and movie titles were added with Adobe Photoshop (Adobe Systems Inc., San Jose, CA) and QuickTime Pro (Apple, Cupertino, CA).

**Immunofluorescence**

Cells were fixed for 10 minutes with 4% paraformaldehyde in PBS, and permeabilized for 5 minutes with 0.2% Triton X-100 in PBS before blocking for 30 minutes with 1% BSA, 0.5% Tween-20 in PBS and immunostaining. Depending on the experiment, cells were stained for cortactin (1:200 dilution), phosphotyrosine (pTyr, 1:100), myc (1:200), HA (1:100), vinculin (1:200), phosphorylated FAK 397 (pFAK; 1:100), α-actinin (1:200) and/or anti-SV (1:200). F-actin was visualized with phalloidin conjugated to Texas Red or fluorescein (Invitrogen). Slides were analyzed with a 40X or 100X Plan-NeoFluor oil immersion objective (NA 1.3) on a Zeiss Axioskop fluorescence microscope, a RETIGA 1300 CCD camera (QImaging), and OpenLab 3.5.2 software. Images were adjusted for contrast and brightness, and merged images were assembled using Adobe Photoshop software. For Z-series, images were acquired with a 100X HCX PLAN APO objective lens (NA 1.35) using step sizes of 0.2 μm on a DM IRE 2 inverted Leica microscope (Leica Microsystems, Bannockburn, IL) with a Retiga Exi cooled CCD camera (QImaging) and OpenLab software. Images were deconvolved using Volocity software (Improvision). Z-series also were obtained with a 100X Plan Apo objective lens (NA 1.4) using a Solamere CSU10 spinning disk confocal microscope (Solamere Technical Group, Salt Lake City, UT) on a Nikon Eclipse TE-2000 microscope (Nikon Instruments Inc., Melville, NY) and a Roper Scientific Cool-Snap HQ2 camera (Photometrics, Tucson, AZ).

**Gelatin-coated coverslips**

The preparation of fluorescently labeled gelatin coated coverslips was carried out as described (Bowden *et al.*, 2001). Briefly, 2.5% gelatin, 225 bloom (Sigma, type B) was conjugated with tetramethylrhodamine-5(and-6)-isothiocyanate (TRITC, Invitrogen T-490), dialyzed extensively to remove unbound dye, and stored in PBS with 2% sucrose. TRITC-gelatin (200 μL) was heated to 45˚C and spread on ethanol-cleaned coverslips (22 mm square). Excess gelatin was removed, and coverslips were inverted onto chilled 0.5% glutaraldehyde in PBS for 15 minutes. Coverslips were then washed with PBS, and unreacted aldehyde groups were quenched with 5 mg/ml sodium borohydride for 5-10 minutes. After washing with PBS, coverslips were then sterilized briefly with 70% ethanol and incubated at 37˚C in serum-free DMEM for one hour prior to plating cells. Cells in complete DMEM then were incubated for 6 hours on the gelatin and fixed with 4% paraformaldehyde, as described above.

**Matrigel invasion assays**

Cell invasion assays were performed using BioCoat™ Matrigel™ Invasion Chambers (BD Biosciences, Franklin Lakes, NJ, No. 354480), according to the manufacturer's instructions. Briefly, ~5 x $10^4$ siRNA-treated MDA-MB-231/WT Src cells in serum-free DMEM were added to the upper wells of invasion chambers that contained DMEM with 10% serum in the bottom wells. Cells were allowed to migrate for 20 hours, when cells remaining on the upper side of the filter were removed with moistened cotton swabs. Migrated cells were fixed and stained with the HEMA 3® Stain Set (Fisher Scientific, Kalamazoo, MI). Five representative images were taken from each

insert with 10X magnification. Cells from the Matrigel inserts were counted using the Cell Counter plugin for ImageJ. Cells from control inserts were counted using the Analyze Particles command in ImageJ after using the Threshold and Watershed commands to identify individual cells. Invasion indices were determined as ratios of cells migrating in the presence *vs.* absence of Matrigel™ to control for changes in cell motility and by normalizing experimental invasion indices against the mean value obtained for cells treated with control siRNA.

**FACS analyses**

The total amounts of cortactin in COS-7 cells expressing EGFP or EGFP-SV were assayed after lifting 1 x $10^6$ cells from plates with 0.1% trypsin, 0.4 mg/ml EDTA. The cells were washed twice with PBS and fixed with 2% paraformaldehyde in PBS for 20 min at room temperature with rotation in a 1.5-ml tube. Fixed cells were washed once and made permeable with 0.1% Triton X-100 in PBS for 5 min at room temperature with rotation. After blocking for 30 minutes with sterile-filtered 4% FBS, 0.05% sodium azide, PBS, the cells were incubated for another 30 minutes on ice in blocking buffer containing either 0.67 μg/ml mouse anti-cortactin antibody or control mouse IgG1 (Leinco Technologies, St. Louis, MO). Cells were washed three times with blocking buffer and then incubated for 15 min on ice with secondary antibody, AlexaFluor647-conjugated goat anti-mouse IgG F($ab_2$) (Invitrogen, 1:5000). The cells were washed three times with blocking buffer and resuspended into 0.5 ml of PBS containing 0.5% BSA in Falcon tubes for FACS analysis.

**Statistical Analyses**

Statistical significance was assessed using InStat 3 for Macintosh (GraphPad Software, Inc., La Jolla, CA). Unless otherwise stated, two-tailed p values were determined by one-way ANOVA with a Tukey-Kramer or Student-Newman-Keuls multiple comparisons post test. As noted in figure legends, some pairs of groups also were compared using unpaired t tests.

## Results

### *SV Promotes Restructuring of the Actin Cytoskeleton.*

**SV overexpression increases F-actin punctae.** Increased levels of SV decrease the numbers of COS-7 cells containing stress fibers (Takizawa *et al.*, 2006). As compared with overexpressed EGFP alone (**Figure 2-1A, panels a-c**), overexpression of either EGFP-tagged SV (EGFP-SV) **(Figure 2-1A, panels d-f)** or untagged SV (**Figure 2-1A, panels g-i**) increases the numbers of F-actin punctae (**Figure 2-1A, panels e, h *vs.* b, insets**). These punctae, which are ~0.5 μm in diameter, can be either round or irregularly shaped. They are prominent at the ventral surfaces of cells expressing EGFP-SV but are also found near nuclei, especially in EGFP-expressing control cells (**Figure 2-2**). In wide-field fluorescence (**Figure 2-1A**), the mean numbers of ventral F-actin punctae in cells expressing EGFP-SV (**Figure 2-1B**) or untagged SV (**Figure 2-1C**) increase ~7-fold, as compared with mock-transfected cells or cells expressing only EGFP, indicating specificity for SV sequences. The increase in ventral F-actin punctae in EGFP-SV transfected cells was not due solely to protein expression levels because even with very high expression of EGFP, the number of these punctae does not increase to levels seen with EGFP-SV (**Figure 2-1D**). This increase in ventral F-actin punctae is apparently a gain of function because RNAi-mediated reduction of endogenous SV to ~20 ± 5% of normal levels does not significantly reduce the low background numbers of F-actin punctae in COS-7 cells (not shown).

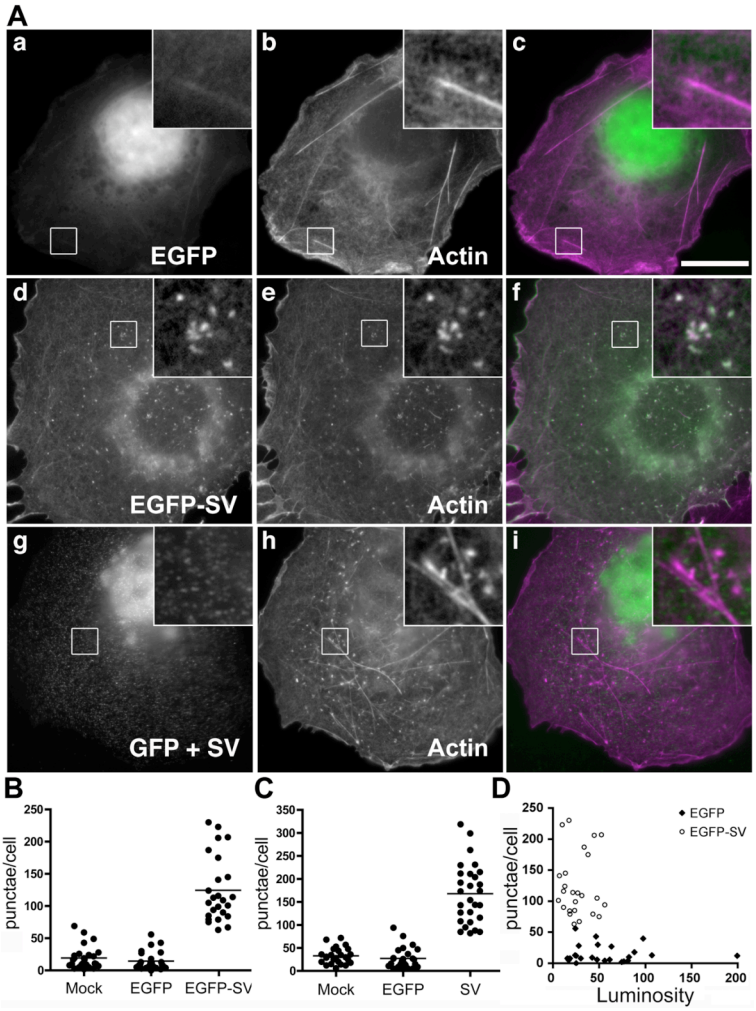


**Figure 2-1.** Overexpression of EGFP-SV in COS-7 cells increases the numbers of cytoplasmic F-actin punctae.

**(A)** COS-7 cells were transfected for 48 hours with vectors encoding EGFP (a-c), EGFP-SV (d-f), or GFP plus untagged supervillin (g-i). Cells were fixed and stained for F-actin using Texas Red phalloidin (b, e, h). Bar, 20 µm. Insets enlarged 4 fold. Overlap in white.

**(B, C)** F-actin punctae were counted in untransfected cells after a mock treatment with transfection agent alone, or in cells expressing EGFP, EGFP-SV, or GFP as a marker for untagged SV. Distributions of individual counts and their means are shown. Both EGFP-SV and untagged SV differed from controls, $p \leq 0.001$, $n = 25 – 28$/group.

**(D)** The relative amounts of EGFP (closed symbols) or EGFP-SV (open symbols) in individual cells were estimated from total luminosities of wide-field microscopic images. The plot shows the number of F-actin punctae per cell vs. luminosity. EGFP-SV expression levels were 12.5 ± 0.7 (mean ± s.d., n=3) times that of endogenous SV. At these expression levels, no significant trend was detected for either data set.

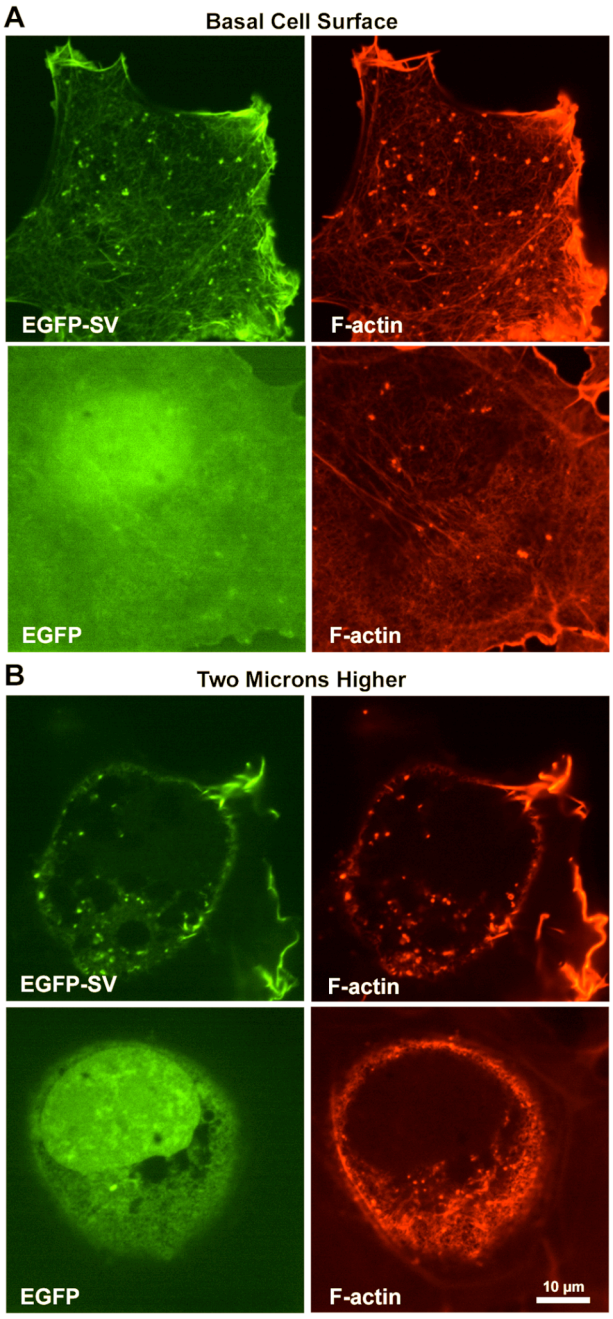


**Figure 2-2.** Confocal images of F-actin punctae at (**A**) basal surfaces and (**B**) 2 µm higher sections of COS-7 cells expressing EGFP-SV or EGFP alone. Bar, 10 µm.

**Most EGFP-SV punctae are dynamic, but these structures are probably heterogeneous in nature.** In live cell imaging, ~94% of the EGFP-SV punctae in the cell periphery were highly dynamic and short-lived (**Figure 2-3; Video 1, available at** http://www.molbiolcell.org/content/vol0/issue2008/images/data/E08-08-0867/DC1/Smov1.mov). Although occasional movements of ~1.0 μm/sec were seen, the instantaneous velocities of these punctae averaged 0.36 ± 0.05 μm/sec (mean ± s.e.m., n = 19) over their lifetimes of 2.9 ± 0.3 min (mean ± s.e.m., n = 93) (**Figure 2-3A, 2-2B**). These dynamic short-lived punctae moved both towards and away from the cell periphery (**Figure 2-3A, arrowheads; Video 1**). The ~6% of the EGFP-SV punctae that were longer lived exhibited lifetimes of at least 30.5 ± 1.6 min (mean ± s.e.m., n = 6) (**Figure 2-3B**) and were largely restricted in localization (**Figure 2-3C**), with signal intensities that could vary over time (**Figure 2-3A, double arrows**). Other longer-lived punctae tumbled in place, as though they might be associated with larger, vesicular structures and exhibited sporadic, rapid movements (**Figure 2-3A, arrow; Figure 2-3C**). The mean instantaneous velocity of EGFP-SV punctae is most consistent with directional movements propelled by kinesins (~0.5 μm/sec), but the variable directionalities and the range of observed velocities suggest the possibility of multiple propulsion mechanisms, including actin comet tails (~0.17 μm/sec), myosin Vb (0.22 μm/sec), and dynein (~0.9 μm/sec) (Porter *et al.*, 1987; Woehlke *et al.*, 1997; Benesch *et al.*, 2002; Toba and Toyoshima, 2004; Paluch *et al.*, 2006; Watanabe *et al.*, 2006).

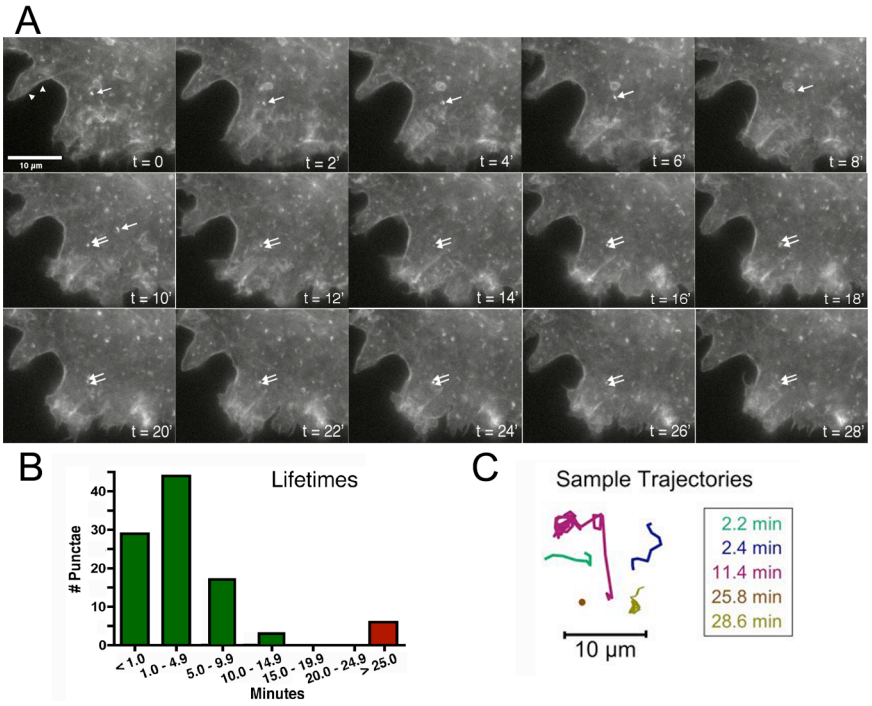


**Figure 2-3**. Most EGFP-SV punctae are dynamic and short lived; a few are longer lived and relatively stable.

**(A)** Time lapse sequence of EGFP-SV punctae in COS-7 cells on glass coverslips. Images were taken every 12 seconds for 60 min. Bar, 10 µm. Examples of short-lived (arrowheads) and long-lived (arrows) punctae are indicated.

**(B)** Distribution of individual punctae lifetimes; n = 99.

**(C)** Sample trajectories of EGFP-SV punctae with associated lifetimes.

**EGFP-SV punctae contain podosome markers, but not focal adhesion proteins.** The lifetimes and dynamic behavior of most EGFP-SV punctae are reminiscent of podosomes or invadopodial precursors (Yamaguchi *et al.*, 2005a; Evans and Matsudaira, 2006). While the localization of some punctae above the ventral cell surface (**Figure 2-2**) argues against a 1:1 identity with podosomes, most ventral EGFP-SV punctae do co-localize with podosome/invadopodial proteins (**Figure 2-4**). For instance, ~91% of the EGFP-SV punctae co-localize with endogenous cortactin (**Figure 2-4A-C, boxes**), a protein required for the formation and function of invadopodia (Bowden *et al.*, 1999; Artym *et al.*, 2006; Clark *et al.*, 2007; Ayala *et al.*, 2008; Clark and Weaver, 2008). Also, ~75% and ~50%, respectively, of the EGFP-SV punctae associate with co-expressed myc-Tks5/FISH (**Figure 2-4D-F**) and HA-Cdc42 (**Figure 2-4G-I**), other proteins important for invadopodial function (Nakahara *et al.*, 2003; Courtneidge *et al.*, 2005; Yamaguchi *et al.*, 2005a). About 27% of the EGFP-SV punctae contain endogenous phosphotyrosine (**Figure 2-4J-L**), a marker for invadopodia, tyrosine kinase-associated intracellular vesicles, and focal adhesions (Zamir *et al.*, 1999; Bowden *et al.*, 2006; Sandilands and Frame, 2008). By contrast, only ~3% or ~5%, respectively, of the EGFP-SV punctae co-localize with vinculin or phosphorylated focal adhesion kinase (pFAK) (**Figure 2-4M-R**), focal adhesion proteins that are present as rings in podosomes but absent from most invadopodia (Bowden *et al.*, 2006; Machesky *et al.*, 2008). Most of the overlap between EGFP-SV and vinculin and pFAK is at focal adhesions, as previously reported (**Figure 2-4M-R, arrows**) (Wulfkuhle *et al.*, 1999; Takizawa *et al.*, 2006).

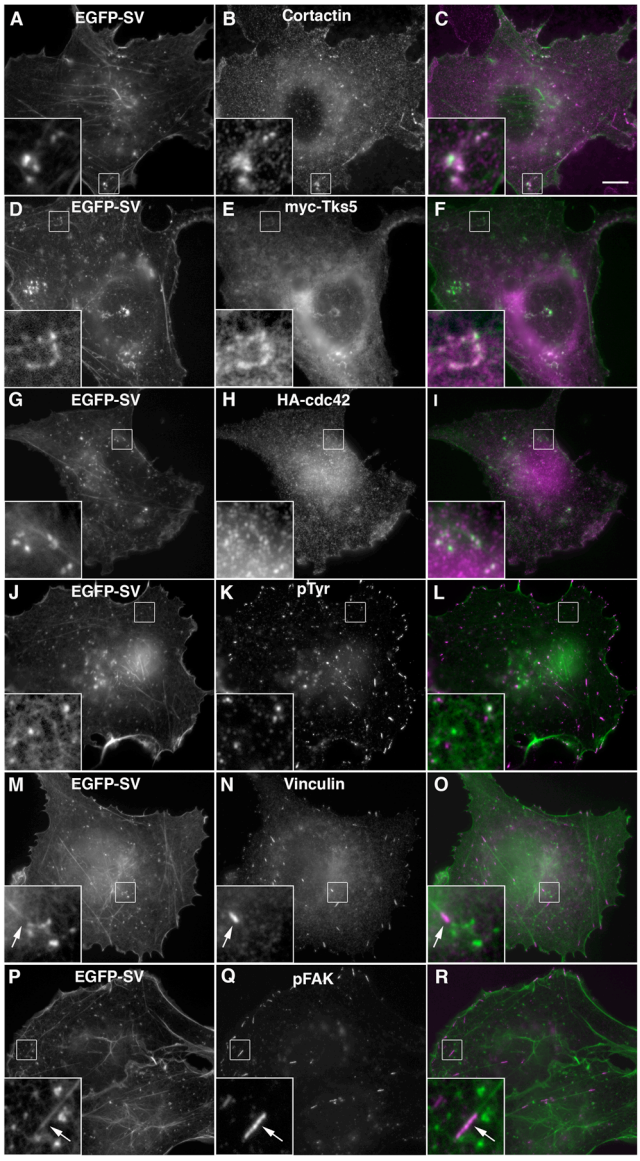


**Figure 2-4.** EGFP-SV punctae co-localize with cortactin and exogenous Tks5 and Cdc42, but not with phosphoFAK or vinculin.

COS-7 cells expressing EGFP-SV **(A, D, G, J, M, P)** were stained with antibodies against endogenous cortactin **(B)**, phosphotyrosine (pTyr, **K**), vinculin **(N)**, or phosphorylated FAK **(**pFAK, **Q)** or with antibodies against tags on exogenously expressed Tks5 **(E)** or Cdc42 **(H)**. EGFP-SV is green in the merged images **(C, F, I, L, O, R)**; other proteins are shown in magenta; overlap appears white. Insets, 4-fold enlargements of areas within boxes. Arrows denote focal adhesions. Bar, 10 µm.

**SV causes a redistribution of cortactin.** Because EGFP-SV reorganizes F-actin and overlaps extensively at punctae with cortactin, a protein that organizes actin at lamellipodial ruffles and is required for podosomes and invadopodia (Buday and Downward, 2007; Ammer and Weed, 2008; Weaver, 2008), we investigated cortactin localization in cells expressing EGFP-SV (**Figure 2-5**). In mock-transfected cells and in cells expressing EGFP alone for 48 hours, ~70% (50-109 cells per experiment, n = 3) of the cells exhibit areas of contiguous, ≥20-μm-long cortactin staining at their peripheries (**Figure 2-5A, arrowheads; Figure 2-5B**), as originally described (Wu and Parsons, 1993). By contrast, only 33.1% ± 5.7 % (~50 cells per experiment, n = 6, $p < 0.0001$) of cells overexpressing EGFP-SV contained strong contiguous peripheral cortactin staining by 48 hours post-transfection (**Figure 2-5A, d-f, arrows; Figure 2-5B**); slight decreases were observed after only 24 hours (not shown). Cortactin was apparently redistributed to the cell interior, as opposed to being differentially stabilized or cleaved by calpain (Perrin *et al.*, 2006), because FACS analyses showed no changes in total amounts of cellular cortactin with increasing expression of either EGFP or EGFP-SV (**Figure 2-5C**).

**Other lamellipodial markers also are displaced.** To determine whether EGFP-SV promotes the selective redistribution of cortactin, we also monitored two other proteins characteristically concentrated at lamellipodia, lamellipodin/RAPH1/PREL1 (**Figure 2-6A-C**) (Krause *et al.*, 2004) and filamin A/ABP280 (**Figure 2-6D-F**) (Stendahl *et al.*, 1980). EGFP-SV induces a significant loss of lamellipodin from the

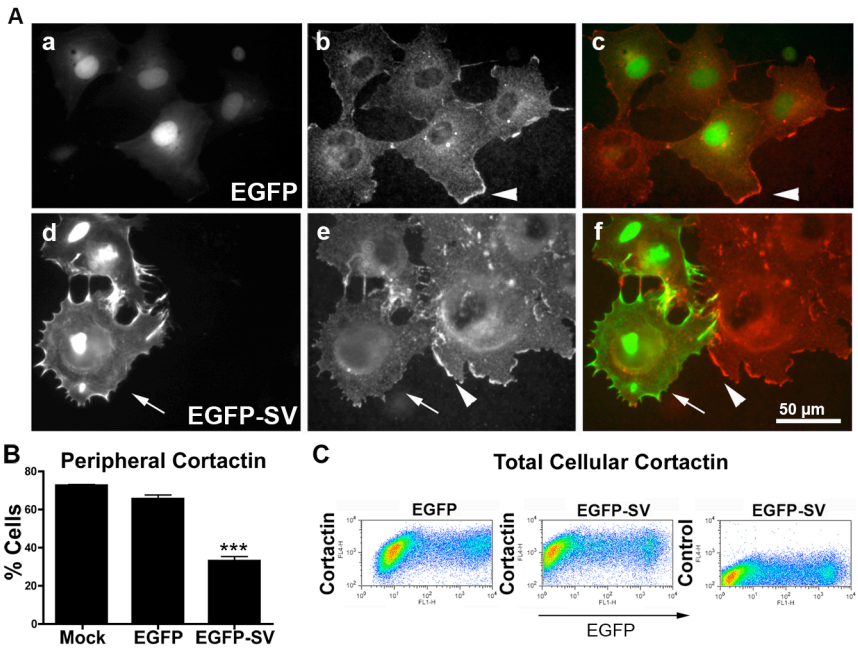


**Figure 2-5.** Expression of EGFP-SV leads to redistribution of cortactin.

**(A)** COS-7 cells expressing EGFP alone **(a;** green in **c)** or EGFP-SV **(d;** green in **f)** for 48 hours were immunostained for endogenous cortactin **(b, e;** red in **c, f)**. Cells were scored as containing (arrowheads) or lacking (arrows) peripheral cortactin. Bar, 50 µm.

**(B)** Percentages of cells with continuous peripheral cortactin staining 48 hours after mock transfection (Mock) or expression of EGFP alone (EGFP) or EGFP-SV (EGFP-SV). Means ± s.d.; ***, $p < 0.0001$.

(**C**) Two-color FACS analyses showing no change in the levels of total cellular cortactin caused by expression of EGFP or EGFP-SV in COS-7 cells.

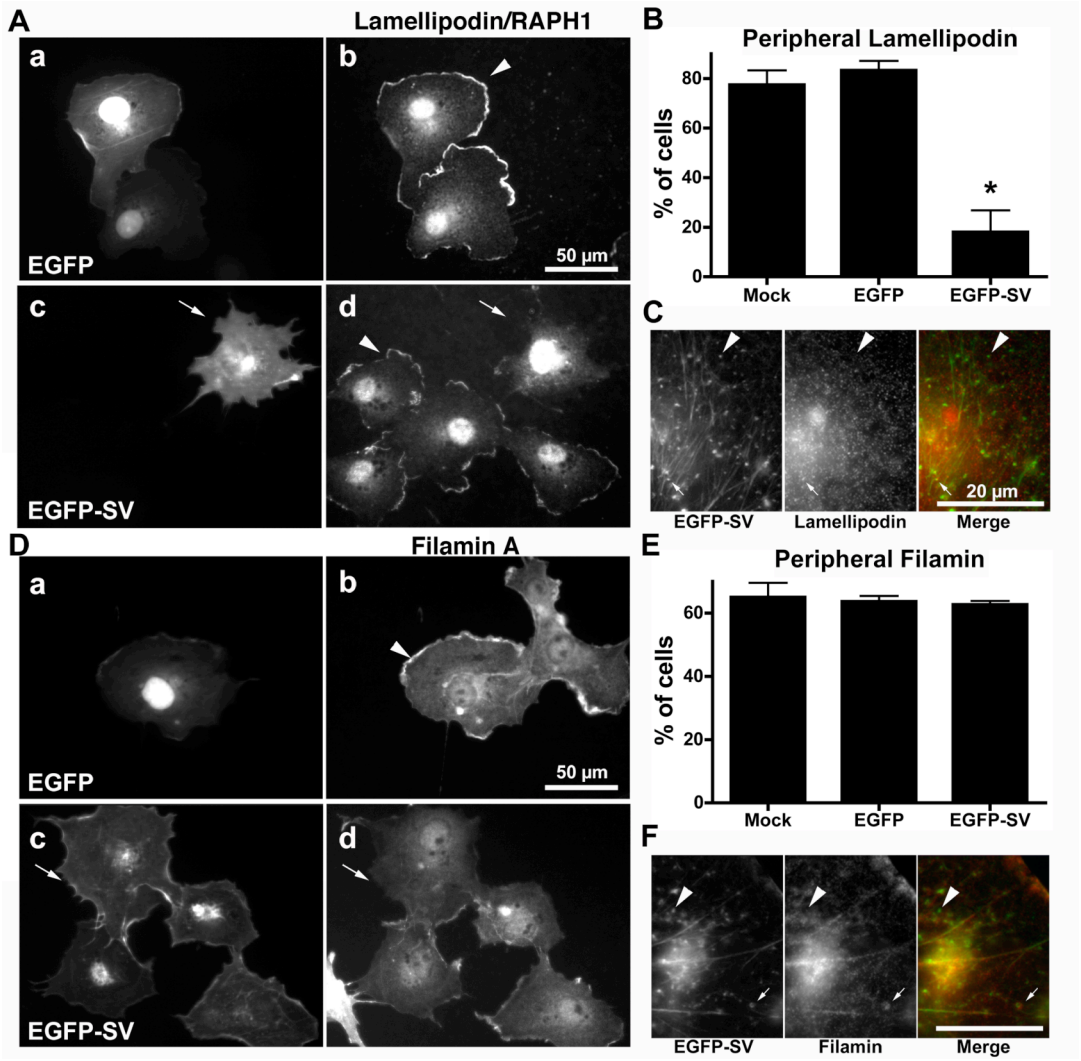


**Figure 2-6.** EGFP-SV redistributes lamellipodin/RAPH1/PREL1, but not filamin A, within 24 hours.

**(A, D)** COS-7 cells expressing EGFP alone **(a)** or EGFP-SV **(c)** for 24 hours were immunostained for endogenous lamellipodin (**b, d** in **A**) or filamin A (**b, d** in **D**). Cells were scored as containing (arrowheads) or lacking (arrows) peripherally localized protein. Bars, 50 µm.

Percentages of cells with peripheral **(B)** lamellipodin or **(E)** filamin staining 24 hours after mock transfection (Mock) or expression of EGFP alone (EGFP) or EGFP-SV (EGFP-SV). Means ± s.d.; *, $p < 0.05$; $n = 2$ (**B**); $n = 3$ (**E**).

Overlap (arrows), or lack of overlap (arrowheads), of EGFP-SV punctae with endogenous (**C**) lamellipodin and (**F**) filamin. Bars, 20 µm.

cell periphery (**Figure 2-6A, 2-6B**). By contrast, filamin remains at the cell periphery in COS-7 cells expressing EGFP-SV, but the extent and intensity of the peripheral filamin signal appears reduced (**Figure 2-6D, 2-6E**). Unlike the nearly perfect overlap seen with cortactin antibody (**Figure 2-4A-C**), most EGFP-SV punctae lack lamellipodin and filamin (**Figure 2-6C, 2-6F, arrowheads**), with only ~38% and ~35%, respectively, of the EGFP-SV punctae overlapping with signal from antibodies against these two proteins (**Figure 2-6C, 2-6F, arrows**).

**Cortactin binds SV in vitro.** Due to the redistribution of cortactin upon EGFP-SV overexpression (**Figure 2-5**) and the striking amount of co-localization of the two proteins (**Figure 2-4A-C**), compared to the relatively weak overlap with lamellipodin and filamin (**Figure 2-6C, 2-6F**), we investigated whether cortactin binds SV directly. GST or GST-tagged SV N-terminal fragments were mixed with His-cortactin(ΔSH3), and interacting proteins were co-sedimented with glutathione-Sepharose™ beads (**Figure 2-7A**). Even with significant His-cortactin(ΔSH3) input (**Figure 2-7A, a-b,** *lanes 1*), there was no detectable binding with GST or beads only (*lanes 2, 3*). His-cortactin(ΔSH3) was pulled down with SV amino acids SV1-340 (*lanes 4*), SV570-830 (*lanes 7*) and SV340-830 (*lanes 8*). The lack of binding with SV171-340 (*lanes 5*) or SV340-570 (*lanes 6*) indicates likely cortactin binding sequences within SV1-171 and SV570-830.

**Cortactin increases the numbers of EGFP-SV F-actin punctae.** To see if cortactin is necessary for the formation of EGFP-SV-induced F-actin punctae, we

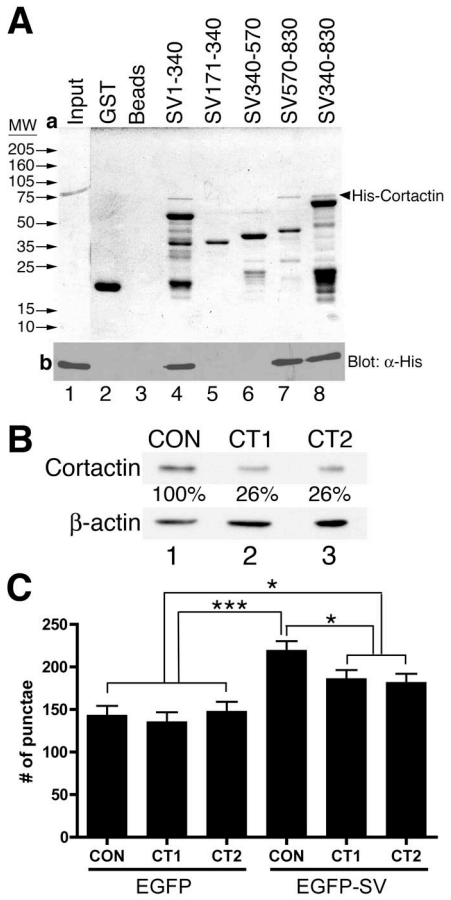


**Figure 2-7.** Cortactin binds SV in vitro and contributes to the formation of EGFP-SV induced punctae in vivo.

(**A**) His-cortactin(ΔSH3) (Input, lane 1) was mixed with glutathione-Sepharose™ beads and the indicated GST fusion proteins (lanes 2, 4-8) or with glutathione-Sepharose™ beads alone (lane 3) for 1 hour. Beads were washed, pelleted and heated in SDS sample buffer and interacting proteins were subjected to SDS-PAGE and (**a**) stained with Coomassie blue or (**b**) transferred to nitrocellulose and immunoblotted for the His tag (n=3). Arrowhead denotes His-cortactin(ΔSH3). Input lane (**a**) was digitally moved to match immunoblot (**b**).

(**B**) Cortactin protein levels in COS-7 cells 4 days post-transfection with control siRNA (CON, lane 1) or cortactin siRNA (CT1, CT2, lanes 2, 3. β-actin was the loading control. Percent of cortactin remaining is shown under cortactin bands (n=1).

(**C**) Cortactin knockdown cells were transfected with plasmids encoding EGFP or EGFP-SV at day 3 of siRNA treatment, and F-actin punctae were visualized with phalloidin after an additional 24 hours (n=3). Statistically significant differences were determined by unpaired two-tailed Student t-tests and with the Student-Newman-Keuls multiple comparison test (*, $p<0.05$, ***, $p<0.001$).

reduced cortactin levels by 74% of control-treated cells (**Figure 2-7B,** *CON, lane 1*) using two different cortactin-specific siRNAs (*CT1, CT2; lanes 2, 3*). Cortactin knockdown cells were transfected with plasmids encoding EGFP or EGFP-SV and scored for the number of F-actin punctae (**Figure 2-7C**). As in the absence of siRNA treatment (**Figure 2-1**), there is a significant difference between EGFP and EGFP-SV transfected cells treated with the control siRNA (***, $p<0.001$) (**Figure 2-7C**). Although cortactin knockdown has no significant effect on the numbers of F-actin punctae in EGFP-transfected cells, the reduction in cortactin levels inhibits ~50% of the increase in numbers induced by EGFP-SV (*, $p<0.05$). Therefore, the podosome and invadopodial protein cortactin contributes to the formation of EGFP-SV punctae.

***Role of SV at Podosomes and Invadopodia***

**Endogenous SV localizes to Src-induced podosomes and areas of matrix degradation in COS-7 cells.** To further examine the relationship between SV and podosomes/invadopodia, we localized endogenous SV in COS-7 cells containing podosomes induced by constitutively active c-Src-Y527F (**Figure 2-8**). Each Src-induced podosome consists of a core of F-actin, cortactin, and other proteins surrounded by a ring of focal adhesion proteins (Linder and Aepfelbacher, 2003). Endogenous SV co-localizes extensively with F-actin and cortactin at the podosome cores (**Figure 2-8A-B**) and less well with α-actinin (**Figure 2-8C**), which associates with both the podosome core and ring (Linder and Aepfelbacher, 2003). Little overlap of SV with the focal

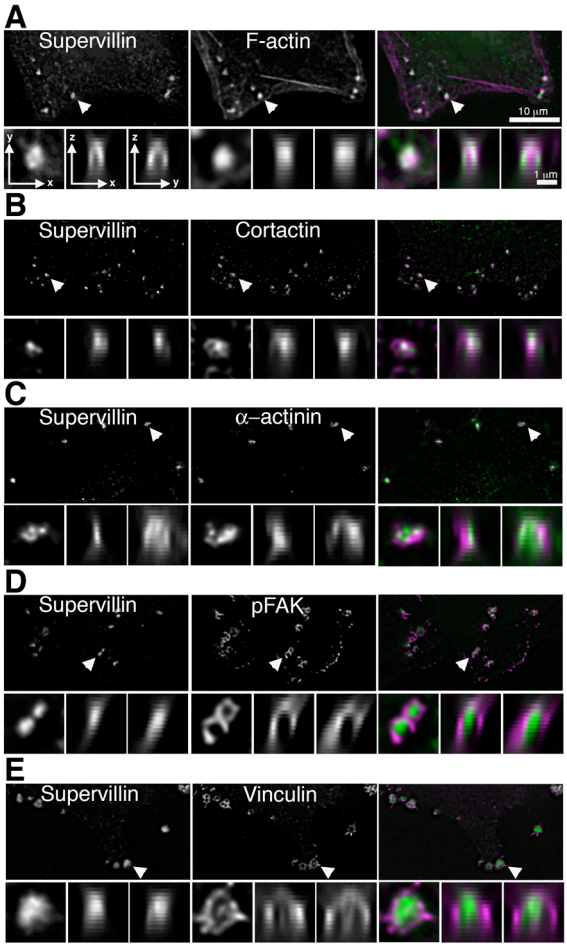


**Figure 2-8.** Endogenous supervillin localizes to the cores of Src-induced podosomes.

COS-7 cells were transfected with Y527F Src, immunostained for SV and stained for (**A**) F-actin with phalloidin or with antibody against endogenous (**B**) cortactin, (**C**) α-actinin, (**D**) pFAK or (**E**) vinculin and visualized after deconvolution of images acquired with 0.2-µm Z-steps. F-actin and cortactin localize to podosome cores, α-actinin to cores + rings, and vinculin and phosphorylated FAK (pFAK) to podosome rings (Linder and Aepfelbacher, 2003).

Individual podosomes in the XY view (**arrowheads**) have been enlarged to the same scale as the XZ and YZ views. SV, green; other proteins magenta; and overlaps in white. Bars, 10 µm in main images, 1 µm in insets.

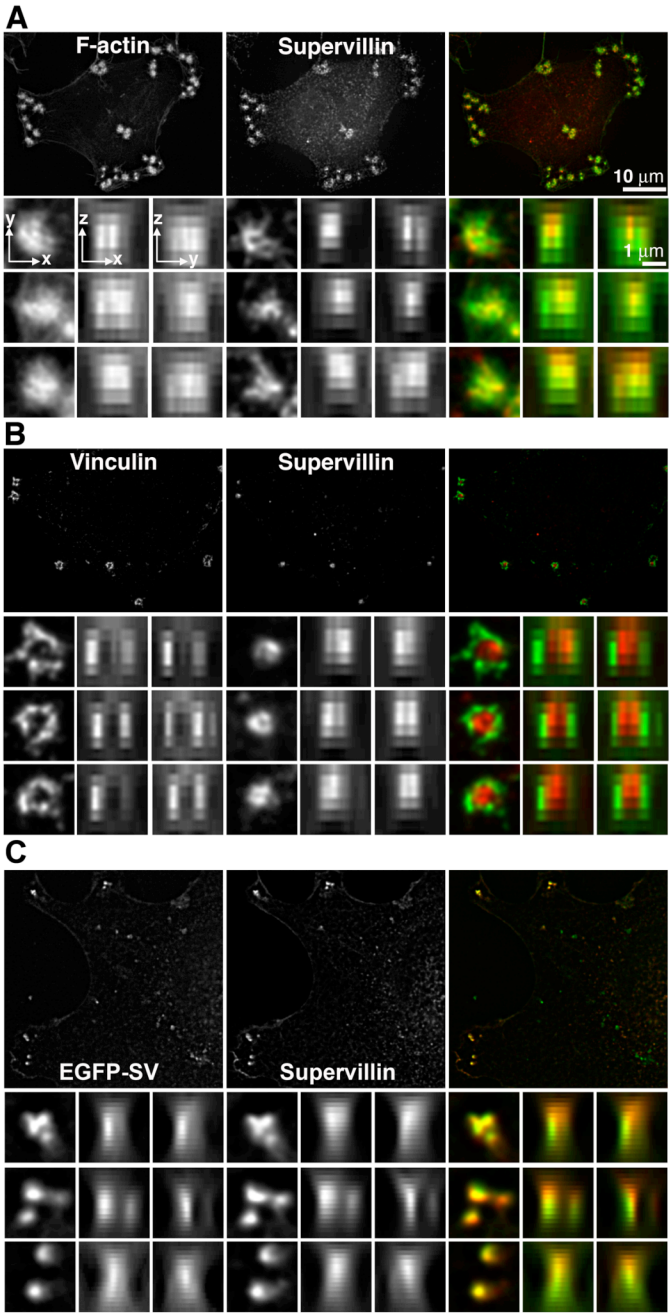


**Figure 2-9.** Controls supporting the localization of SV at the cores of Src-induced podosomes.

**(A, B)** The accessibility of SV epitopes at podosomes is independent of filter sets used for co-localization. COS-7 cells were transfected with Y527F Src, stained for endogenous SV in the red channel, and for F-actin **(A)** or vinculin **(B)** in the green channel, and visualized after deconvolution of images acquired with 0.5-µm Z-steps.

(**C**) EGFP-SV in the green channel localizes throughout the length of the podosome core, whereas the H340 antibody against the SV N-terminus, visualized in the red channel, differentially recognizes the apical ends of podosome cores. Images were acquired with 0.2-µm Z-steps.

(**A – C**) Individual podosomes in the XY view have been enlarged to the same scale as the XZ and YZ views. Bars: 10 µm in main images, 1 µm in insets. Overlaps appear yellow.

adhesion proteins, phosphorylated FAK and vinculin, is observed in podosome rings (**Figure 2-8D-E**). The overall SV staining pattern at podosome cores is generally more punctate than those of the other proteins (**Figure 2-8, left, x-y inset**) although foci of SV and cortactin show frequent overlaps (**Figure 2-8B**). Immunolocalization of SV shows a preferential exposure of the SV epitope at the apical ends of the podosomes, near the interface with the cytoplasm (**Figure 2-8**), regardless of whether SV is imaged with green (**Figure 2-8**) or red (**Figure 2-9A, B**) fluorophores. However, co-localization of EGFP-SV and antibody-stained SV indicates that the N-terminal epitope recognized by the antibody is preferentially shielded near the base of the podosome cores (**Figure 2-9C**). Thus, as has been reported for the transmembrane receptor CD44 (Chabadel *et al.*, 2007), the peripheral membrane protein SV marks podosome cores. EGFP-SV also localizes to areas of matrix degradation in COS-7 cells on fluorescently labeled gelatin although these cells do not efficiently degrade matrix (**Figure 2-10**).

**Many tumor cell lines contain relatively high levels of SV.** To identify an invasive cell line in which we could examine SV function in matrix degradation and invasion, we screened a number of tumor cell lines for the presence of endogenous SV. Abundant levels of SV message have been reported in HeLa cervical adenocarcinoma, SW480 colorectal adenocarcinoma, and A549 lung carcinoma cells (Pope *et al.*, 1998). In agreement with previous results (Pestonjamasp *et al.*, 1997), we find that HeLa cells contain higher levels of endogenous SV than do untransformed cell lines (**Figure 2-11A,**

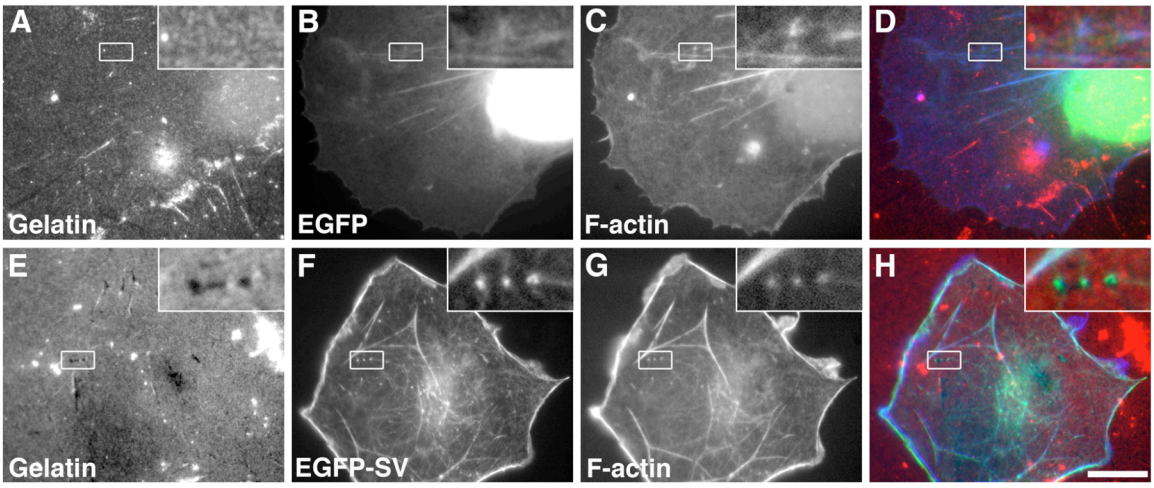


**Figure 2-10.** EGFP-SV induced punctae localize to areas of degraded matrix in COS-7 cells.

COS-7 cells were transfected with either EGFP (**A-D**) or EGFP-SV (**E-H**) and plated on TRITC-labeled gelatin coated coverslips for 24 hours, fixed and stained with Texas Red-phalloidin to visualize F-actin. Bar, 20 $\mu$m. Area within boxes is enlarged 4-fold and shown in inset.

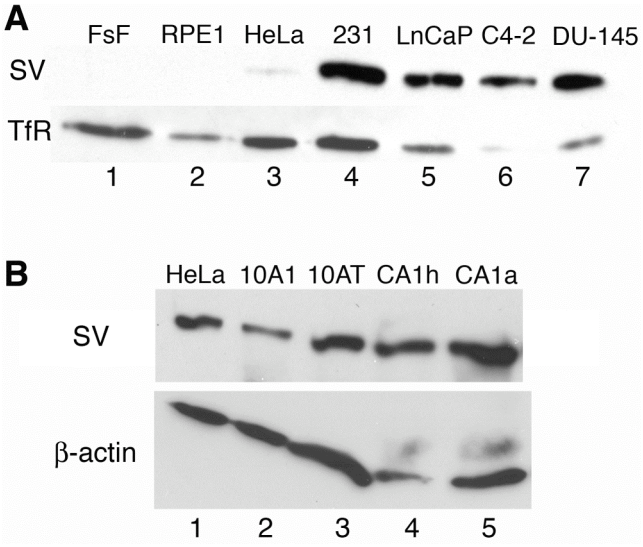


**Figure 2-11.** SV is abundant in many transformed cells.

(**A**) Immunoblot of endogenous SV in primary human foreskin fibroblasts (FsF, lane 1), telomerase-immortalized retinal pigmented epithelial (RPE1) cells (lane 2), HeLa cervical adenocarcinoma cells (lane 3), MDA-MB-231 breast adenocarcinoma cells (231, lane 4), metastatic androgen-dependent LNCaP (lane 5) and androgen-independent C4-2 (lane 6) prostate adenocarcinomas, and metastatic DU-145 carcinoma cells (lane 7).

(**B**) Immunoblot of endogenous SV in HeLa cells (lane 1), spontaneously immortalized MCF10A1 breast epithelial cells (10A1, lane 2), H-Ras expressing hyperplastic MCF10AT1k.cl2 breast cells (10AT, lane 3), MCF10CA1h low-grade breast carcinoma cells (CA1h, lane 4), and MCF10CA1a.cl1 high-grade metastatic breast carcinoma cells (CA1a, lane 5). Antibodies against the transferrin receptor (TfR) or β-actin were used as loading controls.

**lanes 1-3**). A number of human prostate (LNCaP, C4-2, DU-145) (Stone *et al.*, 1978; Thalmann *et al.*, 1994) and breast (MCF10A1, MCF10AT1k.cl2, MCL10CA1h, MCF10ACA1a.cl1, MDA-MB-231) (Tang *et al.*, 2003) epithelial cell lines contain abundant endogenous SV (**Figure 2-11**). The highest SV levels were seen in MDA-MB-231 metastatic breast carcinoma cells, which inherently form invadopodia on ECM substrates (Chen *et al.*, 1994).

**Endogenous SV localizes to invadopodia in MDA-MB-231 cells.** In MDA-MB-231 cells on gelatin, endogenous SV co-localizes with the large ventral accumulations of cortactin and F-actin characteristic of invadopodia (**Figure 2-12A**) (Artym *et al.*, 2006). In addition, mRFP-SV is found in proximity with ~45% of the vesicles or invadopodia that contain EGFP-MT1-MMP (**Figure 2-12B**), the membrane-bound MMP responsible for most matrix degradation in MDA-MB-231 cells (Artym *et al.*, 2006). Endogenous SV also is concentrated at and within regions of matrix degradation, as identified by black areas in thin films of TRITC-labeled gelatin (**Figure 2-12C**). In XZ and YZ views, SV is seen both within and above the holes in the gelatin matrix created by invadopodia (**Figure 2-12C, a-d**). By contrast, little overlap is seen between EGFP-SV and the pY-100 phosphotyrosine antibody (Bowden *et al.*, 2006) (**Figure 2-13**). Taken together, these data support an association between SV and invadopodia.

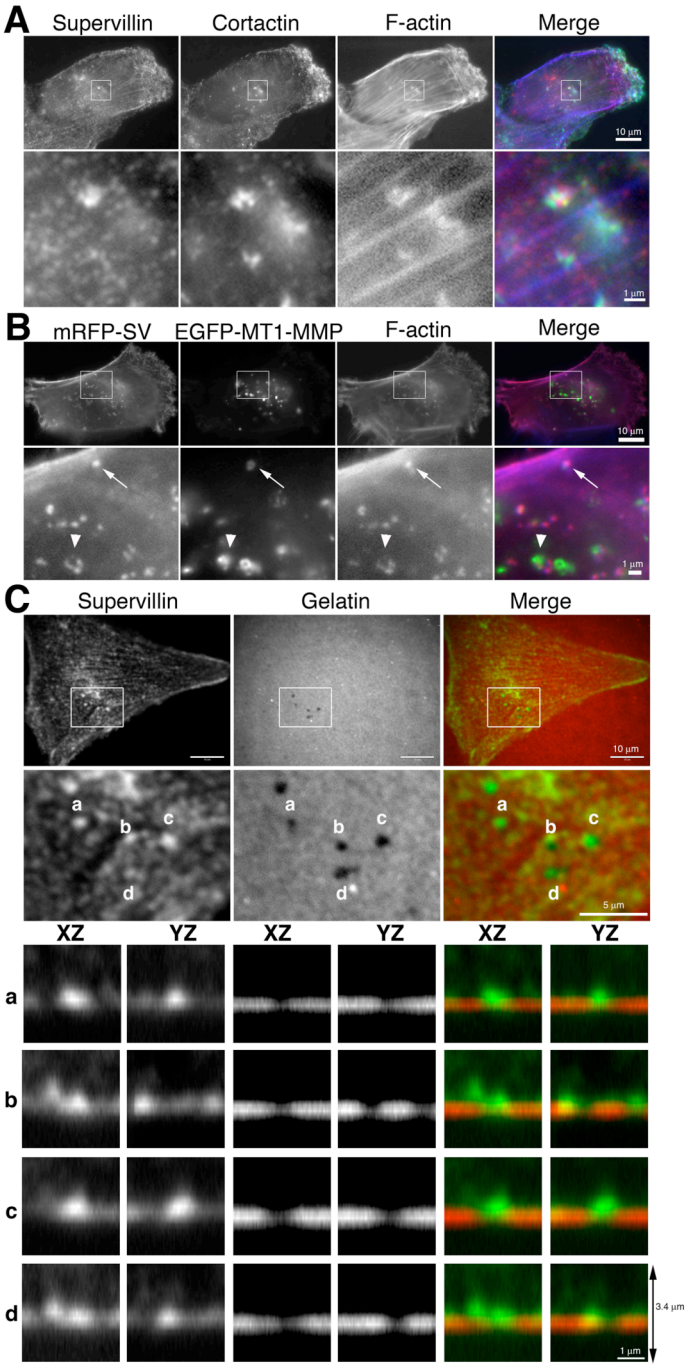


**Figure 2-12.** Supervillin localizes at and within MDA-MB-231 cell invadopodia.

(**A**) MDA-MB-231 cells were plated on unlabeled gelatin-coated coverslips for 3 hours, fixed and stained with antibodies (SV, cortactin) and/or phalloidin (F-actin), as noted, and imaged by wide-field microscopy. Merges show supervillin in red, cortactin in green and F-actin in blue. Bars, 10 µm (top row) and 1 µm (bottom row).

(**B**) MDA-MB-231/WT Src cells were transfected with mRFP-SV and EGFP-MT1-MMP. Cells were plated on unlabeled gelatin-coated coverslips for 6 hours, fixed and stained with phalloidin (F-actin) and imaged by wide-field microscopy. Merges show mRFP-SV in red, EGFP-MT1-MMP in green and F-actin in blue. Arrows indicate co-localization; arrowheads denote mRFP-SV localization surrounding EGFP-MT1-MMP vesicle.

(**C**) MDA-MB-231 cells were plated on TRITC-labeled gelatin-coated coverslips for 6 hours, fixed and stained with anti-SV antibodies and imaged by confocal microscopy as a Z-series with 0.2 µm steps. Merges show supervillin in green and TRITC-gelatin in red. An XY view of such a cell is shown (top row). Areas inside the boxes were enlarged 4 fold (second row). Eight-fold enlargements of XZ and YZ views corresponding to a, b, c, d are shown below XY views. Bars, 10 µm (top row), 5 µm (second row), and 1 µm (bottom row).

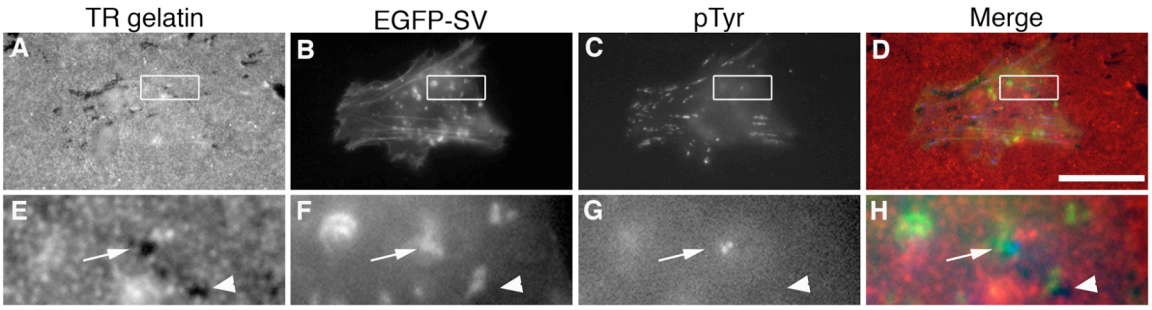


**Figure 2-13.** EGFP-SV overlaps only slightly with phosphotyrosine.

MDA-MB-231/WT Src cells were transfected with EGFP-SV (**B, F**, green in *merge*), plated on TRITC-labeled gelatin coated coverslips (**A, E,** red in *merge*) for 6 hours, fixed and stained with anti-phosphotyrosine antibody (pTyr, **C, G**, blue in *merge*). Bar, 20 $\mu$m. Area within boxes is enlarged 5-fold and shown in bottom row.

**SV overexpression increases the numbers of matrix degradation sites formed per cell.** We tested whether SV affects ECM degradation in highly invasive MDA-MB-231 cells that stably overexpress WT Src (MDA-MB-231/WT Src) (Myoui *et al.*, 2003; Bowden *et al.*, 2006). Transient overexpression of EGFP-SV to levels that were 4.9 ± 1.5 (mean ± s.d., n = 3) times greater than endogenous SV levels doubled the average number of holes per cell in the fluorescent gelatin matrix (**Figure 2-14B** *vs.* **Figure 2-14A, 2-14C; Figure 2-14D**). However, the percentage of cells that made holes did not differ significantly from controls (**Figure 2-14E**). Similar results are seen with MDA-MB-231 cells not transfected with c-Src (**Figure 2-15**). This SV-promoted increase in the numbers of holes per cell corresponds to a 4.2-fold increase in the mean area of degraded matrix per cell (**Figure 2-16**). These results are consistent with a SV-mediated increase in the numbers, efficiency, or dynamics of sites of ECM degradation.

**SV underexpression decreases matrix degradation, especially in the cell center.** Conversely, reduction of endogenous SV levels reduces the apparent numbers of ECM-degrading sites (**Figure 2-17**). Each of two siRNAs reduces SV levels in MDA-MB-231/WT Src cells to about 30% of endogenous levels without adversely affecting the expression level of the related protein, gelsolin (**Figure 2-17A,** *lanes 1-2 vs. lane 3*). While these reduced levels of SV do not affect the percentages of cells associated with degraded matrix (**Figure 2-17B**), the mean numbers of holes per cell (**Figure 2-17C**) and

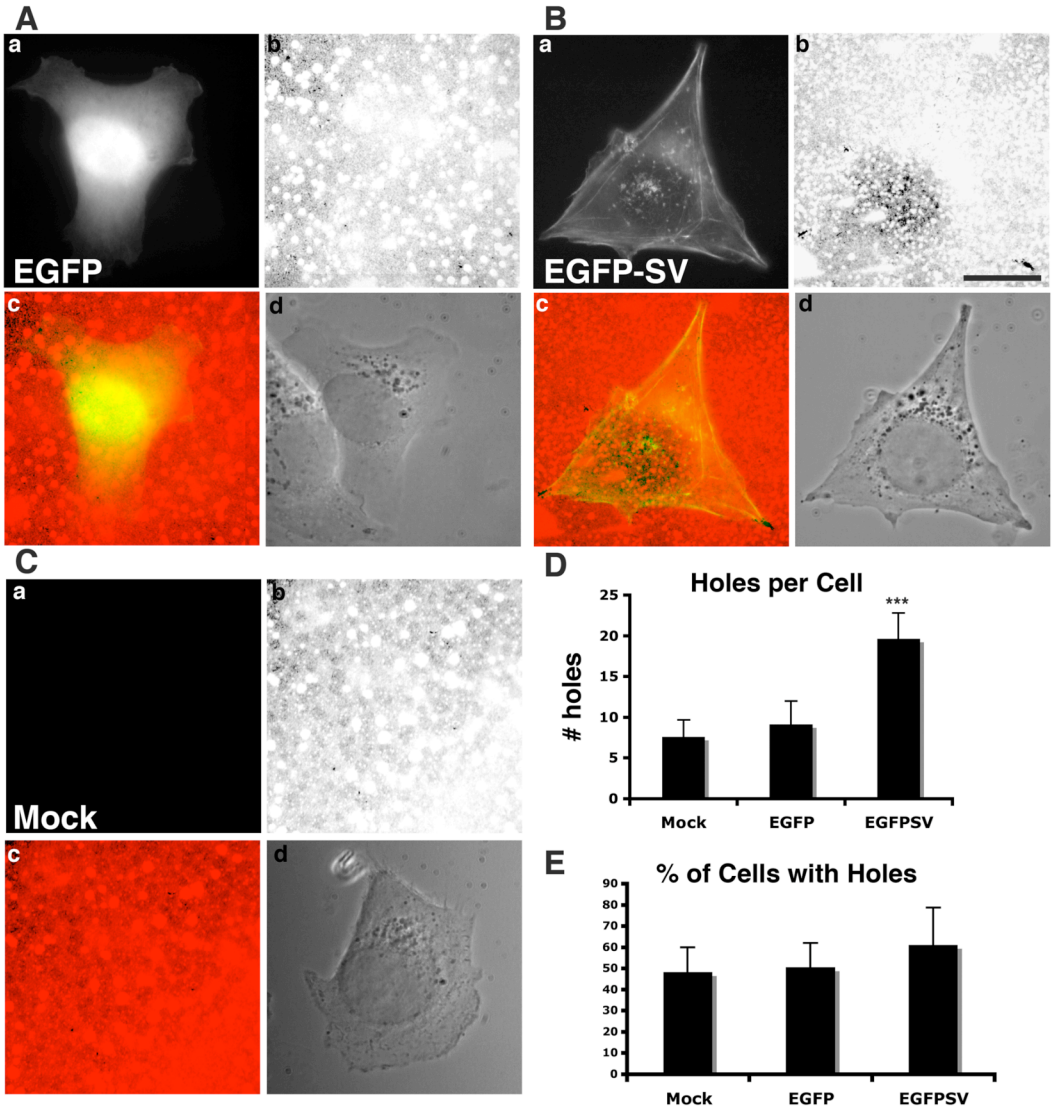


**Figure 2-14.** Overexpression of EGFP-SV increases the number of matrix holes formed per cell.

MDA-MB-231/WT Src cells were transfected with either EGFP alone **(A)**, or EGFP-SV **(B)**, or were mock transfected **(C)**. Cells were plated on TRITC-labeled gelatin coated coverslips for 6 hours before visualization by green (**a**) and red (**b**) fluorescence and phase contrast (**d**); merged green and red images also are shown (**c**). Bar, 20 µm.

**(D)** The numbers of holes in the red gelatin matrix (representative of invadopodia) per cell were counted. EGFP-SV cells had a significant (***, $p < 0.001$, $n = 8$) increase in the number of associated holes per cell.

**(E)** The percentage of cells with some matrix degradation was not significantly different among the three conditions.

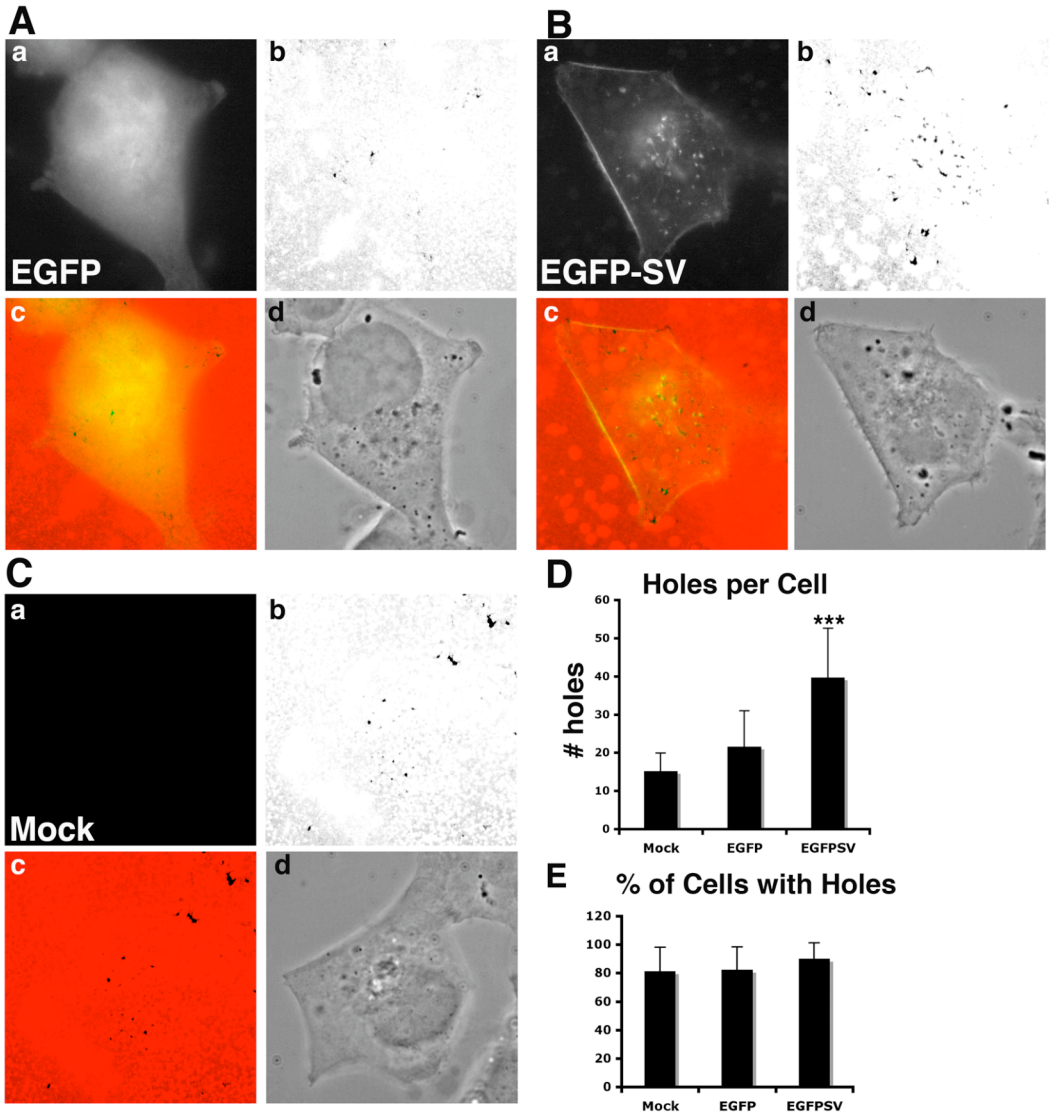


**Figure 2-15.** Increases in the numbers of matrix holes formed per cell induced by EGFP-SV do not require co-overexpression of c-Src.

MDA-MB-231 cells without additional c-Src were transfected with either EGFP alone **(A)**, or EGFP-SV **(B)**, or were mock transfected **(C)**. Cells were plated on TRITC-labeled gelatin coated coverslips for 12 hours before visualization by green (**a**) and red (**b**) fluorescence and phase contrast (**d**); merged green and red images also are shown (**c**). Bar, 20 µm.

**(D)** The numbers of holes in the red gelatin matrix per cell were counted. EGFP-SV cells had a significant increase in the number of associated holes per cell (***, $p < 0.001$, $n = 8$).

**(E)** The percentage of cells with matrix degradation was not significantly different among the three conditions.

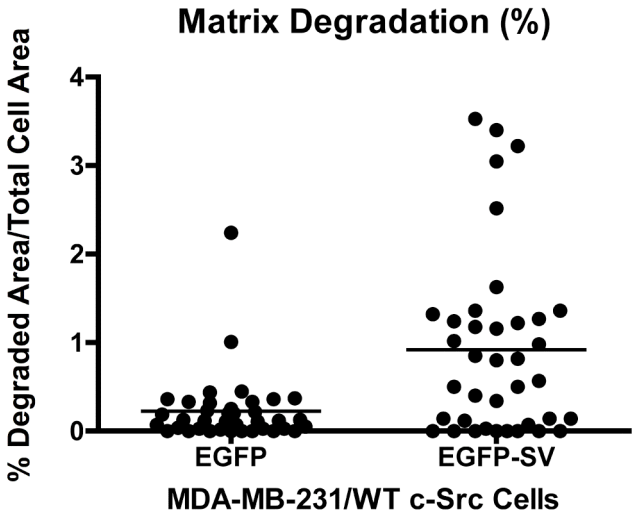


**Figure 2-16.** Overexpression of EGFP-SV in MDA-MB-231/WT c-Src cells increases the extent of matrix degradation.

MDA-MB-231/WT c-Src cells expressing either EGFP or EGFP-SV at comparable levels were plated on TRITC-labeled gelatin coated coverslips for 6 hours before visualization by green and red fluorescence. Regions of interest were drawn to include the matrix surrounding, as well as underneath, the fluorescent cells. Fractional areas of degraded matrix and cellular fluorescence were determined using ImageJ 1.40g, as described at www.nist.gov/lispix/imlab/measure/pctarea.html and plotted as ratios. Means ± s.d. were 0.22 ± 0.39 and 0.92 ± 1.03 for cells expressing EGFP vs. EGFP-SV, respectively; median percentages of degraded matrix were 0.12 and 0.68, respectively; n = 38, P = 0.002.

the percentages of cells with holes underneath the central region of the cell are decreased, as compared with cells treated with a control siRNA (**Figure 2-17D; 2-17E, e *vs.* b**). By contrast, matrix degradation in these assays is unaffected by down-regulation of gelsolin (**Figure 2-17A,** *lane 4***; 2-17B – 2-17D**), a SV family member involved in podosome assembly in osteoclasts and matrix invasion of MDA-MB-231 cells (Chellaiah *et al.*, (Chellaiah *et al.*, 2000; Van den Abbeele *et al.*, 2007). Double knockdowns of SV and gelsolin (**Figure 2-17A,** *lane 5*) result in the same number of total holes per cell as observed for controls (**Figure 2-17C**) and are not significantly more effective than knockdown of SV alone in decreasing the presence of central holes (**Figure 2-17D**). However, the locations of the holes in the matrix for the SV/gelsolin double knockdown tended to be shifted away from the cell centers towards the cell edges, as was also observed for knockdown of SV alone (**Figure 2-17E, panel h**). Thus, SV apparently affects both the numbers and locations of the holes in the fluorescent matrix.

**SV knockdown does not decrease ventral F-actin punctae.** Although SV can increase F-actin bundling in vitro and in vivo (Wulfkuhle *et al.*, 1999; Chen *et al.*, 2003), SV probably is not required for the formation of ventral F-actin structures (**Figure 2-17E**). MDA-MB-231/WT Src cells with reduced levels of SV and significantly reduced sites of matrix degradation (**Figure 2-17E**, **e, h *vs.* b**) still contain apparently normal levels of F-actin structures within the ventral focal plane (**Figure 2-17E**, **d, g *vs.* a**). In addition, COS-7 cells expressing constitutively active c-Src-Y527F form similar numbers of podosomes, regardless of whether their SV levels are normal or have been reduced to

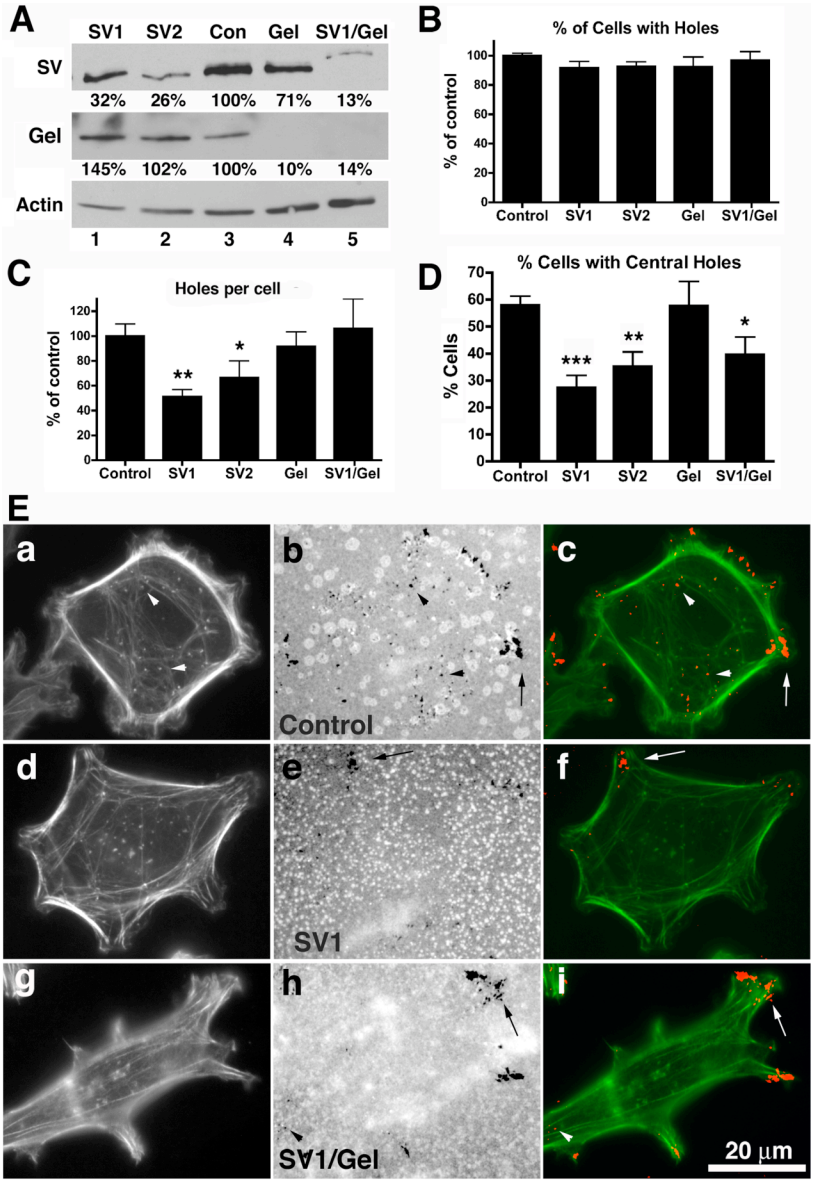


**Figure 2-17.** Underexpression of endogenous SV decreases the numbers of matrix holes per cell, especially under the center of the cell.

MDA-MB-231/WT Src cells were transfected with either control siRNA (Con) or siRNAs targeting SV (SV1, SV2), the related protein, gelsolin (Gel), or both SV and gelsolin (SV1/Gel). These cells were analyzed for (**A**) protein levels by immunoblotting, (**B**) the percentages of cells associated with at least one area of degraded matrix (hole), relative to control-treated cells, (**C**) the mean numbers of holes per cell, relative to control-treated cells, and (**D**) the percentages of cells with holes underneath the cell center. The percentages in panel **A** denote the mean levels (n = 4) of SV and gelsolin, relative to control-treated cells, after normalization to the β-actin loading control. (**B, C, D**) Means ± s.d.; n = 6. Asterisks in panels **C** and **D** denote significant differences (***, $p < 0.001$, **, $p < 0.01$; *, $p < 0.05$) from controls in unpaired t tests.

(**E**) Representative micrographs of cells treated with control siRNA (**a-c**), SV1 siRNA (**d-f**), or both SV1 and gelsolin (SV1/Gel) siRNAs (**g-i**) and stained for F-actin (**a, d, g**) or sites of matrix degradation (**b, e, h**). For merged images (**c, f, i**), holes in the matrix were visualized as red spots by pseudocoloring the images in **b, e** and **h** after inverting and thresholding their luminosities. Note the sites of matrix degradation at the cell periphery (arrows) and underneath the cell center (arrowheads). Overlaps appear yellow or orange. Bar, 20 µm.

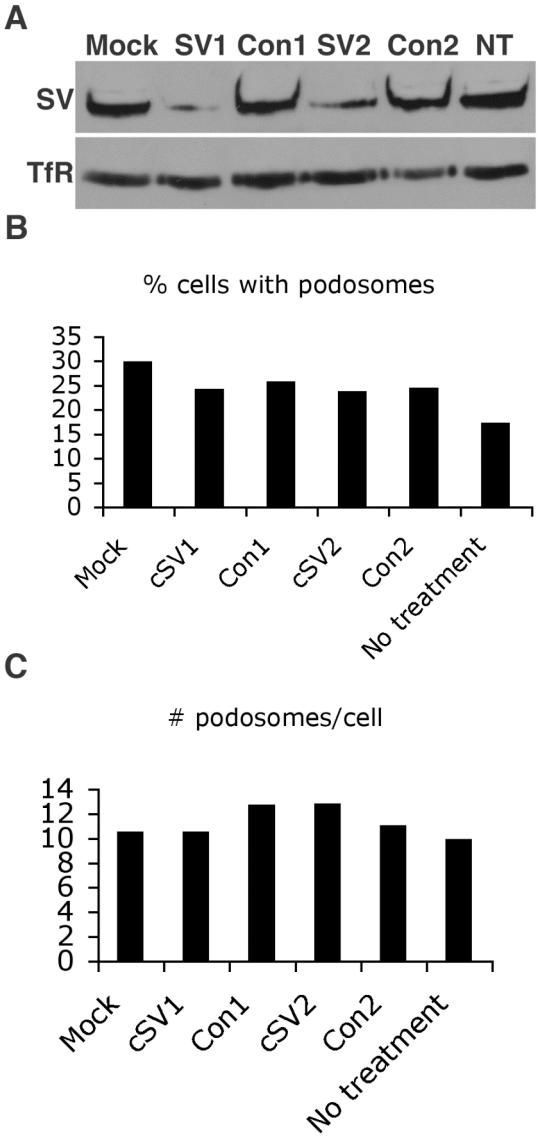


**Figure 2-18.** SV knockdown has no effect on Src-induced podosome formation.

COS-7 cells were transfected for SV knockdown with two siRNAs against SV (SV1, SV2), or two control siRNAs (Con1, Con2) for 4 days. Mock (transfection reagent alone) and no treatment served as additional controls. On day 3 of knockdown, cells were transfected with Y527F activated Src.

**(A)** Western blot showing extent of knockdown; SV (top panel), transferrin receptor (TfR, lower panel) as a loading control.

**(B)** Quantification of the percentages of cells with podosomes.

**(C)** Quantification of the number of podosomes per cell.

20% ± 5% of endogenous levels (**Figure 2-18**). The normal-looking appearance of the ventral F-actin structures in SV knockdown cells, coupled with the reduced numbers of associated ECM holes in MDA-MB-231/WT Src cells, suggest a defect in invadopodial function.

**SV knockdown reduces invasion, but only in the context of reduced levels of gelsolin.** As a direct assay for the roles of SV and gelsolin in invasion, we measured the effects of single and double SV and gelsolin knockdowns on the ability of MDA-MB-231/WT Src cells to invade Matrigel™-coated transwell filters (**Figure 2-19**). Invasion indices are normalized to eliminate effects of changes in cell motility although no statistically significant differences are apparent in the rates of cell transmigration across uncoated filters at this long time point (data not shown). Knockdown of SV alone shows an upward trend in invasion index (**Figure 2-19**), and reduction of gelsolin alone shows a downward trend that compares favorably with previously published results (Van den Abbeele *et al.*, 2007). However, assay-to-assay variances preclude statistical significance for single knockdowns of either SV or gelsolin. By contrast, simultaneously reducing SV and gelsolin significantly decreases the ability of MDA-MB-231 cells to invade Matrigel™-coated filters.

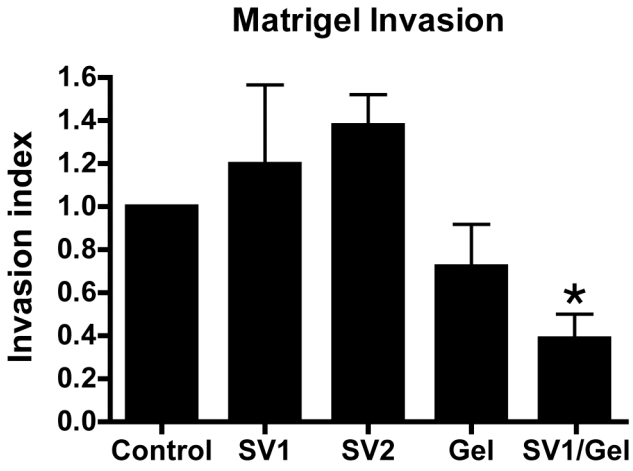


**Figure 2-19.** Matrigel™ invasion is decreased in cells depleted of both SV and gelsolin.

MDA-MB-231/WT Src cells were treated with siRNAs targeting either SV (SV1, SV2), gelsolin (Gel), or both (SV1/Gel) and assayed for invasion through Matrigel™-coated filters. Invasion indices were determined by normalizing against transmigration in the absence of Matrigel™ to control for changes in cell motility and by normalizing experimental invasion indices against the mean value obtained for cells treated with control siRNAs (Control). Cells depleted in both SV and gelsolin were significantly less invasive than controls, based on unpaired t tests (*, $p < 0.05$; $n = 3$).

## Discussion

We show here that SV reorganizes the cortical actin cytoskeleton, stimulating the formation or redistribution of dynamic basal punctae containing F-actin, cortactin, and other podosome/invadopodia proteins while decreasing the extents of cortactin and lamellipodin at the cell periphery. SV and cortactin bind directly in vitro and cooperate to redistribute F-actin in vivo. We also show that SV is a core component of Src-induced podosomes and invadopodia and that SV contributes to ECM degradation and Matrigel™ invasion by Src-expressing MDA-MB-231 breast carcinomas. These results are consistent with the report that the gene encoding SV, SVIL, is among the predisposing factors for non-BRCA1/2 (BRCAx) breast cancer (Hedenfalk *et al.*, 2003).

One possible mechanism of SV action is alteration of signaling pathways upstream of cytoskeletal remodeling. The earliest change that we see in lamellipodial architecture in cells expressing EGFP-SV is the loss of peripheral lamellipodin (**Figure 2-6**). Lamellipodin regulates actin polymerization mediated by Ena/VASP family proteins downstream of Ras activation (Krause *et al.*, 2004; Jenzora *et al.*, 2005). The lack of extensive overlap between lamellipodin and SV in punctae argues against a direct interaction between these two proteins. However, an indirect negative effect of SV on lamellipodial organization at the cell periphery could lead to the loss of broad arcs of peripheral F-actin, cortactin, and lamellipodin that we observe (**Figure 2-5**, **2-6**).

A second possibility is that SV-induced punctae may represent

podosome/invadopodia "building blocks" associated with vesicles and/or molecular motors at various stages of assembly or intracellular transit. SV may help recruit cortactin and F-actin to intracellular membranes. Because SV, cortactin and filamin all bind F-actin, the lack of filamin recruitment to punctae argues for a selective association with cortactin. A membrane-based mechanism for SV is likely based on its intracellular distribution and fractionation behavior (Pestonjamasp *et al.*, 1997; Wulfkuhle *et al.*, 1999; Nebl *et al.*, 2002; Oh *et al.*, 2003; Takizawa *et al.*, 2006). The dot-like appearances of many EGFP-SV punctae (**Figure 2-1, 2-4**) and X-Y views of endogenous SV at podosomes (**Figure 2-8**) are reminiscent of vesicles, as are the circular profiles that are occasionally apparent for larger structures associated with EGFP-SV (**Figure 2-3, Video 1**). EGFP-SV/F-actin/cortactin punctae also resemble cortactin structures described as appearing prior to actin recruitment in phorbol ester-induced podosomes (Webb *et al.*, 2006a) or originating at lamellipodia and moving in association with endosomes (Kaksonen *et al.*, 2000; Boguslavsky *et al.*, 2007; Lladó *et al.*, 2008). Although we did not detect consistent directional trafficking of SV punctae from the cell periphery to the basolateral cell surface, subtle effects on vesicle trafficking or on cortactin recruitment to transport vesicles could lead to the observed shift in cortactin and F-actin distribution over time.

A selective effect of SV on basolateral targeting of cortactin and MMPs would be consistent both with the observed effects of SV knockdown on sites of matrix degradation under the cell center (**Figure 2-17**) and with the role of cortactin in MMP

trafficking and matrix degradation (Bowden *et al.*, 1999; Artym *et al.*, 2006; Clark *et al.*, 2007; Clark and Weaver, 2008). Cortactin recruitment to the ventral cell surface occurs in stages, mediated by at least three convergent regulatory signals (Artym *et al.*, 2006; Webb *et al.*, 2006a; Ayala *et al.*, 2008). Activating mechanisms include cortactin phosphorylation by ERK1/2, Src family kinases, and PAK (Webb *et al.*, 2006b; Tehrani *et al.*, 2007; Ayala *et al.*, 2008). In this context, we note that an isoform of SV is involved in stimulus-mediated activation of ERK1/2 in smooth muscle (Gangopadhyay *et al.*, 2004), and that SV binds directly to and regulates myosin II (Takizawa *et al.*, 2007), which directly affects exocytosis in a number of cell types (Togo and Steinhardt, 2004). The sequential regulated recruitment of MMPs and other proteins to invadopodia suggests that subsequent matrix degradation is a dynamic multi-step process (Artym *et al.*, 2006; Clark *et al.*, 2007; Block *et al.*, 2008). Our SV knockdown results (**Figure 2-17**) are consistent with SV-mediated increases in cortactin activation, enhanced cortactin- or myosin II-mediated MMP secretion, and/or elevation of the rate of invadopodia turnover.

The decreased matrix degradation generated by knockdowns of either SV, cortactin or Tks5 and the co-localization of all three proteins at SV-induced punctae suggests functional cooperation (Seals *et al.*, 2005; Artym *et al.*, 2006; Clark *et al.*, 2007; Webb *et al.*, 2007; Ayala *et al.*, 2008; Clark and Weaver, 2008). Participation in a common pathway is further supported by the interaction of SV with cortactin and by the decreased formation of EGFP-SV induced F-actin punctae in cortactin knockdown cells

(**Figure 2-7**). Thus, these proteins may cooperate in signaling and/or cytoskeletal organization during invadopodia formation. However, F-actin structures form at Src-induced podosomes and at the ventral surfaces of MDA-MB-231 cells after SV knockdown, arguing for SV-independent effects during initial cytoskeletal assembly.

Our results support the hypothesis that SV promotes the loss of large central focal adhesions (Takizawa *et al.*, 2006) by increasing local matrix degradation. The effects of SV overexpression on large focal adhesions and on ECM degradation both represent a gain of function because reduction of endogenous SV exhibits the opposite phenotype (Takizawa *et al.*, 2006, **Figures 2-14, 2-17**). SV targeting to focal adhesions by binding to TRIP6 (Takizawa *et al.*, 2006) could lead to a loss of underlying matrix, causing detachment of integrins and thereby inducing focal adhesion disassembly.

Surprisingly, we find that the outcomes of gelatin degradation experiments with SV and gelsolin (**Figure 2-17**) do not predict the results of Matrigel™ invasion assays (**Figure 2-19**). This might be due to the fine line between degrading enough ECM for transmigration *vs.* destroying too much underlying matrix for the adhesion necessary for movement. These observations are consistent with the report that down-regulation of MT1-MMP can actually increase invasion (Partridge *et al.*, 2007). The long time courses of invasion assays also allow for other mechanisms, such as alterations in cell motility or proliferation, in response to the growth factors that can be released from Matrigel™ (Kleinman and Martin, 2005). Commonalities in signaling mechanisms could explain the

functional redundancy between SV and gelsolin during Matrigel$^{TM}$ invasion, especially if SV can recruit actin to membranes enriched in PIP2, as suggested by the similarities between SV and gelsolin sequences involved in this process (Hartwig *et al.*, 1989; Mere *et al.*, 2005). Gelsolin and CapG, another member of the villin/gelsolin family, also synergize with each other during matrix invasion and have each been implicated in multiple stages of tumorigenesis (Dong *et al.*, 1999; Lee *et al.*, 1999; Silacci *et al.*, 2004; Watari *et al.*, 2006; Kim *et al.*, 2007; Van den Abbeele *et al.*, 2007; Nomura *et al.*, 2008). We conclude that SV plays a nonredundant role in ECM degradation by MDA-MB-231 breast carcinoma cells and has a function overlapping that of gelsolin during invasion, both of which are important facets of tumor cell migration and metastasis.

# Chapter III

## Supervillin and Cytoskeleton-Associated Detergent Resistant Membranes

## Abstract

One property of membrane rafts is resistance to extraction with cold Triton X-100 and flotation to low buoyant densities. The actin cytoskeleton is implicated in membrane raft signaling, but interactions between actin and raft components are not well characterized. Our laboratory isolated a detergent resistant membrane fraction, called DRM-H, that contains ~23 neutrophil plasma membrane proteins (Nebl *et al.*, 2002). DRM-H is rich in cytoskeletal proteins, including fodrin, actin, myosin II, and the F-actin- and myosin II-binding membrane protein supervillin. DRM-H also contains the raft organizing proteins flotillin and stomatin, and signaling proteins, including Lyn kinase, a Src family member, and heterotrimeric G protein subunits. DRM-H exhibits a higher buoyant density (d ~1.16 g/ml) than do most DRMs (d = 1.09-1.13), which are deficient in cytoskeletal proteins. I hypothesize that DRM-H represents cytoskeleton-associated membrane rafts and is involved in trafficking and/or signaling in many cell types. As confirmation for this hypothesis, I find that in COS-7 cells, supervillin, the most tightly bound cytoskeletal protein in neutrophil DRM-H, co-localizes with c-Yes, a Src family kinase and raft protein, at membrane clusters. Domain analysis of supervillin suggests that a major membrane-binding site is located within amino acids 830 – 1010. COS-7 cells also contain cytoskeleton-associated DRMs. Following detergent extraction, flotillin-2 and c-Yes distribute in at least two peaks. Fodrin (non-erythroid spectrin) and supervillin co-migrate with the denser peaks of flotillin-2 and c-Yes in sucrose gradients, using both flotation and sedimentation methods. In addition, when transfected into COS-7 cells, estrogen receptor (ER)α associates with DRM-H, while ERβ is seen in both

DRM-L and DRM-H populations, suggesting a role for DRM-H in non-genomic estrogen signaling. Taken together, these results demonstrate that the cytoskeleton-associated DRM-H not limited to hematopoietic cells and could constitute a scaffold for membrane raft-cytoskeleton signaling events in many cells.

## Introduction

Crucial to the cell's ability to move is the proper organization and compartmentalization of the plasma membrane. One method cells use to organize the plasma membrane is the formation of liquid-ordered membrane domains, or membrane rafts. Membrane rafts, also known as lipid rafts, are defined as "small (10-200 nm), heterogeneous, highly dynamic, sterol- and/or sphingolipid-enriched domains that compartmentalize cellular processes. Small rafts can sometimes be stabilized to form larger platforms through protein-protein and protein-lipid interactions" (Pike, 2006). Proteins can be targeted to rafts by lipid modification, including addition of a myristoyl or palmitoyl moiety (Melkonian *et al.*, 1999; Zacharias *et al.*, 2002) or a glycosylphosphotidylinositol (GPI)-anchor (Brown and Rose, 1992). Rafts participate in many membrane-initiated signaling events as well as trafficking and sorting of proteins and virus particles (reviewed in (Edidin, 2003)).

Participation of the actin cytoskeleton has been implicated in many membrane raft mediated signaling processes. This has been especially well studied in many immune cells (Viola and Gupta, 2007). Membrane rafts are concentrated to form the immunological synapse in T cells at the interface with antigen presenting cells (Viola *et al.*, 1999), and the actin cytoskeleton is key to synapse formation (Monks *et al.*, 1998). Disruption of the actin cytoskeleton by cytochalasin B inhibits raft clustering in Jurkat T cell line (Villalba *et al.*, 2001). Filamin A, an actin crosslinking protein, is responsible for the movement of the co-stimulatory molecule CD28 into the raft

compartment/immunological synapse (Tavano *et al.*, 2006), and filamin A knockdown also disrupts membrane raft accumulation at the synapse (Tavano *et al.*, 2006). It is thought that filamin A "tethers and traps" membrane rafts at the synapse, as opposed to the case in B cells where ezrin (a membrane/actin linker protein) dissociates from rafts upon B cell receptor engagement (Gupta *et al.*, 2006), perhaps leading to an "untethering" of rafts from the actin cytoskeleton (Viola and Gupta, 2007). In mast cells, the actin cytoskeleton is implicated in downregulation of IgE receptor signaling by providing tracks for Lyn kinase to move away from the raft-resident receptor (Holowka *et al.*, 2000). From these studies, as well as others, it is clear that the cytoskeleton is vital to membrane raft processes. However, many details of the interactions between raft components and the cytoskeleton remain to be elucidated.

One particular kind of membrane raft, caveolae, are organized by cholesterol binding proteins called caveolins (Thomas and Smart, 2008) and are sites of nongenomic signaling of estrogen receptors (ER) (Razani *et al.*, 2000; Sak and Everaus, 2004). Aside from its canonical role in nuclear signaling, estrogen can rapidly alter cell signaling through calcium release, mitogen-activated protein (MAP) kinase and phosphatidylinositol 3-kinase (PI3K) pathways, suggesting a role in signal transduction at the membrane in so-called 'nongenomic' signaling (Morley *et al.*, 1992; Le Mellay *et al.*, 1997; Migliaccio *et al.*, 1998; Bjornstrom and Sjoberg, 2005). The membrane receptor that initiates these signals is debated, but both ERα and ERβ, traditional nuclear ERs, can localize to the plasma membrane (Razandi *et al.*, 1999). ERα can be palmitoylated at

cysteine 447, and this residue is important for interaction with caveolin-1, as well as for downstream signaling to MAPK (Acconcia *et al.*, 2004). That cysteine residue is conserved in ERβ, suggesting that this protein also may be palmitoylated (Bourguignon *et al.*, 2005). Additional research into mechanisms of nongenomic estrogen signaling focused on the membrane microenvironment will serve to further illuminate these pathways and their potential for treatment of breast cancer.

One of the hallmarks of membrane rafts is the close packing of saturated lipid acyl chains, which makes these domains resistant to extraction with cold nonionic detergents. This property, coupled with their relatively low buoyant density, has been employed to isolate membrane rafts in vitro. Although some issues have been raised about this method of isolation (Shogomori and Brown, 2003), it remains a good biochemical starting point for understanding which proteins can be associated with such membrane domains.

Our laboratory has isolated a heavy detergent resistant membrane (DRM) fraction, called DRM-H, that contains ~23 neutrophil plasma membrane proteins (Nebl *et al.*, 2002). The DRM-H fraction exhibits a high buoyant density (~1.16 g/ml), relative to most DRMs (d=1.09-1.13), which are deficient in cytoskeletal proteins. However, DRM-H is rich in cytoskeletal proteins (fodrin, actin, myosins IG and II, vimentin, alpha-actinin and the F-actin- and myosin II- binding membrane protein, supervillin), as well as raft organizing proteins (stomatin and flotillin), signaling proteins (lyn kinase, heterotrimeric

G protein subunits) and the GPI-linked matrix metalloproteinase, MT-6-MMP. When total DRMs are isolated from neutrophil plasma membranes and resolved by sucrose gradient, the membrane raft proteins, Lyn, flotillin 2, and $G_{\alpha i\text{-}2}$, show a biphasic distribution, with a significant proportion co-purifying with membrane skeleton proteins (**Figure 3-1A, B**). These membrane skeleton proteins — fodrin, SV, myosin-IG, and actin — peak together in high buoyant density sucrose gradient fractions (DRM-H) (**Figure 3-1A, B**). The heavy chains of myosin-IIA and clathrin are enriched in fractions of intermediate density (**Figure 3-1A, B**). In the case of the $G_{\alpha i\text{-}2}$, SV can co-localize with endogenous raft proteins in isolated neutrophils (**Figure 3-1D**), verifying that isolated DRM-H components exist in complexes in vivo.

Most DRM preparations involve floating membranes through 30-35% sucrose (Brown and Rose, 1992) and discounting denser proteins as the cytoskeleton or Triton-soluble material. However the DRM-H complex isolated from neutrophil plasma membranes by our lab is, in fact, Triton-insoluble and associated with cholesterol-rich membranes, but its density of ~1.16 g/ml corresponds to sucrose concentrations of 37-40%, causing these complexes to not float in ample quantity in conventional sucrose gradients. This may have lead other researchers to overlook DRM-H.

Because lipid raft association with the actin cytoskeleton is crucial for many processes (Viola and Gupta, 2007), I hypothesize that DRM-H represents a subset of

membrane rafts involved in trafficking and/or signaling events at the plasma membrane of many, if not all, cell types.

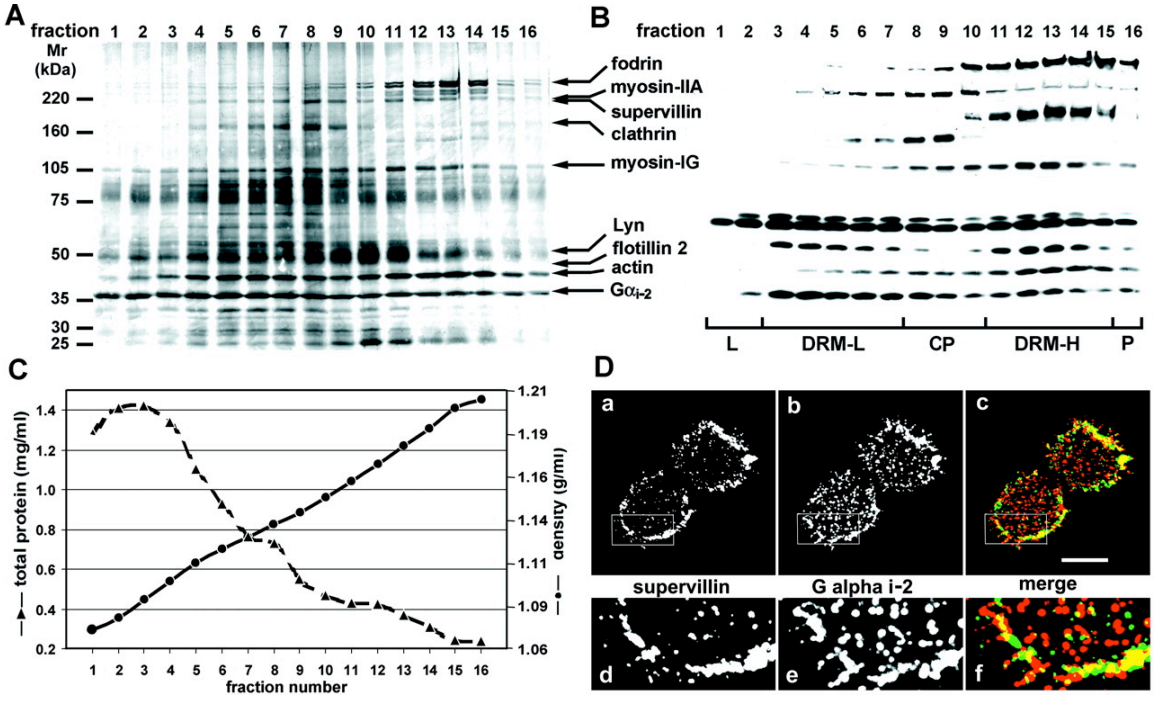


**Figure 3-1.** DRM-H represents a membrane skeleton-associated subset of leukocyte signaling domains.

(**A**) Silver-stained fractions (25µg/lane) after centrifugation of neutrophil plasma membrane DRMs into a linear 20-45% sucrose density gradient. This gradient contains opalescence visualized as DRM-L and DRM-H. Arrows show positions of the proteins visualized by immunoblot analyses.

(**B**) Immunoblot analyses of sucrose density gradient fractions. Fractions (25 µg/lane) from the gradient shown in (**A**) were blotted and probed with antibody against membrane skeleton (fodrin, supervillin, myosin-IG, actin, myosin-IIA), coated pit (clathrin), or lipid raft proteins (Lyn, flotillin 2, $G_{\alpha i\text{-}2}$). Numbers indicate sucrose density gradient fractions from top (1) to bottom (16). Approximate locations are shown for the gradient load (L), low density DRMs (DRM-L), coated pits (CP), high density DRMs (DRM-H), and pellet (P).

(**C**) Densities (circles) and apparent protein concentrations (triangles) of the sucrose gradient fractions shown in (**A**).

(**D**) Confocal immunofluorescence images show partial co-localization of supervillin and $G_{\alpha i\text{-}2}$ in peripheral micropatches of unroofed neutrophils. Neutrophils spread on poly-L-lysine-coated coverslips were mechanically sheared and stained with antibodies against supervillin (green) and $G_{\alpha i\text{-}2}$ (red). Overlap appears yellow (Merge). Bar, 2 µm.

## Materials and Methods

### Cell lines, plasmids and transfection

COS7-2 cells, a highly transfectable clone of COS7 (Kowalczyk *et al.*, 1997), were a generous gift from Dr. Kathleen J. Green (Northwestern University, IL). COS7 cells were grown in Dulbecco's modified Eagle high glucose media (DMEM, Invitrogen, GIBCO #11995) supplemented with 10% fetal calf serum (FCS) for ≤20 passages. Cells transfected with ERα or ERβ were sterol starved 24 hours prior to extraction in phenol red-free DMEM supplemented with 10% charcoal treated FCS.

Plasmids encoding EGFP-SV and EGFP-tagged SV domains have been described (Wulfkuhle *et al.*, 1999, Chen, 2003 #52). The plasmid encoding EGFP-SV-830-1010 was made cutting the EGFP-SV-830-1282 vector with EcoR1, purifying away from the cut fragment and ligating. Full length ERα and ERβ plasmids were kind gifts of Dr. Leigh C. Murphy. COS-7 cells were transfected using Effectene Transfection Reagent (Qiagen Inc.) for either 24 hours for EGFP-tagged SV domains, ERα and ERβ, or for 48 hours for full length EGFP-SV.

### Immunofluorescence

EGFP-SV transfected COS-7 cells were seeded onto gelatin-coated coverslips for 24 hours, and then fixed for 10 minutes with 4% paraformaldehyde in PBS. Cells were permeabilized for 5 minutes with 0.2% Triton X-100 in PBS before blocking for 30 minutes with 1% BSA, 0.5% Tween-20 in PBS and immunostaining for c-Yes at 1:100

dilution (BD Transduction Laboratories). AlexaFluor 568-conjugated secondary antibody against mouse IgG was from Invitrogen (Carlsbad, CA) and used at 1:2000 dilution. Slides were analyzed with a100X Plan-NeoFluor oil immersion objective (NA 1.3) on a Zeiss Axioskop fluorescence microscope, a RETIGA 1300 CCD camera (QImaging), and OpenLab 3.5.2 software.

**Preparation of Crude Membrane Fractions**

Adherent COS-7 cells were lysed and scraped into homogenization buffer (HB, 0.25 M sucrose, 5 mM Tris, pH 7.4, 1 mM $MgCl_2$, (Hiol *et al.*, 2003)) containing 1 mM PMSF, and a protease inhibitor cocktail (PI mix) containing: 1 mg/ml aprotinin, 1 mM antipain, 2 mM ALLM (calpain inhibitor II), 1 mM benzamidine, 10 mM E64, 1 mM leupeptin, and 1 mM pepstatin A. Lysates were homogenized with 10 strokes of a tight-fitting Teflon Dounce homogenizer and nuclei were pelleted by centrifugation for 5 minutes at 3000 x *g*. The precleared lysate was then subjected to a second 30-minute centrifugation of 20,000 x *g*. The resulting pellet is referred to as the crude membrane fraction. Cell equivalents of supernatant and pellet fractions were separated by SDS-PAGE and analyzed by immunoblotting for GFP (Roche).

**Membrane "ripoffs"**

"Footprints" of cells grown on glass coverslips were obtained by directing a stream of 37°C PHEM buffer (60 mM PIPES, 25 mM HEPES, 10 mM EGTA, 2 mM $MgCl_2$, pH 6.9, (Hartwig *et al.*, 1989)) from a 26 gauge needle attached to a 5 mL syringe. Cell patches were immediately fixed in 2% paraformaldehyde in PHEM for 15

minutes, permeabilized for 5 minutes with 0.2% Triton X-100 in PBS before blocking for 30 minutes with 1% BSA, 0.5% Tween-20 in PBS and immunostaining. F-actin was visualized with Texas Red phalloidin (Invitrogen).

**Preparation of DRMs**

*Sedimentation Gradients*

COS-7 cells were grown on 150 mm tissue culture dishes to ~75% confluency, rinsed twice with ice-cold PBS, and then extracted for 15 minutes on ice with 1 ml of Triton extraction buffer (TEB: 1% Triton X-100, 25 mM Tris, 250 mM NaCl, 2.5 mM MgCl2, 1 mM EGTA, 1 mM ATP) containing protease inhibitor cocktail (see above and Appendix B) and 1 mM PMSF. Cell lysate was gathered from the culture dish using a cell scraper, then transferred to a Dounce homogenizer. Lysates were homogenized with 10 strokes of a tight-fitting Teflon Dounce homogenizer and nuclei were pelleted by centrifugation for 10 minutes at 1000 x *g*. Cleared lysate (1 ml) was loaded into a SW55Ti ultracentrifuge tube (Beckman) atop a sucrose step gradient with the following steps: 0.5 ml of 10%, 1 ml of 30%, 1 ml of 40%, 1 ml of 50%, and 0.5 ml 64% sucrose in TEB. Gradients were centrifuged for 16 hours at 300,000 x *g*. All manipulations were performed on ice or at 4°C.

*Flotation Gradients*

COS-7 cells were transfected, as indicated in figure legend, and grown to ~75% confluency in 150 mm tissue culture dishes. Cells were extracted with 2 ml of 1% Triton X-100 in TNE buffer [(25 mM Tris, 150 mM NaCl, 5 mM EDTA) containing protease

inhibitor cocktail, and 1 mM PMSF, 20 μM phenylarsine oxide and 1 μM sodium orthovanadate] for 30 minutes, gathered from the culture dish using a cell scraper, then transferred to a Dounce homogenizer. Lysates were homogenized with 10 strokes of a tight-fitting Teflon Dounce homogenizer and nuclei were pelleted by centrifugation for 10 minutes at 1000 x *g*. 1.3 g of solid sucrose was added to the cleared lysate, then rotated for 15 minutes to mix before adding 1 ml of saturated (64%) sucrose solution and rotating for an additional 5 minutes. This sample was included in a sucrose density gradient with the following steps: 1 ml of 10%, 3 ml of 30%, 3 ml of 40%, 3 ml of sample (~50%) and 0.5 ml of 64% sucrose. Gradients were centrifuged for 16 hours at 200,000 x *g* in a Beckman SW41Ti rotor. All manipulations were performed on ice or at 4°C.

*Gradient fractionation and analysis*

Gradients were fractionated (300 μl) at a rate of 0.5 ml/min using a model 640 density gradient fractionator (Isco Inc., Lincoln, NE). Aliquots were assayed for total protein concentration using BCA assay reagent (Pierce), for density, and for individual proteins by SDS-PAGE (large 6-16% polyacrylamide gradient gels) and immunoblotting. The densities of sucrose solutions and resulting gradient fractions were determined by measuring refractive indices using a model 334610 refractometer (Bausch & Lomb, Rochester, NY).

**Immunoblotting**

For crude membrane preparations, equivalent fractions of initial cellular material

were loaded onto SDS-polyacrylamide gels (Laemmli, 1970), transferred to nitrocellulose membranes (Towbin *et al.*, 1979), blocked with 5% nonfat milk in tris-buffered saline with 0.1% Tween-20 (TBS-T), and probed with primary antibody against GFP (0.4 μg/ml, Roche, Indianapolis, IN). For density gradients, equal volumes of fraction were analyzed by SDS-PAGE followed by immunoblotting for: supervillin (0.2 – 0.4 μg/ml); transferrin receptor (1 μg/ml, Zymed, San Francisco, CA); flotillin 2 (0.125 μg/ml, BD Transduction Laboratories, San Jose, CA); c-Yes (0.25 μg/ml, BD Transduction Laboratories), fodrin (0.1 μg/ml, ICN, Aurora, IL); ERα (1 μg/ml clone D12, Santa Cruz Biotechnology, Santa Cruz, CA); and ERβ (5 μg/ml, GeneTex, San Antonio, TX). HRP-conjugated goat anti-mouse or goat anti-rabbit secondary antibodies (Jackson Laboratories, West Grove, PA), diluted 1:20,000, were detected by SuperSignal WestPico chemiluminescence (Pierce).

**Detection of GM1 ganglioside**

The relative amounts of the GM1 ganglioside were determined as described (Dolganiuc *et al.*, 2003). Briefly, an Immobilon-P membrane was rinsed with methanol, followed by $dH_2O$, and then PBS. Dot blots were made by spotting 10 μl of each gradient fraction onto the pre-treated membrane using the Easy Titer ELIFA system (Pierce). Membranes were allowed to dry overnight, then blocked with 5% nonfat milk in TBS-T and incubated with the peroxidase-conjugated cholera toxin B (0.25 μg/ml) for 30 minutes each. Signal was visualized with SuperSignal West Pico chemiluminescence (Pierce).

## Results

**EGFP-SV co-localizes with some clusters of c-Yes.** To investigate a potential relationship between the DRM-H marker protein, SV, and membrane rafts in COS-7 cells, I first utilized microscopy. Because typical membrane raft sizes are below the limit of light microscopy (Varma and Mayor, 1998; Pralle *et al.*, 2000), I plated EGFP-SV transfected COS-7 cells on a gelatin-coated coverslip in an effort to stimulate the cells and cluster individual rafts. Immunostaining for c-Yes, a Src-family kinase predominant in COS-7 cells, revealed several clusters, some of which co-localized with EGFP-SV; in other clusters, EGFP-SV was noticeably absent (**Figure 3-2**). Upon closer inspection, the c-Yes clusters are punctate structures (**Figure 3-2, inset**); the EGFP-SV does not overlap perfectly with the c-Yes punctae, but clusters within the same boundaries. Thus, SV can associate in the same structures as lipid raft proteins in vivo.

**Primary membrane targeting site of SV lies within amino acids 830-1010; secondary sites may exist in N- and C- termini.** To determine the membrane interaction domain(s) in SV, I expressed a series of EGFP-tagged versions of SV domains in COS-7 cells and fractionated these cells into membrane pellets (P) and cytoplasmic supernatants (S). Analysis by SDS-PAGE followed by immunoblotting shows strong membrane targeting of EGFP-SV-830-1010 (**Figure 3-3A**). The association of EGFP-SV-830-1010 with the membrane pellet is specific to the full-length construct, because apparent breakdown products remain in the supernatant. By the size of the breakdown product I can estimate that the last ~45 amino acids are essential for binding, narrowing the SV membrane

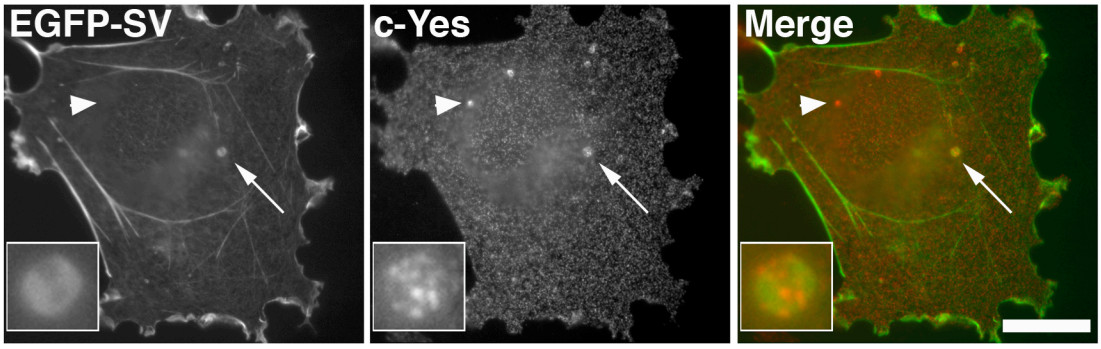


**Figure 3-2.** EGFP-SV co-distributes in some, but not all, c-Yes rich structures.

EGFP-SV transfected COS-7 cells (left panel, green in Merge) were plated on gelatin coated coverslips and immunostained with c-Yes antibody (center panel, red in Merge). Some of the c-Yes clusters are associated with EGFP-SV (arrow, inset); others are not (arrowhead). Insets enlarged 7-fold. Bar, 20 μm.

association domain to amino acids ~965-1010. By fluorescence and light microscopy, I observe punctate EGFP-SV-830-1010 co-localizing with phase dense particles (**Figure 3-3B**), which may represent vesicles from the sheared membrane. In addition, EGFP-SV-830-1010 remains with the cell "footprint" on the coverslip without detectable F-actin after physical disruption of intact cells (**Figure 3-3C**), suggesting that EGFP-SV-830-1010 association with the plasma membrane is independent of F-actin, as expected given that the characterized actin-binding sites in SV lie outside of this sequence.

While EGFP only shows no association with the membrane pellet, EGFP-SV-1-830 is moderately associated, and EGFP-SV-1010-1792 shows a small amount of membrane association (**Figure 3-3A**). In a similar experiment, EGPF-SV-1-171 is also observed in the membrane pellet (data not shown), suggesting that the extreme N-terminus of SV can also potentiate binding to membranes. Thus, SV may have multiple modes of membrane targeting, as is the case for other lipid raft proteins (Resh, 1999, 2004).

In a preliminary experiment with the isolated crude membranes, both EGFP-SV-1-830 and EGFP-SV-830-1010 resist extraction with cold 1% Triton X-100, while much of the EGFP-SV-1010-1792 is extracted from the membrane pellet (data not shown). This suggests that the membrane targeting sequences in SV may also direct the protein to lipid rafts.

**COS-7 cells have complexes similar to DRM-H in neutrophils.** DRM-H fractions can be isolated from COS-7 cells using a protocol similar to that used with neutrophils

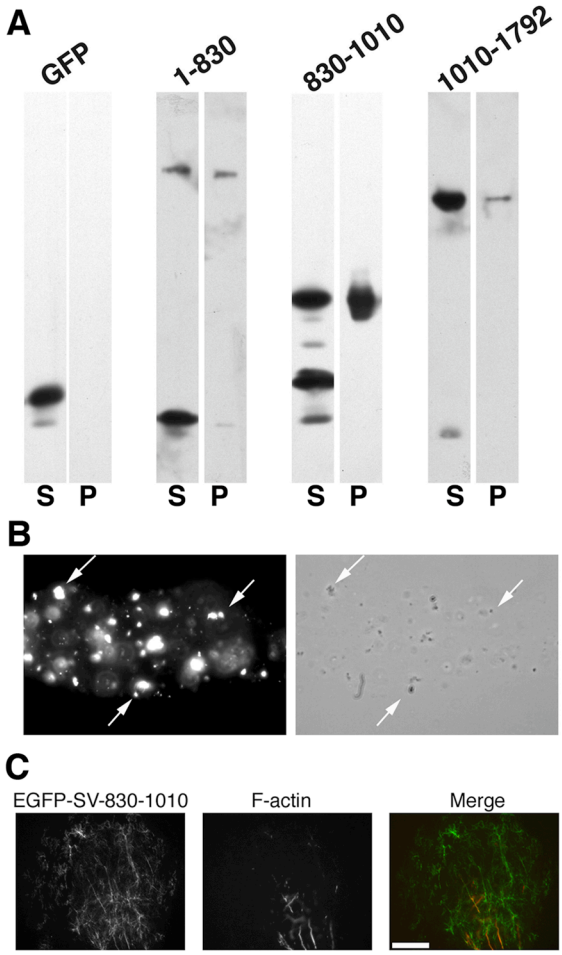


**Figure 3-3.** Primary membrane targeting site of SV lies within amino acids 830-1010; secondary sites may exist in N- and C- termini.

(**A**) Precleared lysates from COS-7 cells transfected with the indicated EGPF-tagged constructs of supervillin domains were separated into a crude membrane pellet (P) and supernatant (S) by a 20,000 x *g* spin.

(**B**) Crude membrane fractions from EGFP-SV-830-1010 transfected COS-7 cells on poly-L-lysine coated coverslips were imaged for green fluorescence (**left panel**) and phase contrast (**right panel**). Arrows indicate examples of areas of membrane associated EGFP-SV-830-1010 that co-localize with phase dense particles.

(**C**) EGFP-SV-830-1010 (**left panel**) remains attached to the coverslip even without detectable F-actin (**center panel**). Image of "unroofed" COS-7 cell expressing EGFP-SV-830-1010. Remaining cell footprints were stained for F-actin with Texas red phalloidin. Bar, 10 μm.

(**Figures 3-4, 3-5**). First, I investigated the density gradient profile of COS-7 cell SV, a tightly associated DRM-H marker in neutrophils (Nebl *et al.*, 2002), when sedimented into a sucrose gradient. COS-7 cells extracted in cold 1% Triton X-100 were loaded at the top of a sucrose step gradient, centrifuged for 16 hours at 300,000 x *g*, fractionated and analyzed by immunoblots (**Figure 3-4**). SV peaks in these gradients at densities ranging from 1.12 to 1.17 g/ml, in accordance with our results with neutrophil DRM-H. Additional SV signal is seen toward the bottom of the gradient, which probably corresponds to the purely cytoskeletal (as opposed to membrane cytoskeletal) population. The presence of different biochemical classes of SV in the density gradient corresponds well with the varying localizations I see in the cell (**Figure 3-2**). Fodrin (non-erythroid spectrin) co-migrates with SV in the gradient. c-Yes and flotillin-2 are lipid raft resident proteins, and accordingly are seen predominantly at DRM-L densities, with relatively smaller amounts at DRM-H densities. Surprisingly, the transferrin receptor (TfR) also peaks in the DRM-H fractions. TfR is a supposed non-lipid raft protein (Harder *et al.*, 1998), although TfR2 has been reported in low-density membrane domains with caveolin 1 (Calzolari *et al.*, 2006). Complexes were most likely at equilibrium density because the gradient profile looks similar for many marker proteins after 42 hours (data not shown). In this case there may have been insufficient detergent solubilization leading to TfR association with lighter membrane fractions.

Although these results obtained by sedimentation into density gradients are consistent with the existence of DRM-H in COS-7 cells, it is not certain that these membrane complexes are completely separated from other protein complexes moving

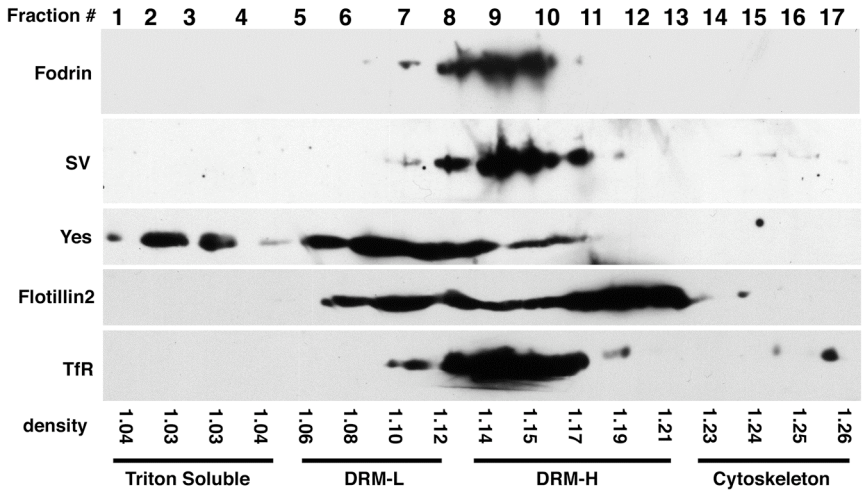


**Figure 3-4.** SV co-sediments with fodrin in a heavy DRM fraction in COS-7 cells, similar to the density of DRM-H in neutrophils.

COS-7 cells were extracted with TEB, and the lysate was sedimented into a sucrose gradient. Gradient fractions were analyzed by SDS-PAGE followed by immunoblotting for fodrin, SV, c-yes, flotillin 2, and TfR, as indicated. Densities of fractions are shown in g/mL (bottom row).

Approximate locations, based on density, of Triton soluble proteins (load), DRM-L, DRM-H and the cytoskeleton are shown.

The majority of SV signal lies within DRM-H densities; additional, less intense signals are found in DRM-L and the cytoskeleton.

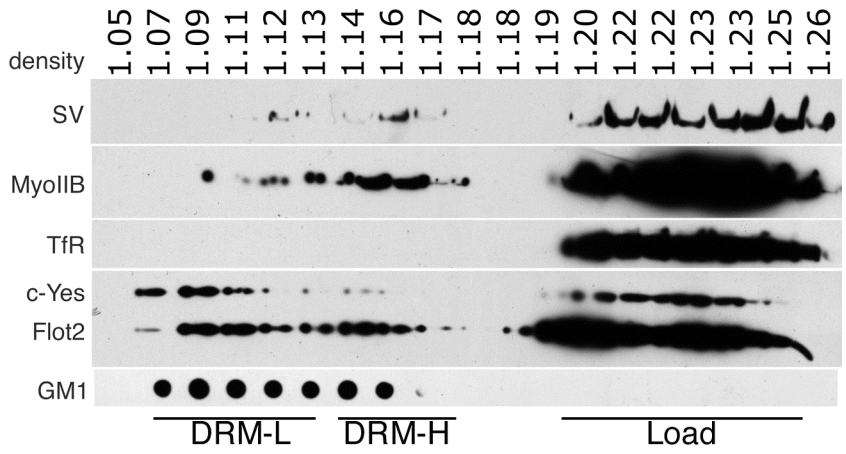


**Figure 3-5.** COS-7 cell DRM-H is also apparent upon flotation through sucrose gradients.

Profile of sucrose density gradient in which COS-7 cells, extracted in cold 1% Triton-X-100 in TNE, were loaded at the bottom of the gradient and centrifuged overnight for complexes to reach equilibrium density. Equal volumes of gradient fractions were analyzed by SDS-PAGE followed by immunoblotting for SV, myosin IIB (MyoIIB), transferrin receptor (TfR), c-Yes, and flotillin 2 (Flot2) and dot blot for ganglioside GM1, as indicated. Densities of fractions are shown in g/mL (top row). Approximate locations of input (Load) and DRM-L, DRM-H are shown.

down the gradient. For additional confirmation of DRM-H in COS-7 cells, I examined whether SV and the other cytoskeleton and lipid raft markers would float to appropriate DRM-H density when loaded at the bottom of a sucrose gradient (**Figure 3-5**). As in the case with neutrophil plasma membranes, two peaks of DRMs are apparent with many of the lipid raft markers, including c-Yes, flotillin 2 and the ganglioside GM1: a lighter peak (DRM-L) with densities of 1.09-1.11 g/ml and a denser peak (DRM-H) with densities of 1.14-1.17 g/ml. SV and myosin IIB mark both DRM populations, but greater intensity is evident in DRM-H. Interestingly, TfR does not isolate to DRM-H densities in this gradient, which was done with increased amounts of detergent (**Figure 3-5**). Together these experiments demonstrate that cytoskeletal-associated light membrane complexes, DRM-H, exist in cells other than bovine neutrophils.

**Estrogen receptors α and β both isolate with DRM-H.** The studies that connected ERα and ERβ to lipid rafts and DRMs did not differentiate between DRM-L and the cytoskeletally associated DRM-H. I investigated the possibility of differential targeting by isolating DRMs from ERα- and ERβ-transfected COS-7 cells (**Figure 3-6**). Indeed, I see that some ERα floats to the DRM-H density of 1.17 g/ml with the peak of SV (**Figure 3-6A**). In these experiments, I cannot detect ERα in the DRM-L fraction. This could be due to many factors. The level of ERα seen floating into the gradient is a very small percentage of the amount remaining in the load. Therefore, COS-7 cells may be limited in necessary factors to target all of the exogenously expressed ERα to the proper compartment. Alternatively, ERα could have a higher affinity for proteins that

preferentially distribute to DRM-H, including SV, which may be relatively more abundant in COS-7 cells. In this context, I note that ERα interacts with SV in a yeast two-hybrid assay (Ting *et al*., 2002). ERβ, on the other hand, seems to be equally distributed between DRM-L and DRM-H fractions (**Figure 3-6B**). Based on these results, I hypothesize that DRM-H could serve as a scaffold for nongenomic estrogen signaling events at the membrane.

The bulk of both exogenously expressed proteins remain at the bottom of the gradient. A study by Razandi, et al. determined that transfection of ERα into an ER-negative breast cancer cell line resulted in only ~5% plasma membrane localization (Razandi *et al.*, 2003). Additional studies indicate that other intracellular populations exist in the mitochondria and the endoplasmic reticulum (Govind and Thampan, 2003; Chen *et al.*, 2004). Thus, it is not surprising that the majority of ERα and ERβ do not float in these assays.

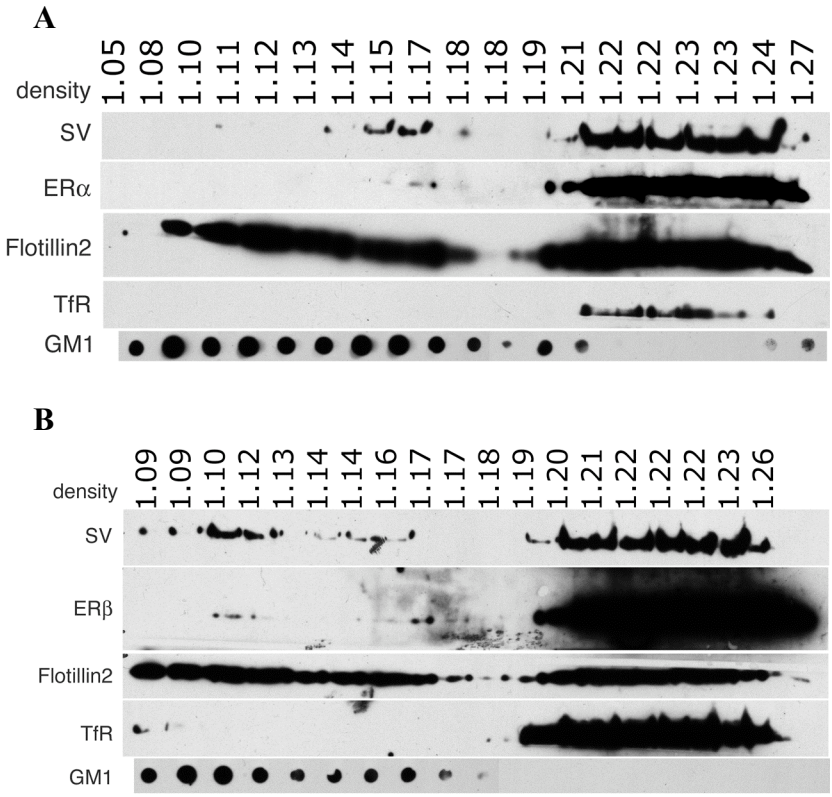


**Figure 3-6.** Some ERα associates with DRM-H; some ERβ associates with both DRM-L and DRM-H.

Gradient profiles of COS-7 cells extracted with cold 1% Triton after transfection with (**A**) ERα or (**B**) ERβ for 24 hours. Aliquots of gradient fraction (100 μl) were analyzed by SDS-PAGE followed by immunoblotting for SV, c-yes, flotillin 2, and TfR, as indicated. Densities of fractions are shown in g/mL (bottom row).

## Discussion

I show here that a DRM-H fraction similar both in composition and buoyant density to the DRM-H complex first isolated from neutrophil plasma membranes (**Figure 3-1**, (Nebl *et al.*, 2002)) exists in COS-7 cells (**Figures 3-4, 3-5)**. In addition, SV, a protein shown to be proximal to the membrane in the neutrophil DRM-H fraction, co-distributes with the membrane raft marker, c-Yes, in these cells (**Figure 3-2**). I have identified a strong membrane interaction domain in SV-830-1010 as well as weaker interaction domains in the amino- and carboxy-termini (**Figure 3-3**). Additional data show ERα associates with DRM-H, while ERβ is seen in both DRM populations (**Figure 3-6**), suggesting a role for DRM-H in non-genomic estrogen signaling.

These studies have provided some preliminary data for SV membrane targeting domains. While I have identified some membrane interaction domains in SV (**Figure 3-3**), it is likely that these membrane preparations contain associated cytoskeletal proteins, making it possible that membrane binding is indirect. However, the SV fragment that showed the strongest association with crude membranes does not contain any of the three F-actin binding domains, or the myosin II, L-MLCK, cortactin or TRIP6 binding sites within SV-1-830, suggesting that this assay is reflective of binding to another protein or lipid tightly associated with the plasma membrane. Liposome binding assays will be necessary to further characterize the membrane binding domains of SV. In addition, the raft association domain of SV was not determined. In my hands, EGFP alone floated to DRM-L densities, making DRM association of all other EGFP-SV constructs suspicious.

EGFP can aggregate, leading to association with membrane rafts. Monomeric-GFP (Zacharias *et al.*, 2002) or other, non-raft epitope tags could be used in future studies to determine the SV raft association site.

The membrane raft field has been somewhat controversial (Lai, 2003; Munro, 2003; Nichols, 2005; Hancock, 2006), in part due to the relationship of isolated DRMs and membrane rafts. DRM analysis can contribute to identification of components, but it is not a substitute for careful in vivo studies of membrane rafts (Edidin, 2003; Lichtenberg *et al.*, 2005). Detergent treatment of membranes can result in artificial clustering of rafts (Heerklotz, 2002), or loss of proteins that do interact with rafts. One study documented 2-3 fold increases in the amount of a GPI-linked protein isolated in DRMs compared to the raft fraction determined by fluorescence correlation spectroscopy in model membranes (Kahya *et al.*, 2005). Another caveat to the bulk biochemical isolation of DRMs is that proteins that co-isolate in the sucrose gradient may have originated from distinct regions of the cell (Gomez-Mouton *et al.*, 2004). A better method of studying membrane rafts is tracking multiple protein movements simultaneously with fluorescence correlation spectroscopy. However, the in vivo tools available for membrane raft analysis require specific proteins to be known. Identification of proteins purified in DRM purification can be used a guideline for designing experiments linking the co-isolating proteins in vivo.

Since our first paper describing DRM-H (Nebl *et al.*, 2002), other studies have

found roles for DRM-H in various signaling processes. Newcastle disease virus proteins associate with DRM-H fractions in transfected (Dolganiuc *et al.*, 2003) and virus-infected (Laliberte *et al.*, 2006; Laliberte *et al.*, 2007) cells, and raft association has a role in infectivity of released virus. The tumor suppressor merlin shifts from a DRM-H to DRM-L-density when acting in its growth suppressive mode; the loss of Triton-insolubility in neurofibromatosis-2 patients with merlin mutations supports the potential significance of membrane raft association (Stickney *et al.*, 2004). Lectins on the surface of the parasitic protozoan Entamoeba histolytica, the causative agent of amoebic dysentery, are present in DRM-H fractions, and raft integrity is necessary for fluid-phase pinocytosis and adhesion to host cell monolayers, both important virulence factors (Laughlin *et al.*, 2004). In addition, the DRM-H proteins fodrin, supervillin, myosin II, vimentin, and actin were found by proteomic analysis to co-isolate with T-cell DRMs (von Haller *et al.*, 2001).

Breast cancers that have gone into remission after antiestrogen treatment often relapse after 12-18 months. One hypothesis is that cancer cells undergo biochemical changes that allow them to adapt to lower estrogen levels. This 'adaptive hypersensitivity' to estrogen is thought to occur through nongenomic signaling (Santen *et al.*, 2004). Although debate exists over the plasma membrane receptor for estrogen, both ERα and ERβ interact with membrane rafts (Chambliss *et al.*, 2002; Acconcia *et al.*, 2005a). However, estrogen elicits different responses when signaling through ERα *vs.* ERβ (Acconcia *et al.*, 2005b). Lateral compartmentalization in the membrane, possibly

represented by the different amounts in of each receptor in DRM-L *vs.* DRM-H seen in these preliminary experiments, could account for the differences in signaling. In vivo functional studies will determine if there is a role for SV, or other DRM-H proteins in nongenomic signaling.

Taken together, I conclude that cytoskeleton-association with membrane rafts, biochemically isolated as DRM-H, is a widespread phenomenon that participates in numerous signaling pathways.

# Chapter IV

## General Discussion

At the beginning of my dissertation, SV was known to be an actin-binding peripheral membrane protein that partially co-localized with focal adhesions, but little was known about its function. Work presented in this dissertation elucidates a function for SV in matrix degradation at invadopodia (**Chapter II**). We also show that SV is closely affiliated with a population of cytoskeleton-associated DRMs (DRM-H) that is found in neutrophils (Nebl *et al.*, 2002), COS-7 cells (**Chapter III**), and possibly skeletal muscle ((Oh *et al.*, 2003), **Appendix A**). DRM-H may represent a subset of membrane rafts that integrate membrane signaling with the underlying actin cytoskeleton. The presence of ERα and ERβ in DRM-H suggest a role in nongenomic estrogen signaling. I have also determined that SV binds to the S2 regulatory region of myosin II ((Chen *et al.*, 2003), **Appendix A**), helping to change the view of SV from an actin-binding focal adhesion protein to a myosin regulatory protein. During the course of my thesis, my colleagues in the lab have expanded on this, showing SV regulation of myosin II during cell spreading by interacting with the long form of myosin light chain kinase (Takizawa *et al.*, 2007). The myosin II-binding site in SV that I identified also regulates focal adhesion integrity, presumably through a similar enhancement of myosin II contractility (Takizawa *et al.*, 2006).

*SV induced F-actin punctae*

SV localizes to and regulates focal adhesions (Wulfkuhle *et al.*, 1999; Takizawa *et al.*, 2006). However, the F-actin punctae induced by EGFP-SV in COS-7 cells are decidedly distinct from focal adhesions (**Chapter II**). The presence of the podosome/invadopodia marker proteins, cortactin, Tks5 and cdc42 in these punctae, coupled with their dynamic nature and the ability, in some cases, to localize over areas of matrix degradation lead to the hypothesis that these structures may represent podosome/invadopodia "building blocks". Consistent with findings on podosomes and invadopodia (Artym *et al.*, 2006; Zhou *et al.*, 2006; Clark *et al.*, 2007), the formation of SV punctae is partially blocked by cortactin knockdown (**Figure 2-7**).

In an effort to understand other contributing pathway(s) involved in the formation of SV punctae, I hypothesized that these punctae are podosome-like structures and/or podosome/invadopodia precursors. Therefore, I attempted several co-expression and drug treatment experiments that affect podosome/invadopodia formation. First, I co-transfected EGFP-SV and two cortactin truncation mutants that interfere with actin polymerization during podosome formation (Webb *et al.*, 2006a) to determine if punctae formation was affected. The C-terminus of cortactin (C-cort), which lacks the ability to bind actin and Arp2/3, but retains N-WASp binding, inhibits podosome formation in smooth muscle cells. Full length cortactin with a point mutation eliminating N-WASp binding has no effect on the percentage of cells with podosomes, but drastically reduces the number of podosomes per cell in smooth muscle cells (Webb *et al.*, 2006a). Both

constructs co-localized slightly with, but did not eliminate the formation of, EGFP-SV induced punctae (data not shown). However, given that there was only a partial decrease in punctae formation following cortactin knockdown (**Figure 2-7**), the results with the cortactin mutants should be similarly quantified. N-WASp is an important activator of F-actin assembly at podosomes and invadopodia(Mizutani *et al.*, 2002; Yamaguchi *et al.*, 2005a). Therefore, I co-expressed mRFP-SV and dominant negative EGFP-N-WASp-ΔA that lacks Arp2/3 binding (Magdalena *et al.*, 2003). SV punctae still formed in the presence of this construct (data not shown). However, I'm not confident that N-WASp is not involved because this construct also allowed formation of Src-induced podosomes, which are dependent on N-WASp (Linder and Aepfelbacher, 2003). I also saw that EGFP-SV punctae formation was not inhibited by co-expression of dynamin2-K44A (gift of Mark McNiven, Mayo Clinic), a dominant negative form of the membrane bound GTPase that inhibits actin turnover at podosomes (Ochoa *et al.*, 2000) and matrix degradation at invadopodia (Baldassarre *et al.*, 2003). Inhibition of Src, a key signaling molecule in podosome and invadopodia formation (Buccione *et al.*, 2009), by co-transfection of dominant negative Src(Y527F/K295R) (gift of Steve Hanks, Vanderbilt University), or treatment with PP2 Src inhibitor also did not prevent EGFP-SV punctae formation (data not shown). Although these experiments should be carefully quantified to be more conclusive, they suggest that multiple, partially redundant pathways may contribute to SV punctae formation, similar to the multiple inputs described for invadopodia formation (Ayala *et al.*, 2008).

*SV role in Src-induced podosome formation*

Knockdown experiments suggest that SV is not required for podosome formation in COS-7 cells expressing constitutively active Src (**Figure 2-18**). Because siRNA treatment does not completely eliminate SV (~10% of SV remains), I also simultaneously investigated whether dominant negative SV constructs would interfere with podosome formation. In addition to its F-actin-binding site, EGFP-SV-342-570 binds to TRIP6 and negatively regulates stress fibers and focal adhesions (Takizawa *et al.*, 2006). EGFP-SV-Δ342-570 lacks this domain, and is largely absent from focal adhesions. EGFP-SV-Δ1-171 lacks the myosin II binding domain. When co-transfected with constitutively active Src, these constructs all allow podosome formation (data not shown). The signal to form podosomes by constitutively active Src is very strong. In fact, I tried to inhibit constitutively active Src in COS-7 cells with 100 μM PP2. After 1 hour, cells still contained numerous podosomes, even though podosome lifetime is 2-12 minutes (Evans *et al.*, 2003). Therefore, SV may be acting upstream of Src, or the dominance of constitutively active Src may mask any contribution from SV. In addition, podosome dynamics were not examined in SV knockdown or dominant negative SV cells. If SV plays an analogous role in podosomes as it does in focal adhesions, it could affect structure turnover. It is also important to note that in MDA-MB-231 cells, SV knockdown affected matrix degradation, but not the formation of F-actin rich structures on the ventral cell surface. This supports a role for SV in the function of invadopodia/podosomes, but not in the initial formation of the actin structure.

*SV effects on invadopodia function*

In this work, we demonstrate that SV functions in the efficient matrix degradation at invadopodia (**Chapter II,** (Crowley *et al.*, 2008)), likely through its interaction with cortactin. However, more work is needed to reveal the full mechanism of SV action at invadopodia. Experiments that determine at which timepoint SV acts in invadopodia formation could contribute our mechanistic understanding. Four stages of invadopodia formation have been described (Artym *et al.*, 2006). First, there is the appearance of cortactin and F-actin at the invadopodial initiation site. The preinvadopodia stage (Stage II) is marked by the appearance of MT1-MMP, with additional accumulation of cortactin and F-actin. A mature invadopodia (Stage III) begins degrading matrix. In late stage invadopodia (Stage IV), cortactin and F-actin diffuse but MT1-MMP remains and can continue matrix degradation. Based on the presence of ventral F-actin clusters in SV knockdown cells without accompanying matrix degradation, it is likely that SV functions at a later stage in invadopodia formation (**Figure 2-17**). It is not clear if the ventral F-actin structures seen are stalled invadopodia initiation sites (Stage I) or preinvadopodia (Stage II).

To determine at which stage SV affects invadopodia function, two approaches could be taken. First, one could take advantage of an invadopodia synchronization technique described by the Buccione laboratory (Ayala *et al.*, 2008). In brief, cells are plated on a gelatin substrate, but their degradative capacity is inhibited by the synthetic reversible broad-spectrum metalloprotease inhibitor batimastat (BB94). Cells can be

transfected with plasmids or siRNA, and incubated for up to 96 hours in the presence of the inhibitor. When the cells are expressing the desired target protein or have downregulated a protein of interest, the inhibitor is washed out and cells can resume normal matrix degradation. At a fixed timepoint following drug washout, SV knockdown cells could be stained for cortactin and MT1-MMP, and amounts of cortactin clusters with and without associated MT1-MMP and localized matrix degradation could be quantified. I would expect SV knockdown to increase the number of invadopodial initiation sites (Stage I invadopodia) compared to control, and SV overexpression to decrease the relative amount of Stage 1 invadopodia by increasing the efficiency of MT1-MMP targeting to invadopodia. This system could also be used to determine the domain(s) of SV necessary for matrix degradation at invadopodia by transfection of a series of SV domain constructs after SV knockdown.

Another technique that could elucidate SV effects on invadopodia is live cell imaging. Based on my results of SV overexpression in MDA-MB-231 cells (**Figure 2-14**), a logical hypothesis is that SV promotes turnover of invadopodia, thereby increasing the amount of matrix holes formed. Movies of EGFP-SV and RFP-cortactin, and/or RFP-SV and EGFP-MT1-MMP on gelatin could provide data on the lifetime of invadopodia, as well as the time of invadopodia initiation to the onset of degradation. Based on COS-7 cell experiments, SV causes a redistribution of cortactin to the ventral cell surface (**Figure 2-5**). SV overexpression in MDA-MB-231 cells could similarly target cortactin to potential invadopodia initiation sites. It would also be interesting to see the dynamics of cortactin and MT1-MMP in SV knockdown cells. The lack of SV

may be blocking a pathway for MT1-MMP or other MMPs to reach the ventral cell surface, especially under the cell center, which may become evident in real-time images.

The recent detection of a direct interaction between SV and cortactin (**Figure 2-7**) further supports a role for SV at invadopodia. While it requires further characterization, it does provide a basis for other observations. For example, the EGFP-SV/F-actin/cortactin punctae we observe closely resemble cortactin structures seen in association with endosomes (Kaksonen *et al.*, 2000), in static images as well as their dynamic properties. Thus, these actin-binding proteins (SV and cortactin) may not be merely playing a structural role in invadopodia formation, but may contribute to their function in matrix degradation through the trafficking of proteases to the cell surface. In fact, secretion and surface expression of MMPs is dependent on cortactin protein levels (Clark *et al.*, 2007). Additionally, cortactin and dynamin2 regulate protein traffic from the *trans*-Golgi network (Cao *et al.*, 2005) and the Golgi has been shown to be oriented toward invadopodia (Baldassarre *et al.*, 2003). Though the role of cortactin in promoting actin nucleation at invadopodia has been well studied, little is known about how cortactin arrives at invadopodia initiation sites. The observation that SV redistributes cortactin to the ventral cell surface in COS-7 cells leads to the hypothesis that SV increases matrix degradation at invadopodia by increasing the efficiency of cortactin targeting. Consequently, SV may act in concert with cortactin to regulate exocytosis of MMPs to the plasma membrane for matrix degradation.

*Membrane rafts and invadopodia*

There are many studies that support the intersection of my data involving SV at membrane rafts and SV at invadopodia. First, focal adhesions show a high degree of membrane order that depends on caveolin and integrin engagement with the ECM (Gaus *et al.*, 2006). Because podosomes and invadopodia share many components of focal adhesions, it is possible that membrane rafts are present in these structures and act to compartmentalize them from the surrounding plasma membrane. Membrane rafts have been shown to positively regulate the activation of integrins (Leitinger and Hogg, 2002), which make the initial contact with the ECM, triggering the cascade of events leading to invadopodia formation (Mueller *et al.*, 1999). Also, inhibition of the epidermal growth factor (EGF) receptor, a protein long identified with membrane raft signaling (Mineo *et al.*, 1996), disrupts invadopodia formation (Yamaguchi *et al.*, 2005a). A recent paper describes EGF-induced coalescence of membrane rafts of different composition, suggesting an ability to assemble signaling platforms (Hofman *et al.*, 2008).

Another overlap of membrane raft and invadopodia signaling involves Arf6 and MT1-MMP. Arf6 is a small GTPase that regulates endosome membrane trafficking to the plasma membrane, actin remodeling and cell migration (Boshans *et al.*, 2000; Palacios *et al.*, 2001; Donaldson and Honda, 2005; D'Souza-Schorey and Chavrier, 2006). This protein is also involved in trafficking of membrane rafts along microtubules to the cell surface for spreading, regulating Rac1 activation and raft recruitment (Balasubramanian *et al.*, 2007). Arf6 is abundant in highly invasive breast cancer cells

and is required for matrix degradation at invadopodia (Hashimoto *et al.*, 2004; Tague *et al.*, 2004; Hoover *et al.*, 2005). In addition, the role of Arf6 in invadopodia formation is dependent on ERK activity (Hashimoto *et al.*, 2004). Here, it is worth noting that the smooth muscle isoform of SV, SmAV, is required for stimulus-mediated contractility through ERK signaling (Gangopadhyay *et al.*, 2004) and that SV co-localizes with Arf6 in membrane tubules (E. Luna and Z. Fang, unpublished data). MT1-MMP activity also promotes the sustained phosphorylation of ERK1/2 (Takino *et al.*, 2006), and MT1-MMP must be released from DRM-confinement to be active (Mazzone *et al.*, 2004). So, it is likely that SV, as a component of DRM-H and its ability to activate the ERK pathway, works in concert with Arf6 to traffic MMPs to invadopodia for efficient matrix degradation.

In light of my data and the existing literature, I propose the following model for matrix degradation at invadopodia involving SV (**Figure 4-1**). SV activates ERK signaling upstream of cortactin in a membrane raft in a recycling endosome compartment with Arf6. SV facilitates exocytosis by possibly binding to microtubule motor proteins (T. Smith, unpublished data) to move exocytic vesicles along microtubules to invadopodia initiation sites, delivering MMPs in the process. The SV-cortactin interaction could contribute to invadopodial targeting of outgoing vesicles. Alternatively, SV could be promoting cortactin trafficking to invadopodia, and cortactin subsequently increases MMP trafficking.

The overall goal of this research was to provide a fundamental understanding of how invasive cells move. Crucial to the cell's ability to move are adhesion and invasion. SV and its many interacting proteins have profound effects on both of these properties. Ideally, the continued molecular dissection of invadopodia could lead to identification of promising targets for medical intervention in the metastatic spread of cancer.

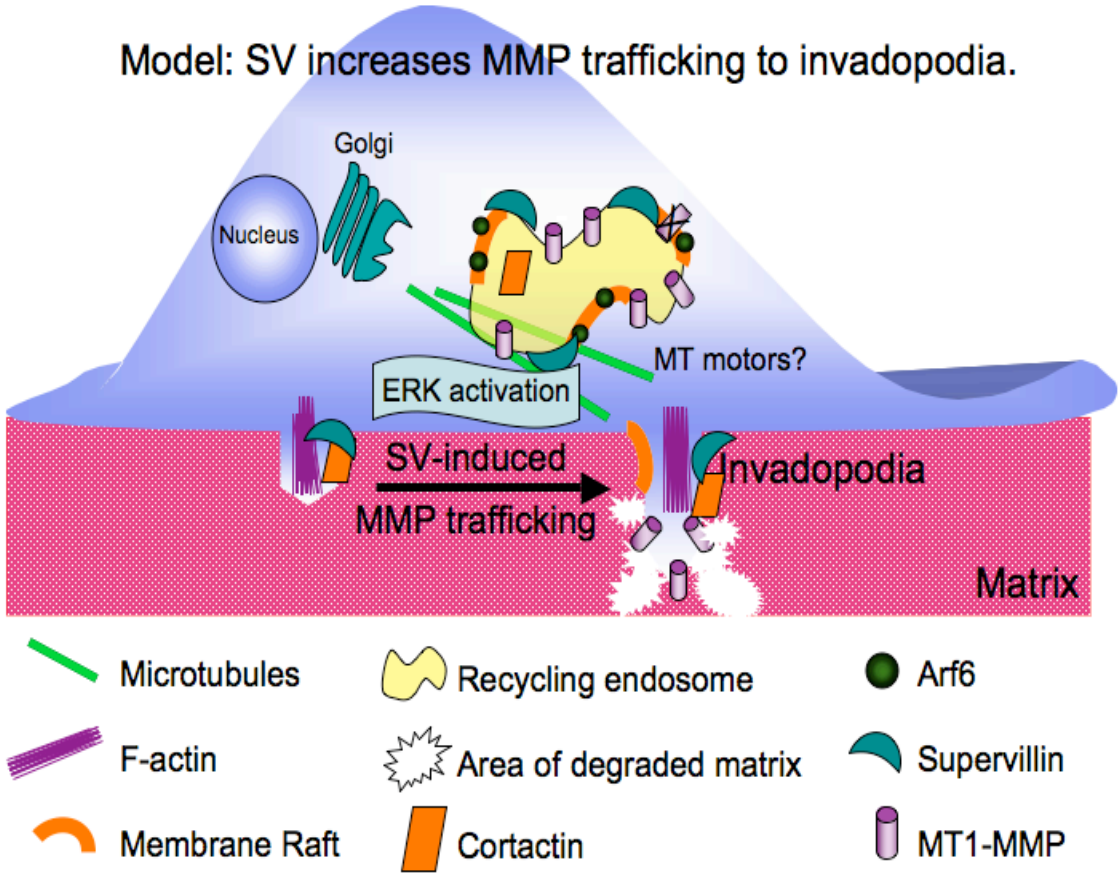


**Figure 4-1.** Model for the role of SV in degrading matrix at invadopodia.

SV promotes ERK activation, stimulating trafficking of cortactin, Arf6, MT1-MMP and SV from an endosome compartment containing membrane rafts to the invadopodia initiation site. This trafficking may involve microtubule (MT) motors that bind to SV (unpublished data). The SV-cortactin interaction may be involved in targeting vesicles to the nascent invadopodia. MT1-MMP is inactive in membrane rafts (X) and may move out of the raft compartment when it reaches the invadopodium.

# Appendix A

## Supervillin/Archvillin binding partners

This body of work explores experiments identifying supervillin and archvillin interacting proteins. These experiments contributed to early understanding of SV function, and were published as part of two manuscripts from the Luna Laboratory (Chen *et al.*, 2003; Oh *et al.*, 2003).

### Archvillin binds F-actin and associates with membranes.

The supervillin C-terminus displays a high degree of homology with the villin/gelsolin family of actin bundling/severing proteins. However, this domain in SV lacks the ability to bind to F-actin (Pestonjamasp *et al.*, 1997; Pope *et al.*, 1998; Wulfkuhle *et al.*, 1999). Instead, the SV F-actin binding activity is confined to the N-terminus (Wulfkuhle *et al.*, 1999). The skeletal muscle form of SV, archvillin (AV), differs from SV by two muscle-specific inserts in the N-terminus. The goal of these experiments was to determine if the muscle-specific inserts interfere with F-actin binding activity.

### Results

### Supervillin-related protein in muscle and myogenic cells

A 250 kDa protein characteristic of mammalian muscle and myogenic cell lines was identified using two affinity-purified polyclonal antibodies specific for different sequences in the 205 kDa non-muscle SV protein (**Figure A-1)**. The α-H340 antibody,

directed against the first 340 residues of human SV, specifically recognizes SV in bovine neutrophils (Nebl *et al.*, 2002). This antibody also recognized SV (205 kDa) in HeLa cells (**Figure A-1A**, lane 1, asterisk) and a larger, 250 kDa polypeptide in human 50MB-1 myoblasts (**Figure A-1A**, lane 2) and in hamster (**Figure A-1A**, lane 3) and rabbit (**Figure A-1B**, lane 1) striated muscle. Specificity of the α-H340 antibody for SV-related sequences in muscle was shown both by immunoblot analyses (**Figure A-1A, B**) and in immunofluorescence micrographs of human (**Figure A-1C**) and murine (data not shown) myogenic cells. The α-pepA antibody, which was previously shown to be specific for amino acids 900-918 in bovine SV (Pestonjamasp *et al.*, 1997), also recognized a 250 kDa polypeptide in rabbit skeletal muscle (**Figure A-1A**, lane 4), 50MB-1 myoblasts (data not shown) and C2C12 myoblasts (data not shown). A similarly sized, immunocrossreactive polypeptide in SDS-solubilized murine leg muscle was specifically immunoprecipitated with α-H340 antibody (**Figure A-1D**). After electrophoresis on SDS-polyacrylamide gels and electrotransfer to nitrocellulose, the immunoprecipitated polypeptide bound directly to α-H340 antibody and to radiolabeled F-actin (**Figure A-1D**, lane 2). Finally, the cross-reactive muscle protein co-fractionated with the sarcolemmal proteins, dystrophin and caveolin-3, as part of a low-density plasma membrane fraction from rabbit skeletal muscle (**Figure A-1E**, light fraction). These results show that the muscle protein (archvillin, AV), which is consistently larger than SV in several species and throughout myogenic differentiation, resembles non-muscle SV in that these proteins contain at least two epitopes in common, bind F-actin on blot overlays and are associated with plasma membranes. These predictions are supported by

molecular cloning, which shows that AV is a larger splice form of non-muscle SV.

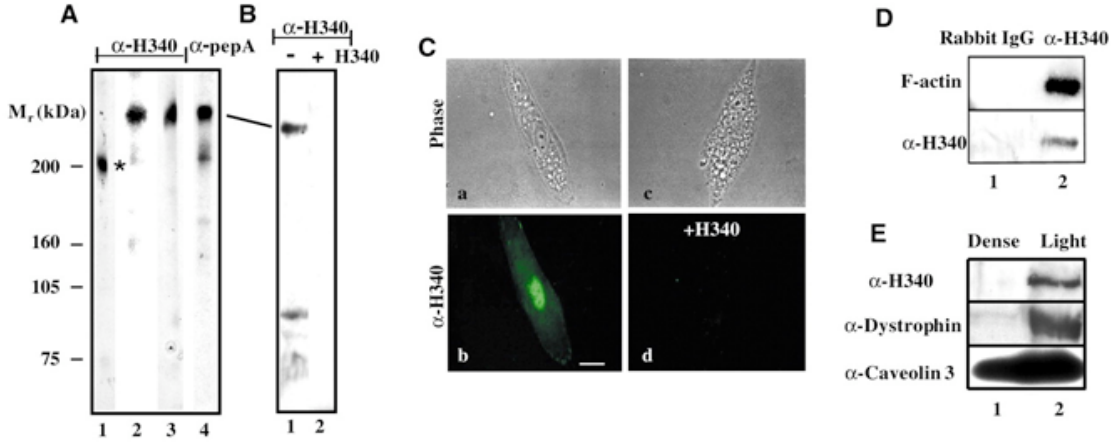


**Figure A-1.** Muscle contains a 250 kDa F-actin binding protein that is related to supervillin.

(**A**) Two antibodies (α-H340, α-pepA) against human supervillin (asterisk) recognize a larger protein in muscle cells (line). Immunoblots of human cervical carcinoma (HeLa S3) cells (lane 1), human 50MB-1 myoblasts (lane 2), hamster skeletal muscle (lane 3) and rabbit skeletal muscle (lane 4) were probed with affinity-purified rabbit polyclonal α-H340 (lanes 1-3) or α-pepA (lane 4) antibodies.

(**B**) Specificity of the α-H340 antibody on immunoblots. Affinity-purified α-H340 antibody (0.5 µg/ml) was pre-incubated for 1 hour at 0-4°C without (–) or with (+) bacterially expressed H340 protein (60 µg/ml) before incubation with blot strips containing rabbit skeletal muscle (100 µg/lane) and visualization by ECL.

(**C**) Specificity of the α-H340 antibody in immunofluorescence. Phase images (a,c) and indirect immunofluorescence micrographs (b,d) of proliferating 50MB-1 cells stained with affinity-purified α-H340 and secondary antibodies. To show specificity, the α-H340 antibody used for (c) and (d) was pre-incubated with 20 µg/ml of the H340 immunogen for 1 hour before use. Bar, 5 µm.

(**D**) Direct binding of $^{32}$P-labeled F-actin to the 250 kDa supervillin-like protein from mouse muscle. Immunoprecipitation with rabbit IgG (lane 1) or with α-H340 (lane 2). The polypeptide specifically immunoprecipitated by α-H340 IgG binds both $^{32}$P-labeled F-actin (top panel) and α-H340 antibody (lower panel).

(**E**) Co-fractionation of the 250 kDa supervillin-like protein with dystrophin and caveolin-3 in the crude plasma membrane fraction from rabbit skeletal muscle (Ohlendieck *et al.*, 1991). Immunoblots with antibodies against H340, dystrophin and caveolin-3 in a higher-density membrane fraction enriched in T-tubules and sarcoplasmic reticulum (lane 1, Dense) and in the low-density membrane fraction enriched in sarcolemmal membranes (lane 2, Light) are shown.

**Discussion**

Archvillin binds directly to F-actin, co-isolates with dystrophin and caveolin-3 in low-density sarcolemmal membranes, and co-localizes with dystrophin at costameres in skeletal muscle. The presence of archvillin in light membrane fractions corresponds well with the data we have on SV in neutrophil (Nebl *et al.*, 2002) and COS-7 DRM-H (Chapter III), supporting a potential role of SV/AV at the interface of membrane and cytoskeleton.

A logical hypothesis is that archvillin serves as an additional linkage between actin filaments and the plasma membrane at costameres, the principle adhesion structures along the length of the myofiber. Although dystrophin is required for sarcolemmal integrity, loss of muscle function develops only over time, suggesting the existence of partially redundant proteins (Hoffman *et al.*, 1987; Blake *et al.*, 2002). One such protein is the dystrophin-related protein, utrophin, but even mice lacking both dystrophin and utrophin exhibit superficially normal muscle function until about four weeks of age (Grady *et al.*, 1997). Other possible actin-membrane linkages at costameres include protein complexes that contain spectrin or focal adhesion proteins, including integrin, vinculin and α-actinin (Stromer, 1995; Berthier and Blaineau, 1997). In support of the idea of at least partial functional redundancy, costameres containing ß-spectrin and vinculin are retained, although frequently disarranged, in sarcolemma of the *mdx* mouse (Williams and Bloch, 1999). Conversely, loss of α- or ß-spectrin in nematodes leads to muscle dysfunction (Hammarlund *et al.*, 2000; Moorthy *et al.*, 2000), suggesting cross-talk among muscle membrane skeleton proteins. Because archvillin contains all the

sequences found in supervillin, archvillin is likely to participate in the cross-talk between the spectrin- and focal adhesion-based membrane skeletons at costameres in muscle.

**SV binds myosin II by yeast two-hybrid.**

As part of an ongoing effort to investigate the functional domains in SV, I generated a series of yeast two-hybrid constructs and performed screens for SV binding partners. The interaction that I found between SV11-171 and nonmuscle myosin IIA was not surprising, based on results from simultaneous experiments using GST pulldowns. Nonetheless, the results from the two-hybrid assay confirmed and extended the binding assays to identify a specific interacting domain of myosin II.

**Results**

Myosin S2 was identified as a key interaction site for the supervillin N-terminus in an untargeted yeast two-hybrid screen of a HeLa cDNA library that was probed with a bait vector encoding supervillin amino acids (11-174) (**Figure A-2**). Out of $10^8$ colonies screened, 10 specifically interacting clones encoding human nonmuscle myosin IIA (MYH-9, NCBI Protein Database accession number P35579 [GenBank]) were obtained. These colonies supported growth on inductive, selective media and induced expression of β-galactosidase activity (**Figure A-2A**). Seven of these clones encoded amino acids 874-1095 in human MYH-9 (**Figure A-2A, B, 1**), two encoded residues 874-1100 (**Figure A-2A, B, 2**), and one encoded amino acids 846-1100 (**Figure A-2A, B, 3**). Thus, in addition to GST pulldown assays (Chen *et al.*, 2003), the untargeted yeast two-hybrid screen also

identified sequences within myosin S2 as important interaction sites for the supervillin N-terminus.

In addition to the multiple myosin II clones that were identified from the yeast two-hybrid screen for SV11-174, sequences were also obtained for helicase (3 clones), hexokinase, hepatitis B virus x interacting protein, lamin B2, and the formally hypothetical proteins, now identified as SIKE (suppressor of IKKε) (Huang *et al.*, 2005) and transmembrane protein 106C. These interactions have not yet been confirmed using other methods.

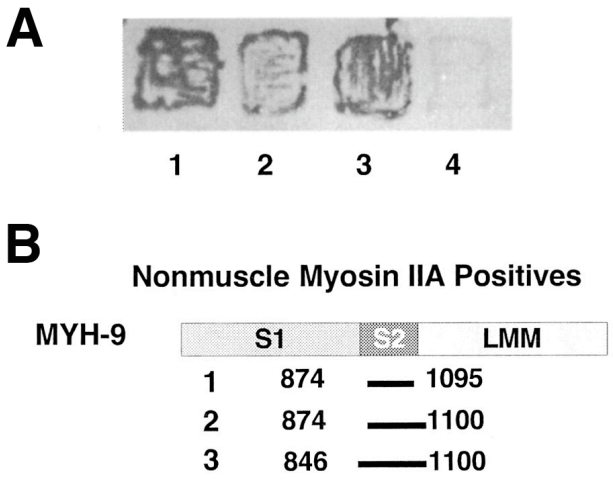


**Figure A-2.** Myosin S2 is sufficient for SV-(1-174) binding.

(**A**) Human nonmuscle myosin IIA sequences (MYH-9, NCBI Protein Database accession number P35579 [GenBank]) interact with supervillin amino acids 11-174 (SV-(11-174)) in a yeast two-hybrid assay. Yeast transformed with pHybLex/Zeo SV-(11-174) and a plasmid encoding one of three separately identified target sequences (lanes 1-3) or control plasmid pYesTrp2 (lane 4) were patched onto inductive, selective media (galactose/raffinose, Zeocin (0.3 mg/ml), -Ura, -Trp). Colonies were transferred to a nitrocellulose membrane and assayed for β-galactosidase activity according to the manufacturer's protocols (Invitrogen).

(**B**) Schematic representation of the locations of the target sequences (lines 1-3) identified by yeast two-hybrid screening with respect to the domain structure of human nonmuscle myosin IIA. All target sequences include most of the S2 domain. The smallest interacting sequence, amino acids 874-1095, corresponds to residues 887-1108 in chicken smooth muscle myosin MYHB (NCBI Protein Database accession number P10587 [GenBank]).

**Discussion**

The results of this untargeted yeast two-hybrid screen provides strong evidence that SV, in addition to being an F-actin binding protein, also binds to myosin II. At the time, we were not sure if the binding was direct, as filamin was also present in GST-SV pulldowns of smooth muscle (Chen *et al.*, 2003). In addition to providing evidence for direct binding, these experiments narrowed down the region in myosin II in which the N-terminal fragment of SV was binding.

The minimal myosin S2 sequence required for binding to supervillin may lie between smooth muscle myosin Lys-887 and Asn-1030. The smallest myosin sequence identified as a strong positive in the yeast two-hybrid screen corresponds to chick smooth muscle myosin residues 887-1109. The prominent binding of $^{35}$S-SV-(1-174) to HMM2 in blot overlays (Chen *et al.*, 2003) indicates that sequences N-terminal to Asn-1030 are sufficient for binding, albeit at a possibly reduced affinity. The greatly diminished binding to rod in blot overlays (Chen *et al.*, 2003) supports the importance of residues at or near the S1-S2 junction (amino acids 849-946 (Ikebe *et al.*, 1998)), a region of smooth muscle myosin II that has been suggested to play an important role in the regulation of myosin activity and assembly, both directly (Ikebe and Hartshorne, 1984, 1985; Konishi *et al.*, 2001) and through binding of regulatory proteins (Ikebe and Reardon, 1988; Kohama *et al.*, 1996; Kunst *et al.*, 2000; Morgan and Gangopadhyay, 2001; Wang, 2001). The S2 region of myosin II is on the surface of the myosin II thick filament, where it may regulate the extension and activation of the myosin II heads (Woodhead *et al.*, 2005; Alamo *et al.*, 2008; Jung *et al.*, 2008).

Supervillin also may mediate the interaction between myosin II and actin filaments. Such a function is well accepted for other proteins known to bind to both myosin and actin filaments. These proteins include myosin light chain kinase, calponin, and caldesmon (Ikebe and Reardon, 1988; Kohama *et al.*, 1996; Gusev, 2001; Morgan and Gangopadhyay, 2001; Wang, 2001). Although calponin and caldesmon have been investigated primarily in smooth muscle, nonmuscle isoforms for all three of these proteins exist. Thus, one hypothesis for the myosin II redistribution induced by overexpressed SV-(1-174) (Chen *et al.*, 2003)is a dominant-negative effect caused by competition with other myosin S2-binding proteins. If true, then the apparently normal distribution of myosin II in the presence of overexpressed SV-(1-342) (Chen *et al.*, 2003), a fragment that contains an actin-binding site as well as the myosin-binding site, implies that supervillin may organize actin and myosin filament interactions in ways similar to those proposed for caldesmon and calponin. The tight association of supervillin with liquid-ordered membrane domains (Nebl *et al.*, 2002) and its localization at actin-rich membrane punctae (Wulfkuhle *et al.*, 1999; Nebl *et al.*, 2002)further suggest that supervillin is well suited to promote the recruitment of, and/or to regulate the interaction between, actin and myosin filaments at these regions of the membrane. As the only protein known so far to be capable of linking liquid-ordered membrane domains to both F-actin and myosin II, supervillin may be an important "adapter" protein for the organization of membrane skeleton attachments at these dynamic regions of the plasma membrane.

## Materials and Methods

### Rabbit muscle fractions

Crude rabbit skeletal muscle plasma membranes were prepared from freshly dissected or frozen back and leg muscles by flotation through 30% (w/v) sucrose, as described (Ohlendieck et al., 1991). The following protease inhibitors (Sigma, St Louis, MO) were included in all buffers: 1 μg/ml aprotinin, 1 μM pepstatin A, 0.5 μg/ml leupeptin, 1 mM benzamidine, 1 μM antipain, 1 mM phenylmethylsulfonyl fluoride (PMSF). Equivalent amounts of protein in the low-density fraction, which was enriched in plasma membranes, and in the higher-density fraction, which was enriched in sarcoplasmic reticulum and T-tubules, were analyzed by SDS polyacrylamide gel electrophoresis (SDS-PAGE) and immunoblotting.

### Muscle extracts

Murine hind leg muscles, or rabbit back and leg muscles, were ground under liquid $N_2$ and extracted twice with 1% SDS for 10 minutes at 70°C. Extracts either were denatured with sample buffer for SDS-PAGE or were diluted 10-fold with 1% Triton X-100 in PBS for immunoprecipitations. Triton X-100 extracts from ~0.3 mg muscle were pre-cleared for 2 hours at 4°C with rabbit immunoglobulin (RIgG) bound to protein A/G beads (Pierce Chemical Company, Rockford, IL) and incubated with 20 μg RIgG or α-H340 bound to protein A/G beads for 5 hours at 4°C. Beads were washed extensively with PBS. Bound immunoprecipitated proteins were eluted by heating for 5 minutes at 95°C in SDS sample buffer and analyzed by α-H340 immunoblot and F-actin blot overlay.

**Immunoblots**

Proteins were separated by SDS-PAGE (Laemmli, 1970) and electrotransferred to nitrocellulose (0.45 μm pore size) (Schleicher and Schuell, Keene, NH). Nitrocellulose blots were blocked with 5% nonfat powdered milk in TBS-T and probed with primary antibodies for 2 hours at room temperature or overnight at 4°C. Concentrations of primary antibodies were as follows: 10 μg/ml affinity-purified α-H340, 20 μg/ml α-pepA, 5 μg/ml anti-caveolin 3 (BD Transduction Laboratories, San Diego, CA), 1:20 dilution of anti-dystrophin (Novocastra Lab, Burlingame, CA). Interacting polypeptides were visualized using either $^{125}$I-labeled protein A or protein A conjugated to horseradish peroxidase and an ECL substrate kit (KPL, Gaithersburg, MD). Reactive polypeptides were detected by exposure to Biomax-MS X-ray film (Eastman Kodak, Rochester, NY). For double labeling with radioactively labeled F-actin, anti-rabbit antibody conjugated to alkaline phosphatase was used with a BCIP/NBT substrate kit (KPL, Gaithersburg, MD) for colorimetric detection.

**F-actin blot overlay**

For F-actin overlays, $^{125}$I-labeled actin was polymerized in the presence of rabbit gelsolin, stabilized with phalloidin and used at a final concentration of 50 μg/ml in 5% nonfat powdered milk in TBS-T(Luna, 1998). In some experiments, actin was labeled with [α-$^{32}$P]ATP (Mackay *et al.*, 1997), using 1 mg of actin and 1 mCi of [α-$^{32}$P]ATP. Nitrocellulose blots were exposed to film for 5 days at –80°C or to an imaging screen for 2 hours. Signal was visualized with a Phosphor Imager SI™optical scanner and ImageQuant software (Molecular Dynamics, Sunnyvale, CA).

**Yeast Two-hybrid Screens**

A bait plasmid encoding supervillin residues 11-174 was constructed and used to screen 1.62 x $10^8$ clones from a library of 1.03 x $10^7$ conditionally expressed target plasmids derived from HeLa S3 cDNA (Hybrid Hunter™ Premade cDNA Library and Two-Hybrid System, Invitrogen). A cDNA encoding bovine supervillin amino acids 11-174 was PCR-amplified using primers containing an *Eco*RI or *Sal*I site (forward primer, 5'-AGGGAATTCTTAGAAGGAATTGAAACCGACACGC-3'; reverse primer, 5'-ATCGTCGACTATAGCCCCGAGAGCTCAGTCCT-3'). The PCR product was cloned into pCR2.1-TOPO® and then into the bait vector pHybLex/Zeo, in-frame with the LexA DNA binding domain. The bait vector (pHybLex/Zeo SV 11-174)) was transformed (Gietz and Woods, 2002) into yeast strain EGY48 containing the reporter plasmid pSH18-34. Transformants with HeLa cDNA target plasmid were screened for leucine prototrophy and for β-galactosidase activity on filter lifts, according to the manufacturer's instructions. Plasmid DNAs were isolated from positively interacting colonies (Hoffman *et al.*, 1987), amplified in bacteria, and sequenced at the University of Massachusetts Nucleic Acid Facility (Worcester, MA).

# Appendix B

## Detailed Protocols

In this section, I provide detailed protocols and notes for assays critical to this dissertation.

### Preparation of gelatin coated coverslips

Adapted from:
Bowden, ET, PJ Coopman and SC Mueller, 2001. Invadopodia: Unique methods for measurement of extracellular matrix degradation in vitro. Methods in Cell Biology, 63, 613-627.

**TRITC-gelatin:** Conjugated Type B gelatin, 225 bloom, 2.5%. Made using above protocol, with following changes: Use 10 mg of TRITC (Molecular Probes T-490) instead of 6 mg. Also add Baker Bond Prepscale Abx resin (40 um, Baker #7269-00) to exterior dialysis solution to capture unbound dye. Pre-mix several scoopfuls of resin (to ~5 ml mark) in 50 ml conical tube, cover with 1 M Tris, pH 8, mix, spin, then resuspend in PBS for addition to dialysis buffer.

**Solutions for 18 coverslips:**

0.5% glutaraldehyde: 312 µl of 8% glutaraldehyde
4.7 ml PBS
Make fresh.

5 mg/ml sodium borohydride: 0.25 g sodium borohydride (stored at RT, desiccated)
50 ml PBS
Make fresh (usually during incubation with glutaraldehyde).

**Coating coverslips:**

1. Pre-clean coverslips (22 x 22 mm, #1.5, or can use round 18 mm in 12 well dish) in 70% ethanol.
2. Heat TRITC-gelatin (or unlabeled gelatin) in heat block to 45°C (fill well with water for better heating). Allow to warm for at least 15 min. In the meantime,

pre-chill 0.5% glutaraldehyde/PBS on ice. Pre-chill trays (lids of 6 well dishes) lined with parafilm in -20°C freezer.

3. Remove trays from the freezer, place on ice and pipette 6 glutaraldehyde drops of 200 μl each on tray.
4. Using a pair of tweezers, take the coverslip at the corner and spread 200 μl of gelatin by tilting in a circular motion for 20 seconds. Remove excess gelatin and let set for 20 seconds. Then invert onto glutaraldehyde droplet. Once you have spread gelatin on 6 coverslips, start a timer for 15 minutes.
5. After glutaraldehyde fixation, move coverslips to 6-well dish (doesn't have to be sterile, but reasonably clean). Wash three times with PBS.
6. Incubate with ~2 ml/well of 5 mg/ml sodium borohydride for 5-10 minutes. Air bubbles will form. Tap the side of dish to ensure coverslips stay submerged.
7. Wash 3 times with PBS.
8. Incubate in 70% ethanol for 10 min. Move to tissue culture hood.
9. Rinse with PBS once or twice. Incubate in serum-free DMEM for at least one hour before plating cells. (I've tested this with phenol-red free media as well, doesn't seem to make a difference with evenness of gelatin fluorescence.)
10. After incubating cells for desired amount of time, fix as usual with 4% paraformaldehyde/PBS, permeabilize and block. Stain as needed.

Notes:

- I routinely made 18 cs (3- 6 well dishes worth). Start ~2.5 hours before you want to plate cells. Set a timer for 3 -15 minute time points.
- Clean coverslips the previous day. Leave them to dry between two pieces of filter paper. Alternatively, clean a lot of coverslips and leave them in a glass dish separated by filter paper.

**Preparation of Protease Inhibitor Mix**

| Inhibitor | Description | F. W. | Amount for 10 mL of 1000X | 1X Concentration |
|---|---|---|---|---|
| Aprotinin | Reversible inhibitor of proteolytic and esterolytic activity and serine proteases | 681.2 | 10 mg | 1 μg/ml |
| Antipain | Reversible inhibitor of cysteine and serine proteases | 677.6 | 6.7 mg | 1 μM |
| ALLM | Calpain inhibitor II | 401.6 | 8 mg | 2 μM |
| Benzamidine | Inhibitor of trypsin and trypsin-like proteases | 156.6 | 1.565 g | 1 mM |
| E64 | Irreversible cysteine protease inhibitor | 357.4 | 35 mg | 10 μM |
| Leupeptin | Trypsin inhibitor | 493.6 | 5 mg | 1 μM |
| Pepstatin A | Inhibitor of aspartic proteases | 658.9 | 6.6 mg | 1 μM |

Mix all protease inhibitors in 10 mL of DMSO. Dissolve and aliquot. Store at -20°C. Use at 1:1000 dilution in lysis buffer.

**Matrigel™ Invasion assay**

**Day 1:**

Remove -20°C Matrigel™ inserts (BD Catalog # 354480, Matrigel, # 354578, Control), to new 24-well plate and bring to room temperature (~30 minutes**)**. Use sterile forceps to manipulate filters.

Re-hydrate the inserts in **complete medium**: add 500 µl of medium to appropriate number of wells of a 24-well plate (special type, with slots for the inserts Falcon # 353504). Add the Matrigel™ inserts and a corresponding number of control inserts, then add 500 µl medium to tops of inserts. Incubate at 37°C, 5% $CO_2$ for 2 hours. **Dislodge any air bubbles on bottom of filters.**

Lift the cells with trypsin; stop reaction with complete medium and move to a conical centrifuge tube. Remove a small aliquot for counting.

Centrifuge at 1000 RPM for 5 minutes. Count cells with hemacytometer.

Remove as much of the medium as possible. **Resuspend cells in serum-free medium**. Final concentration should be $1x10^5$ cells per ml. May need to make dilution. First, resuspend at $10^6$ cells/ml, and then make 1:10 dilution. Mix well. Make more than needed. For example, for an experiment in triplicate, 3 ml of cells plus 0.5 ml to check for cell density is the minimum amount required. Make 4 ml of dilution.

Remove the medium used to hydrate the inserts. **Take care not to damage the Matrigel™!** Add 750 µl of growth medium **(with serum)** to the bottom of the wells. **Be sure there are no trapped air bubbles below the insert.**

Add 500 µl of cell solution to each insert. Incubate in 37°C, 5% $CO_2$ for 20 hours. Add 500 µl of cell solution to 6-well plate with coverslips to check for cell density.

**Day 2:**

Set up a 24 well plate (with slots) with the Diff Quick (or Hema 3 Stain Set, Fisher, #122-911) fix and stain set and 2 large beakers with distilled water for rinsing. (Tip: mark side tabs of insert with sharpie to color code conditions.)

Pre-wet a cotton swab with serum free medium and use it to scrub the top surface of the inserts to remove non-invading cells. (For Matrigel™ coated filters, remove 200-300 µl of media prior to scrubbing; this is not necessary for control filters.) Swirl around the

edge then back and forth across the middle 10 times. Do not press too hard! Use firm, but gentle pressure.

**Immediately** remove media and cell debris from insert and transfer the insert to the fixing solution and incubate 2 minutes. Move to Stain 1 and Stain 2; incubate in each for 2 minutes.

Rinse each insert in distilled water (first in beaker one, then beaker two), tap off excess water, and place in a new plate to dry. Move inserts to the fume hood to dry with lid off.

**Analysis:**

When dry, image on the Zeiss Axioscope with the color camera. Flip plate with inserts upside down and image with 10X objective. Using OpenLab, take 5 non-overlapping pictures, 4 around the edges and one in the center. Can take all pictures for triplicate sets in the same file. Save as TIFs and analyze using ImageJ software.

Count cells from the **Matrigel™ inserts** using the Cell Counter plugin for ImageJ.

For **control inserts**, using ImageJ:

- Process: Binary: Threshold
  (Make a black and white image. Select Threshold twice, if necessary, to get black cells on white.)
- Process: Binary: Watershed
  (May have to wait 1-2 minutes.)
- If there is debris on the image, remove it manually at this point using the Freehand selection and Delete.
- Analyze: Analyze Particles
  To eliminate the pores from the count, use these settings: Minimum = 900 pixels and Maximum = 9999999.9 (default).
  Select "Show Outlines" to be sure that actual cells are being counted.
- Select the count numbers and areas, etc. in the Results panel.
  Copy into a separate Word document under the file name.

To calculate **percent invasion**, ratio the average number of cells that migrated in the presence *vs.* absence of Matrigel™ to control for changes in cell motility. Then ratio experimental percent invasion against the mean value obtained for control cells to obtain the **invasion index**.

To check for cell density loaded on filters, fix cells on coverslips. Take 25 pictures with 10X phase contrast. Count the average number of cells per field.

## Nucleofection of MDA-MB-231 Cells

Modified from Amaxa product literature.

*Notes: MDA-MB-231 cells lift easily/quickly with trypsin. Need $1x10^6$ cells per Nucleofection.

For siRNA, use 1 μl of a 1:5 dilution of the 20 μM stock. Use DEPC water.

For plasmids, use 2 μg of DNA.

Work quickly when cells are in Nucleofection solution; time is 15 minutes before cell viability decreases drastically. Do no more than 6 transfections at once.

Nucleofector program is X-13 or X-013.

Nucleofector solution V: add 100 μl supplement to 450 μl solution V. Good for 3 months after mixing.

**Day 1:**

Split MDA-MB-231 cells from a T-25 flask to 2 - T-75 flasks (= 1: 6 ratio).

Incubate 2 days at 37°C, 5% $CO_2$. (Want cells ~80-90% confluent on day of transfection.

**Day 3:**

Warm growth medium to 37°C and supplemented Nucleofection solution V to room temperature.

Aliquot growth medium to required vessels (*e.g.* 10 cm dish, 6 well plate) and incubate at 37°C, 5% $CO_2$. Also aliquot and incubate 500 μl medium to a 1.5 ml tube (one per Nucleofection).

Prepare 1.5 ml tubes containing plasmid (2 μg) or siRNA (40 nM; see Note, above).

Trypsinize to remove cells from flask; stop trypsin by addition of growth medium and transfer cells to a conical centrifuge tube.

Remove small aliquot to hemacytometer for counting.

Spin for 5 minutes at 1000 RPM on bench top centrifuge; count cells.

Remove as much medium as possible and resuspend cells in PBS.

Remove an aliquot of cells/PBS solution equal to the total number of cells you need to a new conical tube and centrifuge as above. During centrifugation, label cuvettes and transfer pipets appropriately.

Remove as much of the PBS as possible and resuspend the pellet in Nucleofection solution (100 μl per million cells).

Transfer 100 µl of cell solution to prepared tube containing siRNA or plasmid, mix by pupating, then transfer to cuvette. Be sure there are no bubbles and that the solution is at the bottom of the cuvette.

Move to the Nucleofector and take out the 1.5 ml tubes with 500 µl medium. Align the slot in the Nucleofector with the tab of the cuvette. Rotate in the cuvette, and then press the 'X' button to activate the program.

After the beep (machine says OK), immediately add the warmed 500 µl of medium with the transfer pipet to the cuvette and move the cell solution to the 1.5 ml tube. Save the transfer pipet for moving the cells to the growth vessels.

> Occasionally, machine will say "Weak" after Nucleofection. I have proceeded with these samples and the knockdown efficiency has been acceptable.

When all cells are nucleofected, move back to the laminar hood and aliquot the cells between growth vessels with pre-equilibrated medium as appropriate (usually 3-4 drops for 6 well dish for extraction, rest into 10 cm).

Incubate at 37$^{o}$C, 5% $CO_2$ as follows: siRNA - 4 days; over-expression - 24 to 48 hours.

**Deconvolution using Improvision Volocity program**

Obtain a Z-series that you want to deconvolve (in OpenLab liff file or a series of tiff files).

Use 0.2 μm step size for best results.

If Z-series file contains more than one color, separate the channels into separate liff files or separate folders of tiffs.

If you're going to crop the image before deconvolution (for decreases in computing time), crop the file before separating colors, so that they will merge properly after deconvolution.

Open the Volocity program. You will be prompted to create a new library. You can do this by dragging and dropping an OpenLab liff file or a folder of tiffs into the library.

If you want to do batch deconvolution (multiple cells or files at once), drag all OpenLab liff files into the library.

There is no save function in Volocity; the program saves the library upon closing.

Calculate point spread function (PSF), or measure a specific PSF from point source beads.

If deconvolving different colors, you need to calculate a PSF for each color (using command under Tools menu).

If you've already done this for another file, you can copy and paste the PSF from one file to another.

Make liff file or tiff files into volumes. Highlight images, go to actions → make volumes (command + M keys for shortcut).

Go under the properties option (command + I); enter the channel, μm/pixel, wavelength, and objective.

For common use Leica: 25X oil 0.25452 μm/pixel, 63X oil 0.101μm/pixel, 100X oil 0.0635 μm/pixel.

To deconvolve, use the iterative restoration tool. Highlight all volumes you want to deconvolve (can batch deconvolve up to 6 full chip images at a time). Must be all of the same channel, because you can only use one PSF (red or green) per deconvolution. After selecting volumes, go to actions→ iterative deconvolution, choose PSF, enter ~98% confidence interval and 20 iterations, then deconvolve. This is a time-consuming process.

After deconvolution is complete, change the colors of the deconvolved volumes to red or green, as appropriate (Tools → Change colors). Then go to actions→ create new image sequence (new window pops up). Select both channels of a single image, drag into the

window (have to move simultaneously, not individually). Select how many channels, time points, etc. and it will merge the red and green channels. You can now view up and down in the Z direction.

Notes:

In XYZ viewer, the bottom plane is usually at the outside edge (*e.g.*, the left side of the YZ and the top side of the XZ images).

Can capture screen shot of XY, XZ, YZ and export as tiffs.

Use Alt + click to zoom out of an image.

Merge planes makes maximum point projection.

## Preparation of DRMs from COS-7 Cells

**Solutions:**

**TEB**: 1% Triton X-100, 25 mM Tris, 250 mM NaCl, 2.5 mM $MgCl_2$, 1 mM EGTA, 1 mM ATP

**TNE**: 25mM TRIS, 150 mM NaCl, 5 mM EDTA

Make a 10X solution:

25ml 1M TRIS
50 ml 3M NaCl
10 ml 0.5 M EDTA
15 ml $dH_20$

**TNE-T Lysis Buffer**: TNE + 1% Triton X-100

0.5 ml 10% Triton X-100
0.5 ml 10X TNE
4 ml $dH_2O$

**Sucrose solutions**:

Make sucrose solutions in the buffer used for extraction (TEB or TNE).

> For 50 ml of 10% sucrose: 5 g sucrose, 5 ml 10X TNE, bring to volume with $dH_2O$. For all sucrose solutions check refractive index. Sucrose solutions can be made ahead and stored at 4°C.

**Extraction Procedure:**

Notes for an efficient prep

- Pour gels the day before running them. Cover with buffer and store at 4°C.

Prior to starting extraction:

- Turn on Sorvall to 4°C and chill green adaptors
- Chill Dounce homogenizer and PBS for rinsing cells.
- Turn on ultracentrifuge, get to 4°C and run vacuum.
- Label tubes and pre-weigh 1.4 g sucrose in the ~5 ml tubes.

1. Put cells on ice, aspirate media, rinse twice with ice cold PBS. On the last wash, tilt plate to allow PBS to collect at the bottom and aspirate.
2. Add protease inhibitors to TNE-T then extract cells for 30 min on ice with 2 ml chilled TNE-T.
3. Scrape with cell scraper. Collect lysate in chilled Dounce homogenizer.
4. Dounce on ice 10 strokes (avoid creating air bubbles).
5. Remove from homogenizer and place in 2-1.5 ml tubes.

6. Spin out nuclei in Sorvall, SS34 rotor, with green tube adaptors (fill with water before inserting 1.5 ml tubes) at 4°C, 3000 RPM for 10 minutes.
7. Take out supernatant and add to 1.4 g sucrose (in small clear plastic ~ 5 ml round bottom tubes used for the fraction collector).
8. Cap tightly and move to rotator in cold room for 10-15 minutes.
9. Check refractive index and if needed add 64% sucrose to get sample to about 50% sucrose.
10. Place back on rotator and check refractive index again after 5 minutes.
11. Prepare gradient in SW41 thin walled ultracentrifuge tube (Beckman)
    **a.** Add 1ml 10% sucrose.
    **b.** Load the following from bottom using long blunt tip needle: 3 ml 30%, 3 ml 40%, 3 ml sample, 0.5 ml 64% sucrose.
12. Place tubes (very carefully) in SW41Ti centrifuge buckets. Check the weights of the buckets, must be within 0.01 g of each other for proper balance of centrifuge. Use buffer to balance tubes when necessary.
13. Put in chilled (4°C) ultracentrifuge, spin 16 hours 35,000 RPM (200,000 x *g*).

**Fractionation and analysis:**

1. Prepare 1 set of 2ml screw cap tubes and 2 sets of 1.5 ml tubes (numbered 1-19, with experimental designation) ahead of time.
2. Carefully remove gradient from centrifuge and place on ice.
3. Use fractionator in cold room (model 640 density gradient fractionator (Isco Inc., Lincoln, NE)) to fractionate into 19 samples.
    - Make sure line is clear prior to beginning (use $dH_2O$ and a syringe).
    - Run the fractionator in the forward direction before putting tube on to clear any air bubbles from the fluorinert.
    - Add tubes (2 ml screw-cap) to fraction collector tray. Angle slightly so they don't fall through.
    - Place centrifuge tube in appropriate size holder (black cap and white rubber holder). Make sure top of tube is completely level with the rubber holder to avoid leaks. Screw tightly on to fractionator.
    - Put a piece of parafilm under white foam pad prior to piercing tube. (Make sure needle is positioned properly for the size tube being used. Watch your fingers!)
    - Run samples at 0.5-1 ml/min and set the volume collector to 0.6 ml.

- When finished (the pace of drops quicken—a sign that the fluorinert is coming out), switch the machine to reverse to draw the fluorinert back into the syringe for reuse.
- Don't leave machine unattended, as tube collector may stop moving or tube can leak.
- When finished, clean fractionator by squirting $dH_2O$ through the tubing and wiping up any drops of sucrose.

4. After fractionation (or simultaneously), transfer 150 μl of sample to 1.5 ml tube.
5. In the last set of tubes put 25 μl of 5X SDS sample buffer and 100 μl of sample. Vortex, then heat samples in 70°C water bath for 10 min, then vortex, and centrifuge.
6. Load samples onto large 6-16% gradient gel. Run ~100-150 volts, 5-6 hours. Transfer overnight, at least 16 hours.
7. With remaining 50 μl of sample, make a dot blot to check for GM1 levels, determine protein concentration using BCA assay, and measure refractive indices.

## References

Acconcia, F., Ascenzi, P., Bocedi, A., Spisni, E., Tomasi, V., Trentalance, A., Visca, P., and Marino, M. (2005a). Palmitoylation-dependent estrogen receptor alpha membrane localization: regulation by 17beta-estradiol. Mol Biol Cell *16*, 231-237.

Acconcia, F., Ascenzi, P., Fabozzi, G., Visca, P., and Marino, M. (2004). S-palmitoylation modulates human estrogen receptor-alpha functions. Biochem Biophys Res Commun *316*, 878-883.

Acconcia, F., Totta, P., Ogawa, S., Cardillo, I., Inoue, S., Leone, S., Trentalance, A., Muramatsu, M., and Marino, M. (2005b). Survival versus apoptotic 17beta-estradiol effect: role of ER alpha and ER beta activated non-genomic signaling. J Cell Physiol *203*, 193-201.

Alamo, L., Wriggers, W., Pinto, A., Bartoli, F., Salazar, L., Zhao, F.Q., Craig, R., and Padron, R. (2008). Three-dimensional reconstruction of tarantula myosin filaments suggests how phosphorylation may regulate myosin activity. Journal of Molecular Biology *384*, 780-797.

Ammer, A.G., and Weed, S.A. (2008). Cortactin branches out: Roles in regulating protrusive actin dynamics. Cell Motil Cytoskeleton *65*, 687-707.

Archer, S.K., Claudianos, C., and Campbell, H.D. (2005). Evolution of the gelsolin family of actin-binding proteins as novel transcriptional coactivators. Bioessays *27*, 388-396.

Artym, V.V., Zhang, Y., Seillier-Moiseiwitsch, F., Yamada, K.M., and Mueller, S.C. (2006). Dynamic interactions of cortactin and membrane type 1 matrix metalloproteinase at invadopodia: defining the stages of invadopodia formation and function. Cancer Res. *66*, 3034-3043.

Ayala, I., Baldassarre, M., Giacchetti, G., Caldieri, G., Tete, S., Luini, A., and Buccione, R. (2008). Multiple regulatory inputs converge on cortactin to control invadopodia biogenesis and extracellular matrix degradation. J. Cell Sci. *121*, 369-378.

Bai, C.Y., Ohsugi, M., Abe, Y., and Yamamoto, T. (2007). ZRP-1 controls Rho GTPase-mediated actin reorganization by localizing at cell-matrix and cell-cell adhesions. J. Cell Sci. *120*, 2828-2837.

Balasubramanian, N., Scott, D.W., Castle, J.D., Casanova, J.E., and Schwartz, M.A. (2007). Arf6 and microtubules in adhesion-dependent trafficking of lipid rafts. Nat. Cell Biol. *9*, 1381-1391.

Baldassarre, M., Ayala, I., Beznoussenko, G., Giacchetti, G., Machesky, L.M., Luini, A., and Buccione, R. (2006). Actin dynamics at sites of extracellular matrix degradation. Eur. J. Cell Biol. *85*, 1217-1231.

Baldassarre, M., Pompeo, A., Beznoussenko, G., Castaldi, C., Cortellino, S., McNiven, M.A., Luini, A., and Buccione, R. (2003). Dynamin participates in focal extracellular matrix degradation by invasive cells. Mol. Biol. Cell *14*, 1074-1084.

Benesch, S., Lommel, S., Steffen, A., Stradal, T.E., Scaplehorn, N., Way, M., Wehland, J., and Rottner, K. (2002). Phosphatidylinositol 4,5-biphosphate (PIP2)-induced vesicle movement depends on N-WASP and involves Nck, WIP, and Grb2. J. Biol. Chem. *277*, 37771-37776.

Berthier, C., and Blaineau, S. (1997). Supramolecular organization of the subsarcolemmal cytoskeleton of adult skeletal muscle fibers. A review. Biology of the cell / under the auspices of the European Cell Biology Organization *89*, 413-434.

Bjornstrom, L., and Sjoberg, M. (2005). Mechanisms of estrogen receptor signaling: convergence of genomic and nongenomic actions on target genes. Mol. Endocrinol. *19*, 833-842.

Blake, D.J., Weir, A., Newey, S.E., and Davies, K.E. (2002). Function and genetics of dystrophin and dystrophin-related proteins in muscle. Physiological reviews *82*, 291-329.

Block, M.R., Badowski, C., Millon-Fremillon, A., Bouvard, D., Bouin, A.P., Faurobert, E., Gerber-Scokaert, D., Planus, E., and Albiges-Rizo, C. (2008). Podosome-type adhesions and focal adhesions, so alike yet so different. Eur. J. Cell Biol. *87*, 491-506.

Boguslavsky, S., Grosheva, I., Landau, E., Shtutman, M., Cohen, M., Arnold, K., Feinstein, E., Geiger, B., and Bershadsky, A. (2007). p120 catenin regulates lamellipodial dynamics and cell adhesion in cooperation with cortactin. Proc Natl Acad Sci U S A *104*, 10882-10887.

Boshans, R.L., Szanto, S., van Aelst, L., and D'Souza-Schorey, C. (2000). ADP-ribosylation factor 6 regulates actin cytoskeleton remodeling in coordination with Rac1 and RhoA. Mol. Cell. Biol. *20*, 3685-3694.

Bourguignon, L.Y., Gilad, E., Rothman, K., and Peyrollier, K. (2005). Hyaluronan-CD44 interaction with IQGAP1 promotes Cdc42 and ERK signaling, leading to actin binding, Elk-1/estrogen receptor transcriptional activation, and ovarian cancer progression. J. Biol. Chem. *280*, 11961-11972.

Bowden, E.T., Barth, M., Thomas, D., Glazer, R.I., and Mueller, S.C. (1999). An invasion-related complex of cortactin, paxillin and PKCmu associates with invadopodia at sites of extracellular matrix degradation. Oncogene *18*, 4440-4449.

Bowden, E.T., Coopman, P.J., and Mueller, S.C. (2001). Invadopodia: Unique methods for measurement of extracellular matrix degradation *in vitro*. Meth. Cell Biol. *63*, 613-627.

Bowden, E.T., Onikoyi, E., Slack, R., Myoui, A., Yoneda, T., Yamada, K.M., and Mueller, S.C. (2006). Co-localization of cortactin and phosphotyrosine identifies active invadopodia in human breast cancer cells. Exp. Cell Res. *312*, 1240-1253.

Bravo-Cordero, J.J., Marrero-Diaz, R., Megias, D., Genis, L., Garcia-Grande, A., Garcia, M.A., Arroyo, A.G., and Montoya, M.C. (2007). MT1-MMP proinvasive activity is regulated by a novel Rab8-dependent exocytic pathway. EMBO J. *26*, 1499-1510.

Broussard, J.A., Webb, D.J., and Kaverina, I. (2008). Asymmetric focal adhesion disassembly in motile cells. Curr. Opin. Cell Biol. *20*, 85-90.

Brown, D.A., and Rose, J.K. (1992). Sorting of GPI-anchored proteins to glycolipid-enriched membrane subdomains during transport to the apical cell surface. Cell *68*, 533-544.

Buccione, R., Caldieri, G., and Ayala, I. (2009). Invadopodia: specialized tumor cell structures for the focal degradation of the extracellular matrix. Cancer metastasis reviews.

Buday, L., and Downward, J. (2007). Roles of cortactin in tumor pathogenesis. Biochimica et biophysica acta *1775*, 263-273.

Burns, S., Thrasher, A.J., Blundell, M.P., Machesky, L., and Jones, G.E. (2001). Configuration of human dendritic cell cytoskeleton by Rho GTPases, the WAS protein, and differentiation. Blood *98*, 1142-1149.

Calzolari, A., Raggi, C., Deaglio, S., Sposi, N.M., Stafsnes, M., Fecchi, K., Parolini, I., Malavasi, F., Peschle, C., Sargiacomo, M., and Testa, U. (2006). TfR2 localizes in lipid raft domains and is released in exosomes to activate signal transduction along the MAPK pathway. J. Cell Sci. *119*, 4486-4498.

Cao, H., Weller, S., Orth, J.D., Chen, J., Huang, B., Chen, J.L., Stamnes, M., and McNiven, M.A. (2005). Actin and Arf1-dependent recruitment of a cortactin-dynamin complex to the Golgi regulates post-Golgi transport. Nat. Cell Biol. *7*, 483-492.

Chabadel, A., Banon-Rodriguez, I., Cluet, D., Rudkin, B.B., Wehrle-Haller, B., Genot, E., Jurdic, P., Anton, I.M., and Saltel, F. (2007). CD44 and beta3 integrin organize two functionally distinct actin-based domains in osteoclasts. Mol. Biol. Cell *18*, 4899-4910.

Chambliss, K.L., Yuhanna, I.S., Anderson, R.G., Mendelsohn, M.E., and Shaul, P.W. (2002). ERbeta has nongenomic action in caveolae. Mol. Endocrinol. *16*, 938-946.

Chellaiah, M., Kizer, N., Silva, M., Alvarez, U., Kwiatkowski, D., and Hruska, K.A. (2000). Gelsolin deficiency blocks podosome assembly and produces increased bone mass and strength. J. Cell Biol. *148*, 665-678.

Chen, J.Q., Delannoy, M., Cooke, C., and Yager, J.D. (2004). Mitochondrial localization of ERalpha and ERbeta in human MCF7 cells. Am. J. Physiol. *286*, E1011-1022.

Chen, W.T. (1989). Proteolytic activity of specialized surface protrusions formed at rosette contact sites of transformed cells. J. Exp. Zool. *251*, 167-185.

Chen, W.T., Lee, C.C., Goldstein, L., Bernier, S., Liu, C.H., Lin, C.Y., Yeh, Y., Monsky, W.L., Kelly, T., Dai, M., and et al. (1994). Membrane proteases as potential diagnostic and therapeutic targets for breast malignancy. Breast Cancer Res Treat *31*, 217-226.

Chen, W.T., and Wang, J.Y. (1999). Specialized surface protrusions of invasive cells, invadopodia and lamellipodia, have differential MT1-MMP, MMP-2, and TIMP-2 localization. Ann N Y Acad Sci *878*, 361-371.

Chen, Y., Takizawa, N., Crowley, J.L., Oh, S.W., Gatto, C.L., Kambara, T., Sato, O., Li, X., Ikebe, M., and Luna, E.J. (2003). F-actin and myosin II binding domains in supervillin. J. Biol. Chem. *278*, 46094-46106.

Clark, E.S., and Weaver, A.M. (2008). A new role for cortactin in invadopodia: Regulation of protease secretion. Eur. J. Cell Biol. *87*, 581-590.

Clark, E.S., Whigham, A.S., Yarbrough, W.G., and Weaver, A.M. (2007). Cortactin is an essential regulator of matrix metalloproteinase secretion and extracellular matrix degradation in invadopodia. Cancer Res. *67*, 4227-4235.

Condeelis, J., and Segall, J.E. (2003). Intravital imaging of cell movement in tumours. Nat Rev Cancer *3*, 921-930.

Condeelis, J., Singer, R.H., and Segall, J.E. (2005). The great escape: when cancer cells hijack the genes for chemotaxis and motility. Annu Rev Cell Dev Biol *21*, 695-718.

Coopman, P.J., Do, M.T., Thompson, E.W., and Mueller, S.C. (1998). Phagocytosis of cross-linked gelatin matrix by human breast carcinoma cells correlates with their invasive capacity. Clin Cancer Res *4*, 507-515.

Courtneidge, S.A., Azucena, E.F., Pass, I., Seals, D.F., and Tesfay, L. (2005). The SRC substrate Tks5, podosomes (invadopodia), and cancer cell invasion. Cold Spring Harb Symp Quant Biol *70*, 167-171.

Crowley, J.L., Smith, T.C., Fang, Z., Takizawa, N., and Luna, E.J. (2008). Supervillin Reorganizes the Actin Cytoskeleton and Increases Invadopodial Efficiency. Mol. Biol. Cell.

D'Souza-Schorey, C., and Chavrier, P. (2006). ARF proteins: roles in membrane traffic and beyond. Nat Rev Mol Cell Biol *7*, 347-358.

De Corte, V., Bruyneel, E., Boucherie, C., Mareel, M., Vandekerckhove, J., and Gettemans, J. (2002). Gelsolin-induced epithelial cell invasion is dependent on Ras-Rac signaling. EMBO J. *21*, 6781-6790.

Deryugina, E.I., Ratnikov, B., Monosov, E., Postnova, T.I., DiScipio, R., Smith, J.W., and Strongin, A.Y. (2001). MT1-MMP initiates activation of pro-MMP-2 and integrin alphavbeta3 promotes maturation of MMP-2 in breast carcinoma cells. Exp. Cell Res. *263*, 209-223.

Destaing, O., Saltel, F., Geminard, J.C., Jurdic, P., and Bard, F. (2003). Podosomes display actin turnover and dynamic self-organization in osteoclasts expressing actin-green fluorescent protein. Mol. Biol. Cell *14*, 407-416.

Destaing, O., Sanjay, A., Itzstein, C., Horne, W.C., Toomre, D., De Camilli, P., and Baron, R. (2008). The tyrosine kinase activity of c-Src regulates actin dynamics and organization of podosomes in osteoclasts. Mol. Biol. Cell *19*, 394-404.

Dolganiuc, V., McGinnes, L., Luna, E.J., and Morrison, T.G. (2003). Role of the cytoplasmic domain of the Newcastle disease virus fusion protein in association with lipid rafts.J. Virol. *77*, 12968-12979.

Donaldson, J.G., and Honda, A. (2005). Localization and function of Arf family GTPases. Biochemical Society transactions *33*, 639-642.

Dong, Y., Asch, H.L., Medina, D., Ip, C., Ip, M., Guzman, R., and Asch, B.B. (1999). Concurrent deregulation of gelsolin and cyclin D1 in the majority of human and rodent breast cancers. Int J Cancer *81*, 930-938.

Echarri, A., Muriel, O., and Del Pozo, M.A. (2007). Intracellular trafficking of raft/caveolae domains: insights from integrin signaling. Seminars in cell & developmental biology *18*, 627-637.

Edidin, M. (2003). The state of lipid rafts: from model membranes to cells. Annual review of biophysics and biomolecular structure *32*, 257-283.

Evans, J.G., Correia, I., Krasavina, O., Watson, N., and Matsudaira, P. (2003). Macrophage podosomes assemble at the leading lamella by growth and fragmentation. J. Cell Biol. *161*, 697-705.

Evans, J.G., and Matsudaira, P. (2006). Structure and dynamics of macrophage podosomes. Eur. J. Cell Biol. *85*, 145-149.

Furmaniak-Kazmierczak, E., Crawley, S.W., Carter, R.L., Maurice, D.H., and Cote, G.P. (2007). Formation of extracellular matrix-digesting invadopodia by primary aortic smooth muscle cells. Circ Res *100*, 1328-1336.

Galvez, B.G., Matias-Roman, S., Yanez-Mo, M., Sanchez-Madrid, F., and Arroyo, A.G. (2002). ECM regulates MT1-MMP localization with beta1 or alphavbeta3 integrins at distinct cell compartments modulating its internalization and activity on human endothelial cells. J. Cell Biol. *159*, 509-521.

Gangopadhyay, S.S., Takizawa, N., Gallant, C., Barber, A.L., Je, H.D., Smith, T.C., Luna, E.J., and Morgan, K.G. (2004). Smooth muscle archvillin: A novel regulator of signaling and contractility in vascular smooth muscle. J. Cell Sci. *117*, 5043-5057.

Gaus, K., Le Lay, S., Balasubramanian, N., and Schwartz, M.A. (2006). Integrin-mediated adhesion regulates membrane order. J. Cell Biol. *174*, 725-734.

Gavazzi, I., Nermut, M.V., and Marchisio, P.C. (1989). Ultrastructure and gold-immunolabelling of cell-substratum adhesions (podosomes) in RSV-transformed BHK cells. J. Cell Sci. *94 ( Pt 1)*, 85-99.

Geiger, B., Bershadsky, A., Pankov, R., and Yamada, K.M. (2001). Transmembrane extracellular matrix--cytoskeleton crosstalk. Nat Rev Mol Cell Biol *2*, 793-805.

Gietz, R.D., and Woods, R.A. (2002). Transformation of yeast by lithium acetate/single-stranded carrier DNA/polyethylene glycol method. Methods in enzymology *350*, 87-96.

Gimona, M., Buccione, R., Courtneidge, S.A., and Linder, S. (2008). Assembly and biological role of podosomes and invadopodia. Curr. Opin. Cell Biol. *20*, 235-241.

Gimona, M., Kaverina, I., Resch, G.P., Vignal, E., and Burgstaller, G. (2003). Calponin repeats regulate actin filament stability and formation of podosomes in smooth muscle cells. Mol. Biol. Cell *14*, 2482-2491.

Gomez-Mouton, C., Abad, J.L., Mira, E., Lacalle, R.A., Gallardo, E., Jimenez-Baranda, S., Illa, I., Bernad, A., Manes, S., and Martinez, A.C. (2001). Segregation of leading-edge and uropod components into specific lipid rafts during T cell polarization. Proc Natl Acad Sci U S A *98*, 9642-9647.

Gomez-Mouton, C., Lacalle, R.A., Mira, E., Jimenez-Baranda, S., Barber, D.F., Carrera, A.C., Martinez, A.C., and Manes, S. (2004). Dynamic redistribution of raft domains as an organizing platform for signaling during cell chemotaxis. J. Cell Biol. *164*, 759-768.

Govind, A.P., and Thampan, R.V. (2003). Membrane associated estrogen receptors and related proteins: localization at the plasma membrane and the endoplasmic reticulum. Molecular and cellular biochemistry *253*, 233-240.

Grady, R.M., Teng, H., Nichol, M.C., Cunningham, J.C., Wilkinson, R.S., and Sanes, J.R. (1997). Skeletal and cardiac myopathies in mice lacking utrophin and dystrophin: a model for Duchenne muscular dystrophy. Cell *90*, 729-738.

Gupta, N., Wollscheid, B., Watts, J.D., Scheer, B., Aebersold, R., and DeFranco, A.L. (2006). Quantitative proteomic analysis of B cell lipid rafts reveals that ezrin regulates antigen receptor-mediated lipid raft dynamics. Nature immunology *7*, 625-633.

Gusev, N.B. (2001). Some properties of caldesmon and calponin and the participation of these proteins in regulation of smooth muscle contraction and cytoskeleton formation. Biochemistry (Moscow) *66*, 1112-1121.

Hai, C.M., Hahne, P., Harrington, E.O., and Gimona, M. (2002). Conventional protein kinase C mediates phorbol-dibutyrate-induced cytoskeletal remodeling in a7r5 smooth muscle cells. Exp. Cell Res. *280*, 64-74.

Hammarlund, M., Davis, W.S., and Jorgensen, E.M. (2000). Mutations in beta-spectrin disrupt axon outgrowth and sarcomere structure. J. Cell Biol. *149*, 931-942.

Hancock, J.F. (2006). Lipid rafts: contentious only from simplistic standpoints. Nat Rev Mol Cell Biol *7*, 456-462.

Harder, T., Scheiffele, P., Verkade, P., and Simons, K. (1998). Lipid domain structure of the plasma membrane revealed by patching of membrane components. J. Cell Biol. *141*, 929-942.

Hartwig, J.H., Chambers, K.A., and Stossel, T.P. (1989). Association of gelsolin with actin filaments and cell membranes of macrophages and platelets. J. Cell Biol. *108*, 467-479.

Hashimoto, S., Onodera, Y., Hashimoto, A., Tanaka, M., Hamaguchi, M., Yamada, A., and Sabe, H. (2004). Requirement for Arf6 in breast cancer invasive activities. Proc Natl Acad Sci U S A *101*, 6647-6652.

Hedenfalk, I., Ringner, M., Ben-Dor, A., Yakhini, Z., Chen, Y., Chebil, G., Ach, R., Loman, N., Olsson, H., Meltzer, P., Borg, A., and Trent, J. (2003). Molecular classification of familial non-BRCA1/BRCA2 breast cancer. Proc Natl Acad Sci U S A *100*, 2532-2537.

Heerklotz, H. (2002). Triton promotes domain formation in lipid raft mixtures. Biophysical journal *83*, 2693-2701.

Hiol, A., Davey, P.C., Osterhout, J.L., Waheed, A.A., Fischer, E.R., Chen, C.K., Milligan, G., Druey, K.M., and Jones, T.L. (2003). Palmitoylation regulates regulators of G-protein signaling (RGS) 16 function. I. Mutation of amino-terminal cysteine residues on RGS16 prevents its targeting to lipid rafts and palmitoylation of an internal cysteine residue. J. Biol. Chem. *278*, 19301-19308.

Hoffman, E.P., Brown, R.H., Jr., and Kunkel, L.M. (1987). Dystrophin: the protein product of the Duchenne muscular dystrophy locus. Cell *51*, 919-928.

Hofman, E.G., Ruonala, M.O., Bader, A.N., van den Heuvel, D., Voortman, J., Roovers, R.C., Verkleij, A.J., Gerritsen, H.C., and van Bergen En Henegouwen, P.M. (2008). EGF induces coalescence of different lipid rafts. J. Cell Sci. *121*, 2519-2528.

Holowka, D., Sheets, E.D., and Baird, B. (2000). Interactions between Fc(epsilon)RI and lipid raft components are regulated by the actin cytoskeleton. J. Cell Sci. *113 ( Pt 6)*, 1009-1019.

Hoover, H., Muralidharan-Chari, V., Tague, S., and D'Souza-Schorey, C. (2005). Investigating the role of ADP-ribosylation factor 6 in tumor cell invasion and extracellular signal-regulated kinase activation. Methods in enzymology *404*, 134-147.

Huang, J., Liu, T., Xu, L.G., Chen, D., Zhai, Z., and Shu, H.B. (2005). SIKE is an IKK epsilon/TBK1-associated suppressor of TLR3- and virus-triggered IRF-3 activation pathways. EMBO J. *24*, 4018-4028.

Ikebe, M., and Hartshorne, D.J. (1984). Conformation-dependent proteolysis of smooth-muscle myosin. J. Biol. Chem. *259*, 11639-11642.

Ikebe, M., and Hartshorne, D.J. (1985). Proteolysis of smooth muscle myosin by Staphylococcus aureus protease: preparation of heavy meromyosin and subfragment 1 with intact 20 000-dalton light chains. Biochemistry *24*, 2380-2387.

Ikebe, M., and Reardon, S. (1988). Binding of caldesmon to smooth muscle myosin. J. Biol. Chem. *263*, 3055-3058.

Ikebe, M., Yamada, M., Mabuchi, K., Kambara, T., and Ikebe, R. (1998). A specific amino acid sequence at the head-rod junction is not critical for the phosphorylation-dependent regulation of smooth muscle myosin. Biochemistry *37*, 13285-13290.

Ingley, E. (2008). Src family kinases: regulation of their activities, levels and identification of new pathways. Biochimica et biophysica acta *1784*, 56-65.

Inui, T., Ishibashi, O., Origane, Y., Fujimori, K., Kokubo, T., and Nakajima, M. (1999). Matrix metalloproteinases and lysosomal cysteine proteases in osteoclasts contribute to bone resorption through distinct modes of action. Biochemical and biophysical research communications *258*, 173-178.

Jenzora, A., Behrendt, B., Small, J.V., Wehland, J., and Stradal, T.E. (2005). PREL1 provides a link from Ras signalling to the actin cytoskeleton via Ena/VASP proteins. FEBS Lett *579*, 455-463.

Jung, H.S., Komatsu, S., Ikebe, M., and Craig, R. (2008). Head-head and head-tail interaction: a general mechanism for switching off myosin II activity in cells. Mol. Biol. Cell *19*, 3234-3242.

Kahya, N., Brown, D.A., and Schwille, P. (2005). Raft partitioning and dynamic behavior of human placental alkaline phosphatase in giant unilamellar vesicles. Biochemistry *44*, 7479-7489.

Kaksonen, M., Peng, H.B., and Rauvala, H. (2000). Association of cortactin with dynamic actin in lamellipodia and on endosomal vesicles. J. Cell Sci. *113 Pt 24*, 4421-4426.

Khurana, S., and George, S.P. (2008). Regulation of cell structure and function by actin-binding proteins: Villin's perspective. FEBS Lett *582*, 2128-2139.

Kim, C.S., Furuya, F., Ying, H., Kato, Y., Hanover, J.A., and Cheng, S.Y. (2007). Gelsolin: a novel thyroid hormone receptor-beta interacting protein that modulates tumor progression in a mouse model of follicular thyroid cancer. Endocrinology *148*, 1306-1312.

Kleinman, H.K., and Martin, G.R. (2005). Matrigel: basement membrane matrix with biological activity. Semin Cancer Biol *15*, 378-386.

Kohama, K., Ye, L.-H., Hayakawa, K., and Okagaki, T. (1996). Myosin light chain kinase: an actin-binding protein that regulates an ATP-dependent interaction with myosin. TiPS *17*, 284-287.

Konishi, K., Kojima, S., Katoh, T., Yazawa, M., Kato, K., Fujiwara, K., and Onishi, H. (2001). Two new modes of smooth muscle myosin regulation by the interaction between the two regulatory light chains, and by the S2 domain. J Biochem (Tokyo) *129*, 365-372.

Kowalczyk, A.P., Bornslaeger, E.A., Borgwardt, J.E., Palka, H.L., Dhaliwal, A.S., Corcoran, C.M., Denning, M.F., and Green, K.J. (1997). The amino-terminal domain of desmoplakin binds to plakoglobin and clusters desmosomal cadherin-plakoglobin complexes. J. Cell Biol. *139*, 773-784.

Krause, M., Leslie, J.D., Stewart, M., Lafuente, E.M., Valderrama, F., Jagannathan, R., Strasser, G.A., Rubinson, D.A., Liu, H., Way, M., Yaffe, M.B., Boussiotis, V.A., and Gertler, F.B. (2004). Lamellipodin, an Ena/VASP ligand, is implicated in the regulation of lamellipodial dynamics. Dev Cell *7*, 571-583.

Kunst, G., Kress, K.R., Gruen, M., Uttenweiler, D., Gautel, M., and Fink, R.H. (2000). Myosin binding protein C, a phosphorylation-dependent force regulator in muscle that controls the attachment of myosin heads by its interaction with myosin S2. Circ Res *86*, 51-58.

Kusumi, A., Nakada, C., Ritchie, K., Murase, K., Suzuki, K., Murakoshi, H., Kasai, R.S., Kondo, J., and Fujiwara, T. (2005). Paradigm shift of the plasma membrane concept from the two-dimensional continuum fluid to the partitioned fluid: high-speed single-molecule tracking of membrane molecules. Annual review of biophysics and biomolecular structure *34*, 351-378.

Laemmli, U.K. (1970). Cleavage of structural proteins during the assembly of the head of bacteriophage T4. Nature (Lond.) *227*, 680-685.

Lai, E.C. (2003). Lipid rafts make for slippery platforms. J. Cell Biol. *162*, 365-370.

Lai, Y.J., Chen, C.S., Lin, W.C., and Lin, F.T. (2005). c-Src-mediated phosphorylation of TRIP6 regulates its function in lysophosphatidic acid-induced cell migration. Mol. Cell. Biol. *25*, 5859-5868.

Lai, Y.J., Lin, W.C., and Lin, F.T. (2007). PTPL1/FAP-1 negatively regulates TRIP6 function in lysophosphatidic acid-induced cell migration. J. Biol. Chem. *282*, 24381-24387.

Laliberte, J.P., McGinnes, L.W., and Morrison, T.G. (2007). Incorporation of functional HN-F glycoprotein-containing complexes into newcastle disease virus is dependent on cholesterol and membrane lipid raft integrity.J. Virol. *81*, 10636-10648.

Laliberte, J.P., McGinnes, L.W., Peeples, M.E., and Morrison, T.G. (2006). Integrity of membrane lipid rafts is necessary for the ordered assembly and release of infectious Newcastle disease virus particles.J. Virol. *80*, 10652-10662.

Lauffenburger, D.A., and Horwitz, A.F. (1996). Cell migration: A physically integrated molecular process. Cell *84*, 359-369.

Laughlin, R.C., McGugan, G.C., Powell, R.R., Welter, B.H., and Temesvari, L.A. (2004). Involvement of raft-like plasma membrane domains of Entamoeba histolytica in pinocytosis and adhesion. Infection and immunity *72*, 5349-5357.

Le Mellay, V., Grosse, B., and Lieberherr, M. (1997). Phospholipase C beta and membrane action of calcitriol and estradiol. J. Biol. Chem. *272*, 11902-11907.

Lee, H.K., Driscoll, D., Asch, H., Asch, B., and Zhang, P.J. (1999). Downregulated gelsolin expression in hyperplastic and neoplastic lesions of the prostate. Prostate *40*, 14-19.

Leitinger, B., and Hogg, N. (2002). The involvement of lipid rafts in the regulation of integrin function. J. Cell Sci. *115*, 963-972.

Li, Y., Tondravi, M., Liu, J., Smith, E., Haudenschild, C.C., Kaczmarek, M., and Zhan, X. (2001). Cortactin potentiates bone metastasis of breast cancer cells. Cancer Res. *61*, 6906-6911.

Lichtenberg, D., Goni, F.M., and Heerklotz, H. (2005). Detergent-resistant membranes should not be identified with membrane rafts. Trends in biochemical sciences *30*, 430-436.

Linder, S. (2007). The matrix corroded: podosomes and invadopodia in extracellular matrix degradation. Trends Cell Biol *17*, 107-117.

Linder, S., and Aepfelbacher, M. (2003). Podosomes: adhesion hot-spots of invasive cells. Trends Cell Biol *13*, 376-385.

Linder, S., Higgs, H., Hufner, K., Schwarz, K., Pannicke, U., and Aepfelbacher, M. (2000). The polarization defect of Wiskott-Aldrich syndrome macrophages is linked to dislocalization of the Arp2/3 complex. J Immunol *165*, 221-225.

Linder, S., Nelson, D., Weiss, M., and Aepfelbacher, M. (1999). Wiskott-Aldrich syndrome protein regulates podosomes in primary human macrophages. Proc Natl Acad Sci U S A *96*, 9648-9653.

Lladó, A., Timpson, P., Vila de Muga, S., Moreto, J., Pol, A., Grewal, T., Daly, R.J., Enrich, C., and Tebar, F. (2008). Protein Kinase C{delta} and Calmodulin Regulate Epidermal Growth Factor Receptor Recycling from Early Endosomes through Arp2/3 Complex and Cortactin. Mol. Biol. Cell *19*, 17-29.

Lo, S.H. (2006). Focal adhesions: what's new inside. Dev Biol *294*, 280-291.

Lock, P., Abram, C.L., Gibson, T., and Courtneidge, S.A. (1998). A new method for isolating tyrosine kinase substrates used to identify fish, an SH3 and PX domain-containing protein, and Src substrate. EMBO J. *17*, 4346-4357.

Luna, E.J. (1998). F-actin blot overlays. Methods in enzymology *298*, 32-42.

Machesky, L., Jurdic, P., and Hinz, B. (2008). Grab, stick, pull and digest: the functional diversity of actin-associated matrix-adhesion structures. Workshop on Invadopodia, Podosomes and Focal Adhesions in Tissue Invasion. EMBO Rep *9*, 139-143.

Mackay, D.J.G., Esch, F., Furthmayr, H., and Hall, A. (1997). Rho- and Rac-dependent assembly of focal adhesion complexes and actin filaments in permeabilized fibroblasts: An essential role for ezrin/radixin/moesin proteins. J. Cell Biol. *138*, 927-938.

MacLennan, A.J., Orringer, M.B., and Beer, D.G. (1999). Identification of intestinal-type Barrett's metaplasia by using the intestine-specific protein villin and esophageal brush cytology. Mol Carcinog *24*, 137-143.

Magdalena, J., Millard, T.H., Etienne-Manneville, S., Launay, S., Warwick, H.K., and Machesky, L.M. (2003). Involvement of the Arp2/3 complex and Scar2 in Golgi polarity in scratch wound models. Mol. Biol. Cell *14*, 670-684.

Manes, S., Ana Lacalle, R., Gomez-Mouton, C., and Martinez, A.C. (2003). From rafts to crafts: membrane asymmetry in moving cells. Trends in immunology *24*, 320-326.

Marchisio, P.C., Cirillo, D., Naldini, L., Primavera, M.V., Teti, A., and Zambonin-Zallone, A. (1984). Cell-substratum interaction of cultured avian osteoclasts is mediated by specific adhesion structures. J. Cell Biol. *99*, 1696-1705.

Marchisio, P.C., Cirillo, D., Teti, A., Zambonin-Zallone, A., and Tarone, G. (1987). Rous sarcoma virus-transformed fibroblasts and cells of monocytic origin display a peculiar dot-like organization of cytoskeletal proteins involved in microfilament-membrane interactions. Exp. Cell Res. *169*, 202-214.

Mareel, M., and Leroy, A. (2003). Clinical, cellular, and molecular aspects of cancer invasion. Physiological reviews *83*, 337-376.

Martinez-Quiles, N., Ho, H.Y., Kirschner, M.W., Ramesh, N., and Geha, R.S. (2004). Erk/Src phosphorylation of cortactin acts as a switch on-switch off mechanism that controls its ability to activate N-WASP. Mol. Cell. Biol. *24*, 5269-5280.

Mazzone, M., Baldassarre, M., Beznoussenko, G., Giacchetti, G., Cao, J., Zucker, S., Luini, A., and Buccione, R. (2004). Intracellular processing and activation of membrane type 1 matrix metalloprotease depends on its partitioning into lipid domains. J. Cell Sci. *117*, 6275-6287.

Melkonian, K.A., Ostermeyer, A.G., Chen, J.Z., Roth, M.G., and Brown, D.A. (1999). Role of lipid modifications in targeting proteins to detergent-resistant membrane rafts. Many raft proteins are acylated, while few are prenylated. J. Biol. Chem. *274*, 3910-3917.

Mere, J., Chahinian, A., Maciver, S.K., Fattoum, A., Bettache, N., Benyamin, Y., and Roustan, C. (2005). Gelsolin binds to polyphosphoinositide-free lipid vesicles and simultaneously to actin microfilaments. Biochem J *386*, 47-56.

Migliaccio, A., Piccolo, D., Castoria, G., Di Domenico, M., Bilancio, A., Lombardi, M., Gong, W., Beato, M., and Auricchio, F. (1998). Activation of the Src/p21ras/Erk pathway by progesterone receptor via cross-talk with estrogen receptor. EMBO J. *17*, 2008-2018.

Mineo, C., James, G.L., Smart, E.J., and Anderson, R.G. (1996). Localization of epidermal growth factor-stimulated Ras/Raf-1 interaction to caveolae membrane. J. Biol. Chem. *271*, 11930-11935.

Mizushima, S., and Nagata, S. (1990). pEF-BOS, a powerful mammalian expression vector. Nucl. Acids Res. *18*, 5322.

Mizutani, K., Miki, H., He, H., Maruta, H., and Takenawa, T. (2002). Essential role of neural Wiskott-Aldrich syndrome protein in podosome formation and degradation of extracellular matrix in src-transformed fibroblasts. Cancer Res. *62*, 669-674.

Monks, C.R., Freiberg, B.A., Kupfer, H., Sciaky, N., and Kupfer, A. (1998). Three-dimensional segregation of supramolecular activation clusters in T cells. Nature *395*, 82-86.

Moorthy, S., Chen, L., and Bennett, V. (2000). Caenorhabditis elegans beta-G spectrin is dispensable for establishment of epithelial polarity, but essential for muscular and neuronal function. J. Cell Biol. *149*, 915-930.

Morgan, K.G., and Gangopadhyay, S.S. (2001). Cross-bridge regulation by thin filament-associated proteins. J Appl Physiol *91*, 953-962.

Morley, P., Whitfield, J.F., Vanderhyden, B.C., Tsang, B.K., and Schwartz, J.L. (1992). A new, nongenomic estrogen action: the rapid release of intracellular calcium. Endocrinology *131*, 1305-1312.

Mueller, S.C., and Chen, W.T. (1991). Cellular invasion into matrix beads: localization of beta 1 integrins and fibronectin to the invadopodia. J. Cell Sci. *99 ( Pt 2)*, 213-225.

Mueller, S.C., Ghersi, G., Akiyama, S.K., Sang, Q.X., Howard, L., Pineiro-Sanchez, M., Nakahara, H., Yeh, Y., and Chen, W.T. (1999). A novel protease-docking function of integrin at invadopodia. J. Biol. Chem. *274*, 24947-24952.

Munro, S. (2003). Lipid rafts: elusive or illusive? Cell *115*, 377-388.

Myoui, A., Nishimura, R., Williams, P.J., Hiraga, T., Tamura, D., Michigami, T., Mundy, G.R., and Yoneda, T. (2003). C-SRC tyrosine kinase activity is associated with tumor colonization in bone and lung in an animal model of human breast cancer metastasis. Cancer Res. *63*, 5028-5033.

Nakahara, H., Mueller, S.C., Nomizu, M., Yamada, Y., Yeh, Y., and Chen, W.T. (1998). Activation of beta1 integrin signaling stimulates tyrosine phosphorylation of p190RhoGAP and membrane-protrusive activities at invadopodia. J. Biol. Chem. *273*, 9-12.

Nakahara, H., Otani, T., Sasaki, T., Miura, Y., Takai, Y., and Kogo, M. (2003). Involvement of Cdc42 and Rac small G proteins in invadopodia formation of RPMI7951 cells. Genes Cells *8*, 1019-1027.

Nebl, T., Pestonjamasp, K.N., Leszyk, J.D., Crowley, J.L., Oh, S.W., and Luna, E.J. (2002). Proteomic analysis of a detergent-resistant membrane skeleton from neutrophil plasma membranes. J. Biol. Chem. *277*, 43399-43409.

Nichols, B. (2005). Cell biology: without a raft. Nature *436*, 638-639.

Nitsch, L., Gionti, E., Cancedda, R., and Marchisio, P.C. (1989). The podosomes of Rous sarcoma virus transformed chondrocytes show a peculiar ultrastructural organization. Cell Biol Int Rep *13*, 919-926.

Nomura, H., Uzawa, K., Ishigami, T., Kouzu, Y., Koike, H., Ogawara, K., Siiba, M., Bukawa, H., Yokoe, H., Kubosawa, H., and Tanzawa, H. (2008). Clinical significance of gelsolin-like actin-capping protein expression in oral carcinogenesis: an immunohistochemical study of premalignant and malignant lesions of the oral cavity. BMC Cancer *8*, 39.

Ochoa, G.C., Slepnev, V.I., Neff, L., Ringstad, N., Takei, K., Daniell, L., Kim, W., Cao, H., McNiven, M., Baron, R., and De Camilli, P. (2000). A functional link between dynamin and the actin cytoskeleton at podosomes. J. Cell Biol. *150*, 377-389.

Oh, S.W., Pope, R.K., Smith, K.P., Crowley, J.L., Nebl, T., Lawrence, J.B., and Luna, E.J. (2003). Archvillin, a muscle-specific isoform of supervillin, is an early expressed component of the costameric membrane skeleton. J. Cell Sci. *116*, 2261-2275.

Ohlendieck, K., Ervasti, J.M., Snook, J.B., and Campbell, K.P. (1991). Dystrophin-glycoprotein complex is highly enriched in isolated skeletal muscle sarcolemma. J. Cell Biol. *112*, 135-148.

Oikawa, T., Itoh, T., and Takenawa, T. (2008). Sequential signals toward podosome formation in NIH-src cells. J. Cell Biol. *182*, 157-169.

Osiak, A.E., Zenner, G., and Linder, S. (2005). Subconfluent endothelial cells form podosomes downstream of cytokine and RhoGTPase signaling. Exp. Cell Res. *307*, 342-353.

Palacios, F., Price, L., Schweitzer, J., Collard, J.G., and D'Souza-Schorey, C. (2001). An essential role for ARF6-regulated membrane traffic in adherens junction turnover and epithelial cell migration. EMBO J. *20*, 4973-4986.

Paluch, E., van der Gucht, J., Joanny, J.F., and Sykes, C. (2006). Deformations in actin comets from rocketing beads. Biophysical journal *91*, 3113-3122.

Partridge, J.J., Madsen, M.A., Ardi, V.C., Papagiannakopoulos, T., Kupriyanova, T.A., Quigley, J.P., and Deryugina, E.I. (2007). Functional analysis of matrix metalloproteinases and tissue inhibitors of metalloproteinases differentially expressed by variants of human HT-1080 fibrosarcoma exhibiting high and low levels of intravasation and metastasis. J. Biol. Chem. *282*, 35964-35977.

Perrin, B.J., Amann, K.J., and Huttenlocher, A. (2006). Proteolysis of cortactin by calpain regulates membrane protrusion during cell migration. Mol. Biol. Cell *17*, 239-250.

Pestonjamasp, K., Amieva, M.R., Strassel, C.P., Nauseef, W.M., Furthmayr, H., and Luna, E.J. (1995). Moesin, ezrin, and p205 are actin-binding proteins associated with neutrophil plasma membranes. Mol. Biol. Cell *6*, 247-259.

Pestonjamasp, K.N., Pope, R.K., Wulfkuhle, J.D., and Luna, E.J. (1997). Supervillin (p205): A novel membrane-associated, F-actin-binding protein in the villin/gelsolin superfamily. J. Cell Biol. *139*, 1255-1269.

Pike, L.J. (2006). Rafts defined: a report on the Keystone Symposium on Lipid Rafts and Cell Function. Journal of lipid research *47*, 1597-1598.

Pope, R.K., Pestonjamasp, K.N., Smith, K.P., Wulfkuhle, J.D., Strassel, C.P., Lawrence, J.B., and Luna, E.J. (1998). Cloning, characterization, and chromosomal localization of human supervillin (SVIL). Genomics *52*, 342-351.

Porter, M.E., Scholey, J.M., Stemple, D.L., Vigers, G.P., Vale, R.D., Sheetz, M.P., and McIntosh, J.R. (1987). Characterization of the microtubule movement produced by sea urchin egg kinesin. J. Biol. Chem. *262*, 2794-2802.

Pralle, A., Keller, P., Florin, E.L., Simons, K., and Horber, J.K. (2000). Sphingolipid-cholesterol rafts diffuse as small entities in the plasma membrane of mammalian cells. J. Cell Biol. *148*, 997-1008.

Razandi, M., Pedram, A., Greene, G.L., and Levin, E.R. (1999). Cell membrane and nuclear estrogen receptors (ERs) originate from a single transcript: studies of ERalpha and ERbeta expressed in Chinese hamster ovary cells. Mol. Endocrinol. *13*, 307-319.

Razandi, M., Pedram, A., Park, S.T., and Levin, E.R. (2003). Proximal events in signaling by plasma membrane estrogen receptors. J. Biol. Chem. *278*, 2701-2712.

Razani, B., Schlegel, A., and Lisanti, M.P. (2000). Caveolin proteins in signaling, oncogenic transformation and muscular dystrophy. J. Cell Sci. *113*, 2103-2109.

Resh, M.D. (1999). Fatty acylation of proteins: new insights into membrane targeting of myristoylated and palmitoylated proteins. Biochimica et biophysica acta *1451*, 1-16.

Resh, M.D. (2004). Membrane targeting of lipid modified signal transduction proteins. Sub-cellular biochemistry *37*, 217-232.

Ridley, A.J., Schwartz, M.A., Burridge, K., Firtel, R.A., Ginsberg, M.H., Borisy, G., Parsons, J.T., and Horwitz, A.R. (2003). Cell migration: integrating signals from front to back. Science (New York, N.Y *302*, 1704-1709.

Rieder, G., Tessier, A.J., Qiao, X.T., Madison, B., Gumucio, D.L., and Merchant, J.L. (2005). Helicobacter-induced intestinal metaplasia in the stomach correlates with Elk-1 and serum response factor induction of villin. J. Biol. Chem. *280*, 4906-4912.

Romer, L.H., Birukov, K.G., and Garcia, J.G. (2006). Focal adhesions: paradigm for a signaling nexus. Circ Res *98*, 606-616.

Sak, K., and Everaus, H. (2004). Nongenomic effects of 17beta-estradiol--diversity of membrane binding sites. J Steroid Biochem Mol Biol *88*, 323-335.

Sandilands, E., and Frame, M.C. (2008). Endosomal trafficking of Src tyrosine kinase. Trends Cell Biol *18*, 322-329.

Santen, R.J., Song, R.X., Zhang, Z., Yue, W., and Kumar, R. (2004). Adaptive hypersensitivity to estrogen: mechanism for sequential responses to hormonal therapy in breast cancer. Clin Cancer Res *10*, 337S-345S.

Schuuring, E., Verhoeven, E., Mooi, W.J., and Michalides, R.J. (1992). Identification and cloning of two overexpressed genes, U21B31/PRAD1 and EMS1, within the amplified chromosome 11q13 region in human carcinomas. Oncogene *7*, 355-361.

Seals, D.F., Azucena, E.F., Jr., Pass, I., Tesfay, L., Gordon, R., Woodrow, M., Resau, J.H., and Courtneidge, S.A. (2005). The adaptor protein Tks5/Fish is required for podosome formation and function, and for the protease-driven invasion of cancer cells. Cancer Cell *7*, 155-165.

Seveau, S., Eddy, R.J., Maxfield, F.R., and Pierini, L.M. (2001). Cytoskeleton-dependent membrane domain segregation during neutrophil polarization. Mol. Biol. Cell *12*, 3550-3562.

Shinjo, K., Koland, J.G., Hart, M.J., Narasimhan, V., Johnson, D.I., Evans, T., and Cerione, R.A. (1990). Molecular cloning of the gene for the human placental GTP-binding protein Gp (G25K): identification of this GTP-binding protein as the human homolog of the yeast cell-division-cycle protein CDC42. Proc Natl Acad Sci U S A *87*, 9853-9857.

Shogomori, H., and Brown, D.A. (2003). Use of detergents to study membrane rafts: the good, the bad, and the ugly. Biological chemistry *384*, 1259-1263.

Silacci, P., Mazzolai, L., Gauci, C., Stergiopulos, N., Yin, H.L., and Hayoz, D. (2004). Gelsolin superfamily proteins: key regulators of cellular functions. Cell Mol Life Sci *61*, 2614-2623.

Simons, K., and Toomre, D. (2000). Lipid rafts and signal transduction. Nat Rev Mol Cell Biol *1*, 31-39.

Singer, S.J., and Nicolson, G.L. (1972). The fluid mosaic model of the structure of cell membranes. Science (New York, N.Y *175*, 720-731.

Sohail, A., Sun, Q., Zhao, H., Bernardo, M.M., Cho, J.A., and Fridman, R. (2008). MT4-(MMP17) and MT6-MMP (MMP25), A unique set of membrane-anchored matrix metalloproteinases: properties and expression in cancer. Cancer metastasis reviews *27*, 289-302.

Spinardi, L., and Marchisio, P.C. (2006). Podosomes as smart regulators of cellular adhesion. Eur. J. Cell Biol. *85*, 191-194.

Stenbeck, G., and Horton, M.A. (2000). A new specialized cell-matrix interaction in actively resorbing osteoclasts. J. Cell Sci. *113 ( Pt 9)*, 1577-1587.

Stendahl, O.I., Hartwig, J.H., Brotschi, E.A., and Stossel, T.P. (1980). Distribution of actin-binding protein and myosin in macrophages during spreading and phagocytosis. J. Cell Biol. *84*, 215-224.

Stickney, J.T., Bacon, W.C., Rojas, M., Ratner, N., and Ip, W. (2004). Activation of the tumor suppressor merlin modulates its interaction with lipid rafts. Cancer Res. *64*, 2717-2724.

Stone, K.R., Mickey, D.D., Wunderli, H., Mickey, G.H., and Paulson, D.F. (1978). Isolation of a human prostate carcinoma cell line (DU 145). Int J Cancer *21*, 274-281.

Stromer, M.H. (1995). Immunocytochemistry of the muscle cell cytoskeleton. Microscopy research and technique *31*, 95-105.

Stylli, S.S., Kaye, A.H., and Lock, P. (2008). Invadopodia: At the cutting edge of tumour invasion. J Clin Neurosci *15*, 725-737.

Tague, S.E., Muralidharan, V., and D'Souza-Schorey, C. (2004). ADP-ribosylation factor 6 regulates tumor cell invasion through the activation of the MEK/ERK signaling pathway. Proc Natl Acad Sci U S A *101*, 9671-9676.

Takino, T., Watanabe, Y., Matsui, M., Miyamori, H., Kudo, T., Seiki, M., and Sato, H. (2006). Membrane-type 1 matrix metalloproteinase modulates focal adhesion stability and cell migration. Exp. Cell Res. *312*, 1381-1389.

Takizawa, N., Ikebe, R., Ikebe, M., and Luna, E.J. (2007). Supervillin slows cell spreading by facilitating myosin II activation at the cell periphery. J. Cell Sci. *120*, 3792-3803.

Takizawa, N., Smith, T.C., Nebl, T., Crowley, J.L., Palmieri, S.J., Lifshitz, L.M., Ehrhardt, A.G., Hoffman, L.M., Beckerle, M.C., and Luna, E.J. (2006). Supervillin modulation of focal adhesions involving TRIP6/ZRP-1. J. Cell Biol. *174*, 447-458.

Tang, B., Vu, M., Booker, T., Santner, S.J., Miller, F.R., Anver, M.R., and Wakefield, L.M. (2003). TGF-beta switches from tumor suppressor to prometastatic factor in a model of breast cancer progression. J Clin Invest *112*, 1116-1124.

Tavano, R., Contento, R.L., Baranda, S.J., Soligo, M., Tuosto, L., Manes, S., and Viola, A. (2006). CD28 interaction with filamin-A controls lipid raft accumulation at the T-cell immunological synapse. Nat. Cell Biol. *8*, 1270-1276.

Tehrani, S., Tomasevic, N., Weed, S., Sakowicz, R., and Cooper, J.A. (2007). Src phosphorylation of cortactin enhances actin assembly. Proc Natl Acad Sci U S A *104*, 11933-11938.

Thalmann, G.N., Anezinis, P.E., Chang, S.M., Zhau, H.E., Kim, E.E., Hopwood, V.L., Pathak, S., von Eschenbach, A.C., and Chung, L.W. (1994). Androgen-independent cancer progression and bone metastasis in the LNCaP model of human prostate cancer. Cancer Res. *54*, 2577-2581.

Thomas, C.M., and Smart, E.J. (2008). Caveolae structure and function. Journal of cellular and molecular medicine *12*, 796-809.

Ting, H.J., Yeh, S., Nishimura, K., and Chang, C. (2002). Supervillin associates with androgen receptor and modulates its transcriptional activity. Proc Natl Acad Sci U S A *99*, 661-666.

Toba, S., and Toyoshima, Y.Y. (2004). Dissociation of double-headed cytoplasmic dynein into single-headed species and its motile properties. Cell Motil Cytoskeleton *58*, 281-289.

Togo, T., and Steinhardt, R.A. (2004). Nonmuscle myosin IIA and IIB have distinct functions in the exocytosis-dependent process of cell membrane repair. Mol. Biol. Cell *15*, 688-695.

Towbin, H., Stahelin, T., and Gordon, J. (1979). Electrophoretic transfer of proteins from polyacrylamide gels to nitrocellulose sheets: Procedure and some applications. Proc. Natl. Acad. Sci. U.S.A. *76*, 4350-4354.

Uruno, T., Liu, J., Zhang, P., Fan, Y., Egile, C., Li, R., Mueller, S.C., and Zhan, X. (2001). Activation of Arp2/3 complex-mediated actin polymerization by cortactin. Nat. Cell Biol. *3*, 259-266.

Van den Abbeele, A., De Corte, V., Van Impe, K., Bruyneel, E., Boucherie, C., Bracke, M., Vandekerckhove, J., and Gettemans, J. (2007). Downregulation of gelsolin family proteins counteracts cancer cell invasion in vitro. Cancer Lett *255*, 57-70.

Varma, R., and Mayor, S. (1998). GPI-anchored proteins are organized in submicron domains at the cell surface. Nature *394*, 798-801.

Varon, C., Tatin, F., Moreau, V., Van Obberghen-Schilling, E., Fernandez-Sauze, S., Reuzeau, E., Kramer, I., and Genot, E. (2006). Transforming growth factor beta induces rosettes of podosomes in primary aortic endothelial cells. Mol. Cell. Biol. *26*, 3582-3594.

Villalba, M., Bi, K., Rodriguez, F., Tanaka, Y., Schoenberger, S., and Altman, A. (2001). Vav1/Rac-dependent actin cytoskeleton reorganization is required for lipid raft clustering in T cells. J. Cell Biol. *155*, 331-338.

Viola, A., and Gupta, N. (2007). Tether and trap: regulation of membrane-raft dynamics by actin-binding proteins. Nature reviews *7*, 889-896.

Viola, A., Schroeder, S., Sakakibara, Y., and Lanzavecchia, A. (1999). T lymphocyte costimulation mediated by reorganization of membrane microdomains. Science (New York, N.Y *283*, 680-682.

von Haller, P.D., Donohoe, S., Goodlett, D.R., Aebersold, R., and Watts, J.D. (2001). Mass spectrometric characterization of proteins extracted from Jurkat T cell detergent-resistant membrane domains. Proteomics *1*, 1010-1021.

Wang, C.-L.A. (2001). Caldesmon and smooth-muscle regulation. Cell Biochem. Biophys. *35*, 275-288.

Watanabe, S., Mabuchi, K., Ikebe, R., and Ikebe, M. (2006). Mechanoenzymatic characterization of human myosin Vb. Biochemistry *45*, 2729-2738.

Watari, A., Takaki, K., Higashiyama, S., Li, Y., Satomi, Y., Takao, T., Tanemura, A., Yamaguchi, Y., Katayama, I., Shimakage, M., Miyashiro, I., Takami, K., Kodama, K., and Yutsudo, M. (2006). Suppression of tumorigenicity, but not anchorage independence, of human cancer cells by new candidate tumor suppressor gene CapG. Oncogene *25*, 7373-7380.

Weaver, A.M. (2006). Invadopodia: specialized cell structures for cancer invasion. Clin Exp Metastasis *23*, 97-105.

Weaver, A.M. (2008). Cortactin in tumor invasiveness. Cancer Lett *265*, 157-166.

Weaver, A.M., Karginov, A.V., Kinley, A.W., Weed, S.A., Li, Y., Parsons, J.T., and Cooper, J.A. (2001). Cortactin promotes and stabilizes Arp2/3-induced actin filament network formation. Curr Biol *11*, 370-374.

Webb, B.A., Eves, R., and Mak, A.S. (2006a). Cortactin regulates podosome formation: roles of the protein interaction domains. Exp. Cell Res. *312*, 760-769.

Webb, B.A., Jia, L., Eves, R., and Mak, A.S. (2007). Dissecting the functional domain requirements of cortactin in invadopodia formation. Eur. J. Cell Biol. *86*, 189-206.

Webb, B.A., Zhou, S., Eves, R., Shen, L., Jia, L., and Mak, A.S. (2006b). Phosphorylation of cortactin by p21-activated kinase. Arch Biochem Biophys *456*, 183-193.

Wehrle-Haller, B., and Imhof, B. (2002). The inner lives of focal adhesions. Trends Cell Biol *12*, 382-389.

Wehrle-Haller, B., and Imhof, B.A. (2003). Actin, microtubules and focal adhesion dynamics during cell migration. Int J Biochem Cell Biol *35*, 39-50.

Williams, M.W., and Bloch, R.J. (1999). Extensive but coordinated reorganization of the membrane skeleton in myofibers of dystrophic (mdx) mice. J. Cell Biol. *144*, 1259-1270.

Woehlke, G., Ruby, A.K., Hart, C.L., Ly, B., Hom-Booher, N., and Vale, R.D. (1997). Microtubule interaction site of the kinesin motor. Cell *90*, 207-216.

Woodhead, J.L., Zhao, F.Q., Craig, R., Egelman, E.H., Alamo, L., and Padron, R. (2005). Atomic model of a myosin filament in the relaxed state. Nature *436*, 1195-1199.

Wu, H., and Parsons, J.T. (1993). Cortactin, an 80/85-kilodalton pp60src substrate, is a filamentous actin-binding protein enriched in the cell cortex. J. Cell Biol. *120*, 1417-1426.

Wulfkuhle, J.D., Donina, I.E., Stark, N.H., Pope, R.K., Pestonjamasp, K.N., Niswonger, M.L., and Luna, E.J. (1999). Domain analysis of supervillin, an F-actin bundling plasma membrane protein with functional nuclear localization signals. J. Cell Sci. *112*, 2125-2136.

Yamaguchi, H., and Condeelis, J. (2007). Regulation of the actin cytoskeleton in cancer cell migration and invasion. Biochimica et biophysica acta *1773*, 642-652.

Yamaguchi, H., Lorenz, M., Kempiak, S., Sarmiento, C., Coniglio, S., Symons, M., Segall, J., Eddy, R., Miki, H., Takenawa, T., and Condeelis, J. (2005a). Molecular mechanisms of invadopodium formation: the role of the N-WASP-Arp2/3 complex pathway and cofilin. J. Cell Biol. *168*, 441-452.

Yamaguchi, H., Pixley, F., and Condeelis, J. (2006). Invadopodia and podosomes in tumor invasion. Eur. J. Cell Biol. *85*, 213-218.

Yamaguchi, H., Wyckoff, J., and Condeelis, J. (2005b). Cell migration in tumors. Curr. Opin. Cell Biol. *17*, 559-564.

Yi, J., Kloeker, S., Jensen, C.C., Bockholt, S., Honda, H., Hirai, H., and Beckerle, M.C. (2002). Members of the Zyxin family of LIM proteins interact with members of the p130Cas family of signal transducers. J. Biol. Chem. *277*, 9580-9589.

Zacharias, D.A., Violin, J.D., Newton, A.C., and Tsien, R.Y. (2002). Partitioning of lipid-modified monomeric GFPs into membrane microdomains of live cells. Science (New York, N.Y *296*, 913-916.

Zaidel-Bar, R., Cohen, M., Addadi, L., and Geiger, B. (2004). Hierarchical assembly of cell-matrix adhesion complexes. Biochemical Society transactions *32*, 416-420.

Zamir, E., Katz, B.Z., Aota, S., Yamada, K.M., Geiger, B., and Kam, Z. (1999). Molecular diversity of cell-matrix adhesions. J. Cell Sci. *112 ( Pt 11)*, 1655-1669.

Zhou, S., Webb, B.A., Eves, R., and Mak, A.S. (2006). Effects of tyrosine phosphorylation of cortactin on podosome formation in A7r5 vascular smooth muscle cells. Am J Physiol Cell Physiol *290*, C463-471.